Ideal Hydrocracking Catalysts for the Conversion of FT Wax to Diesel

Conrad Ndimande

submitted in partial fulfillment of the requirements for the degree of
Master of Science in Engineering

Center for Catalysis Research
Department of Chemical Engineering
University of Cape Town

Synopsis

The Fischer-Tropsch wax synthesis process and the subsequent upgrade of the wax to useful distillate fuels by mild hydrocracking is a well-known, economically viable method of producing liquid fuels, in particular diesel fuel. This project seeks to develop an ideal hydrocracking catalyst (i.e. a hydrocracking unit in which only primary cracking occurs) for the conversion of Fischer-Tropsch (FT) wax to diesel and to determine the effect of carbon monoxide on the activity and selectivity of the hydrocracking catalyst for possible integration of low temperature FT wax synthesis with wax hydrocracking into a single stage. Theoretically, a combination of the Fischer-Tropsch unit with an ideal hydrocracking unit can produce diesel yields of up to 80 wt%. A non-ideal hydrocracking catalyst would lower the middle distillate yields due to the occurrence of secondary cracking. Primary cracking of the paraffins produced by the low temperature FT process occurs only when the activity of the metal is high and the rate limiting step occurs on the acid site.

Integrating the wax synthesis process with the subsequent work up of the wax to produce distillate fuels is not without challenges, mainly the low reaction temperature and pressure (225°C and 20 bar), in which the hydrocracking catalyst is to operate. Noble metals, combined with zeolites are known to be active for hydrocracking at such conditions. Carbon monoxide, a feedstock of the FT process poisons noble metal catalysts; therefore knowledge of its effect on the hydrocracking catalysts performance is essential.

The hydrocracking catalysts were tested when the metal and the acid sites were segregated (i.e. the metal supported on an inert carrier, physically mixed with the zeolite), and when the two sites are in close proximity (i.e. the metal impregnated into the zeolite). The tests were carried out both in the presence and absence of CO consistent with the FT feed ratio. The noble metals, Rh, Ru and Pd were used as co-catalysts to H-MFI-90.

It was found that the physical distance between the metal and the acid sites has disturbs the balance of the two sites by introduction of a transport steps, this seen through both the activity and selectivity of the catalyst. Pd exhibited higher activity than Rh and Ru. Primary cracking was found to be unattainable when the metal and the acid sites are segregated. When the metal and the acid sites were in close proximity (impregnated catalyst), near primary hydrocracking performance was observed at metal loading of 0.9 wt% Pd. Secondary cracking was aggravated upon the introduction of CO on both the segregated and impregnated catalyst.

Acknowledgements

Many thanks go to Prof. Jack C.Q Fletcher the director of the UCT Center for Catalysis Research for the opportunity to undertake this research and his guidance.

Many thanks to Dr Roald Brosius and Walter Böhringer for their guidance and assistance.

Acknowledgment is also made to, C*Change, the Centre for Catalysis Research and the Department of Chemical Engineering at the University of Cape Town for research facilities and funding.

Declaration

I declare that this is my own unaided work and that material that is not my own has been adequately referenced.

Name: ……

Signature: .....

Table of contents

CONTENTS

FIGURES

List of Figures

FIGURES

FIGURES

FIGURES

TABLES

List of Tables

TABLES

1 Introduction

In recent years, the production of liquid fuels from various sources (coal, biomass and natural gas) via the Fischer-Tropsch (FT) process has enjoyed a renewed interest [Bouchy et al., 2009]. This is because of increasing demand for middle distillate fuels, in particular diesel. Unfortunately, whatever the catalyst and reaction conditions, the FT process produces a broad spectrum of hydrocarbon molecular weights and a maximum diesel yield of about 40% [Bouchy et al., 2009]. In spite of efforts, improvement of the intrinsic selectivity of the Fischer-Tropsch Synthesis (FTS) towards the middle distillates (diesel) has met with little success [Calemma et al., 2009]. Higher diesel yields of up to 80% may be achieved by a two-step approach. The FTS is carried out at low temperatures (220°C-230°C) using a cobalt catalyst, in order to produce long chain paraffins (wax), which is followed by selective hydrocracking of the wax to high quality diesel [Dry, 2001].

Hydrocracking is a catalytic process which converts heavy feedstocks to mostly saturated lighter products. A variety of hydrocracking catalysts have been developed and extensively studied. These include sulfided base-metals on amorphous silica-alumina supports [Leckel, 2005], the type of catalysts used in crude oil refineries, platinum-loaded sulphated or tungstated zirconia supported catalysts [Zhang et al., 2001], or noble metal promoted amorphous silica-alumina catalysts [Sie et al., 1991]. These hydrocracking catalysts are bifunctional, comprised of a metal component dispersed on an acidic carrier such as amorphous silica-alumina. The metal provides a dehydrogenation/hydrogenation function while the acid provides the isomerization and cracking function [Coonradt et al., 1964]. The cracking reactions are responsible for conversion of the heavy feedstock to produce gasoline and middle distillates, while isomerization leads to a marked improvement of the gasoline octane number and the diesel cold flow properties. The relative strength of the two functions of the hydrocracking catalyst determines the type and distribution of the products. If a metal which provides a strong hydrogenation or hydrogen activation function such as platinum is used, high selectivity for hydro isomerization and pure primary cracking can be obtained [Steijns et al., 1981].

There exists an opportunity for catalysts and processes that effect an integration of the wax selective FTS and hydrocracking processes into one unit. Integrating the two processes reduces the scale of the plant and lowers the capital investment [Hamelinck et al., 2004]. Conventional hydrocracking catalysts (oxidic CoMo on amorphous silica-alumina) [Böhringer et al., 2007] are not active in the 200°C-240°C temperature window of the cobalt FT wax synthesis process, while noble-metal-on-acid-carrier catalysts have been found to be active in this temperature

window [Akhmedov and Al-Khowaiter, 2000]. However, reaction temperature and pressure are not the only critical factors to the combination of FTS and hydrocracking, as the hydrocracking catalyst must tolerate high carbon monoxide concentrations. Carbon monoxide is known to affect the hydrogenation/dehydrogenation activity of noble metals by adsorbing strongly on the metal, blocking the active sites [Scherzer and Gruia, 1996]. In addition, water vapour, one of the major products of FTS may affect the hydro isomerization/hydrocracking activity of the acid support, especially at high syngas conversions. In addition, the conventional hydrocracking process operates at high hydrogen partial pressures and high hydrogen to hydrocarbon ratios. For a combination of hydrocracking and FTS, the hydrogen to wax ratio will be lower and low hydrogen to wax ratio has been shown to decrease wax conversion [Leckel, 2005].

A common method for the preparation of a hydrocracking catalyst involves wet coating the acid support with a metal salt solution, drying and finally reducing the metal under hydrogen flow [Pinna, 1998]. While procedures can be optimized for a certain technical application, for scientific purposes such as the comparison of different acid functions, loading the metal directly on the acid support presents its own problems as the uncertainty as to the dispersion of the metal on the acid support makes it difficult to produce a desired metal to acid site ratio. An alternative is to synthesize a single batch of the metal co-catalyst by loading the metal onto an inert support. The dispersion of the supported metal will be known and fixed. To make a hydrocracking catalyst with a particular metal to acid site ratio would require just the addition of enough acid co-catalyst. However, for a hydrocracking catalyst to be practically effective, it is important that there be rapid molecular transfer between acid and metal sites to avoid undesired secondary cracking [Scherzer and Gruia, 1996], and segregating the metal and acid sites increases the distance between these two functions.

The focus of this investigation was firstly to understand the effect of CO on the metal co-catalyst (Rh, Ru and Pd) of a hydrocracking catalyst. This was done both with the metal impregnated on an inert carrier and with the metal directly impregnated on the acid function. Zeolite H-MFI, with molar silica to alumina ratio of 90 was used as the acid co-catalyst and n-hexadecane was used as a model compound for wax.

2 Background

2.1 Liquid Fuels from FTS

A synthetic method for the production of liquid fuels is the conversion of carbonaceous material to a mixture of hydrogen and carbon monoxide (known as syngas), followed by its conversion to hydrocarbons over a suitable catalyst via the Fischer-Tropsch synthesis process, and the subsequent hydrocracking of these intermediates to produce liquid fuels. Currently, commercial FTS has two operating modes, the high temperature process and the low temperature process [Khodakov et al., 2006]. Irrespective of the mode of operation, FTS products are characterized by a wide carbon number distribution. The high temperature process (240°C – 350°C) produces hydrocarbons mainly from C_1 to about C_{15} over an iron catalyst [Khodakov et al., 2006]. This process is primarily used to produce lower olefins and liquid fuels in the gasoline range. Low temperature FTS (200°C – 240°C) produces mostly long chain linear paraffins which can then be hydrocracked to produce middle-distillate fuels (diesel). The FTS product carbon number distribution is described by the Anderson-Schultz-Flory (ASF) polymerization model, which presents the carbon number distribution of the FTS products as a function of the chain growth probability, α, as shown in Figure 2.3.

The kinetics of FTS limits selectivity to specific carbon number fractions. An example is the yield of diesel fuels, with a maximum yield of 40%. To increase diesel yield, it therefore becomes necessary to run the FTS so as to produce wax (chain growth probability close to 1), followed by hydrocracking to upgrade the wax from the LTFT process to maximize diesel yields, as shown in Figure 2.1.

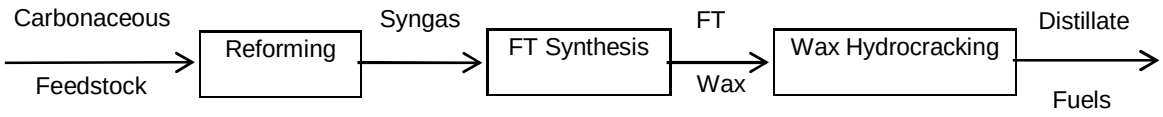

Figure 2.1: Distillate production from carbonaceous material, redrawn from Dry, [2001]

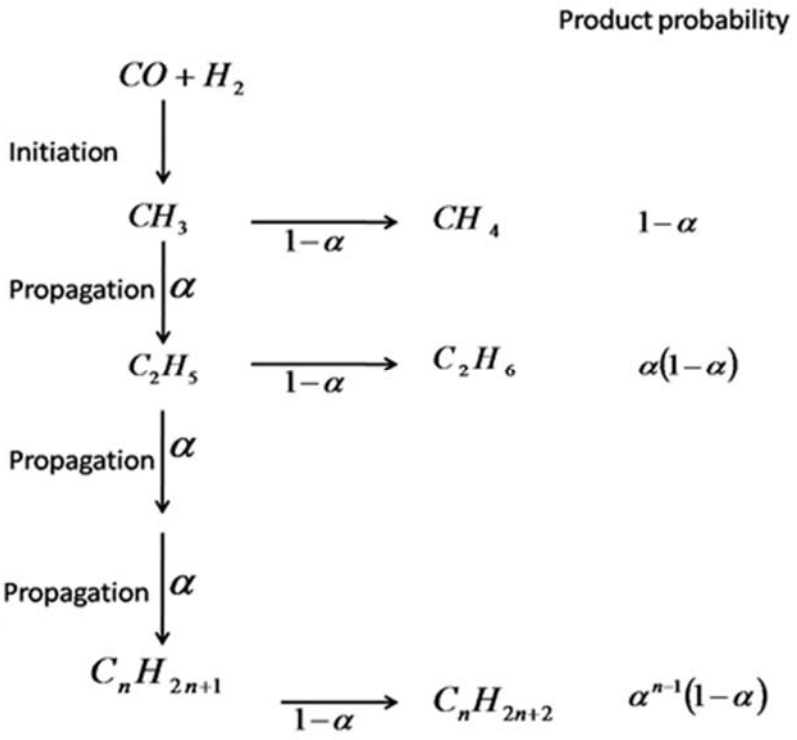

Figure 2.2: FTS product formation according to ASF polymerization model. Reproduced from Bouchy et al. [2009]

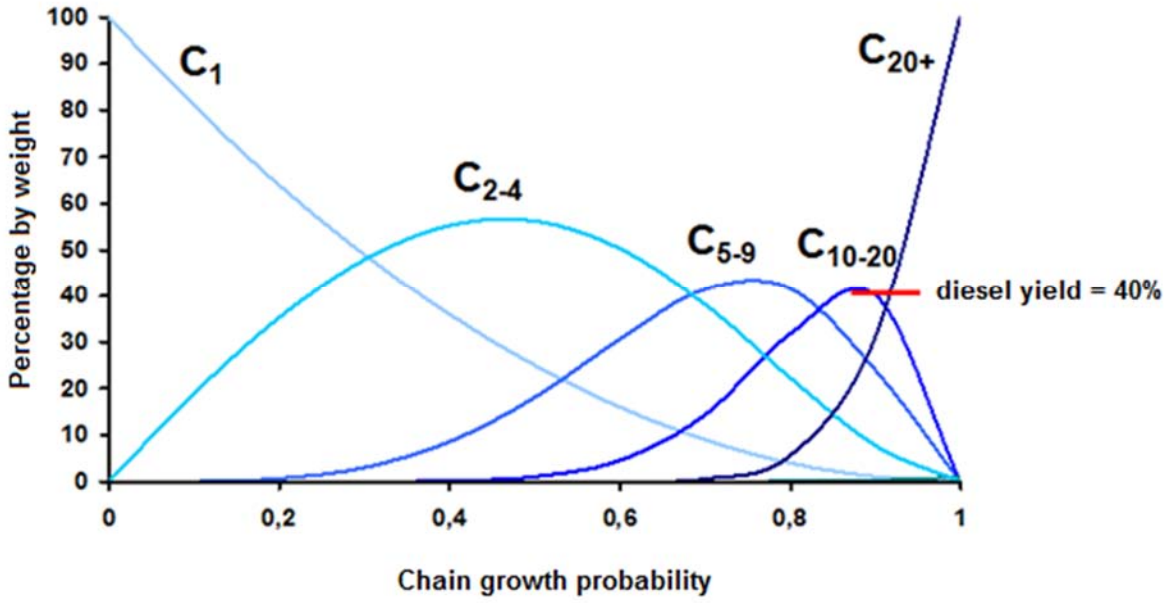

Figure 2.3: FT product carbon number distribution as a function of chain growth probability (according to ASF model)

2.2 Hydrocracking

2.2.1.1 Hydrocracking Catalysts and Process

Hydrocracking is commonly applied to upgrade heavy hydrocarbon fractions to lighter marketable liquid fuels. This is achieved by cleavage of carbon-carbon bonds followed by saturation of the resulting fragments. The formation of these cracked products generally involves two successive reaction steps [Bouchy et al., 2009], namely isomerisation and the actual cracking step.
Ideally, hydrocracking should fulfill certain requirements which are the following:

1. Selectively convert heavy feedstock to light products, for instance, middle distillates,
2. Minimize cracking of middle distillate already present in the feed,
3. Minimize further cracking of middle distillate produced
4. Limit the extent of isomerization in order to optimize the balance between cetane number requirements and cold flow properties.

Hydrocracking is carried out over a bifunctional catalyst containing a hydrogenation/ dehydrogenation function or hydrogen activation function (a metal or metal sulphide or oxides) and an acid function of the Brönsted type. The acid function may be an amorphous oxide (in particular silica-alumina), a zeolite or a mixture of the two aforementioned. These combinations are summarized in Figure 2.4.

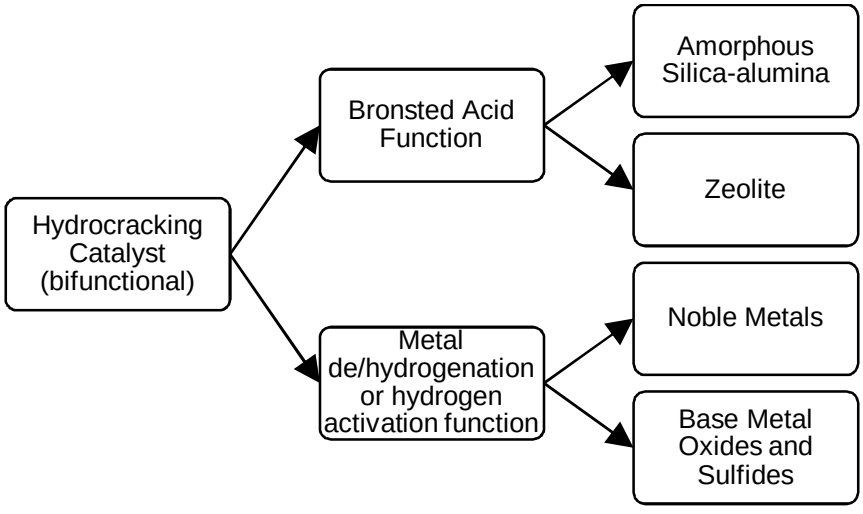

Figure 2.4: Possible compositions of hydrocracking catalysts

For crude oil fractions, only the base metal option (because of the sulfur containing feed) together with the amorphous silica-alumina option is possible (because of size of the poly-cyclic feed molecules). All the options shown in Figure 2.4 are applicable for FT-wax hydrocracking.

High conversion of LTFT wax is obtained at rather mild conditions compared to hydrocracking of conventional petroleum based feed stocks [Bouchy et al., 2009]. This is partly because of the high chemical reactivity of the heavy paraffin molecules and because of the more active catalysts that can be applied to the former, sulfur-free feed stocks. Conventional crude oil hydrocracking is performed over a bifunctional catalyst at high H_2/feedstock ratio, usually in the range 800 - 2000 m^3/m^3. High hydrogen pressures enable the deep hydrogenation of polynuclear aromatics and deep hydrodenitrification. It further improves catalyst life by reducing the rate of coke formation [Dufresne et al., 1987].

Typical feedstock for the conventional hydrocracking process includes, atmospheric gas oil and vacuum gas oil. The conventional hydrocracking process may be operated in a single or two stage configuration [Dufresne et al., 1987]. The two stage configuration consists of a hydro-treatment step with the option for intermediate removal of H_2S and NH_3 before the product is fed to the second hydrocracking step, in which the unconverted heavy fraction from the hydro-treatment step is hydrocracked to produce middle distillate fuels, naphtha, butane and propane. The catalysts employed compromise a variety of group VIA metals (Mo, W) and some group VIIIA metals (Co, Ni). For the acid co-catalyst, typically amorphous silica-alumina and zeolites are used.
Mild hydrocracking is conducted in a single-stage process operated in the range 380°C - 440°C [Marcilly, 2003; Dufresne et al., 1987]. The feed stock for mild hydrocracking typically includes vacuum gas oil and the Catalysts employed are similar to those applied for conventional crude oil hydrocracking, the only difference being that milder acid co-catalysts are used. A comparison of the process conditions for conventional crude oil fractions and FT wax hydrocracking is summarized in Table 2.1.

Table 2.1: Process conditions for conventional, mild and FT wax hydrocracking

	Conventional Hydrocracking*	**Mild hydrocracking****	**FT wax Hydrocracking*****
Type of Catalyst	(Mo, W, Co, Ni) or noble metals on amorphous silica-alumina	(Mo, W, Co, Ni) or noble metals on amorphous silica-alumina	Ni/Mo on amorphous silica-alumina
Reactor technology	Trickle bed	Trickle bed	Trickle bed
Conversion (%)	70-100	20-40	20-100
Pressure	100-200	50-80	35-70
Temperature (°C)	350-430	380-440	324-372
H_2/feedstock (m^3/m^3)	800-2000	400-800	500-1800
Products	Diesel, jet fuel, gasoline	Middle distillates and low sulfur oil	80% diesel, 15% gasoline

[* Marcilly, 2003; Dufresne et al., 1987; ** Leckel, 2007; ***Calemma et al., 2005]

An example of an existing application of low temperature FTS (LTFT) and hydrocracking for middle distillate production is the Shell Middle Distillate Synthesis (SMDS) process (Figure 2.5). The first of such came online in 1993 [Dry, 2002]. The first stage of the two-stage SMDS is the conversion of syngas to wax by LTFT, and is referred to as the 'Heavy Paraffin Synthesis'. It is operated such that the chain growth probability is above 0.9, in order to produce mostly wax. This stage is followed by hydrocracking of the wax to produce middle distillates, a stage referred to as 'Heavy Paraffin Conversion'. A trickle-flow reactor is employed at mild conditions (300°C - 350°C and 30-50 bar) [Sie et al., 1991; Eilers et al., 1990]. A fractionation stage follows the hydrocracking step where the hydrocarbons boiling above the diesel range are recycled to the hydrocracking unit.

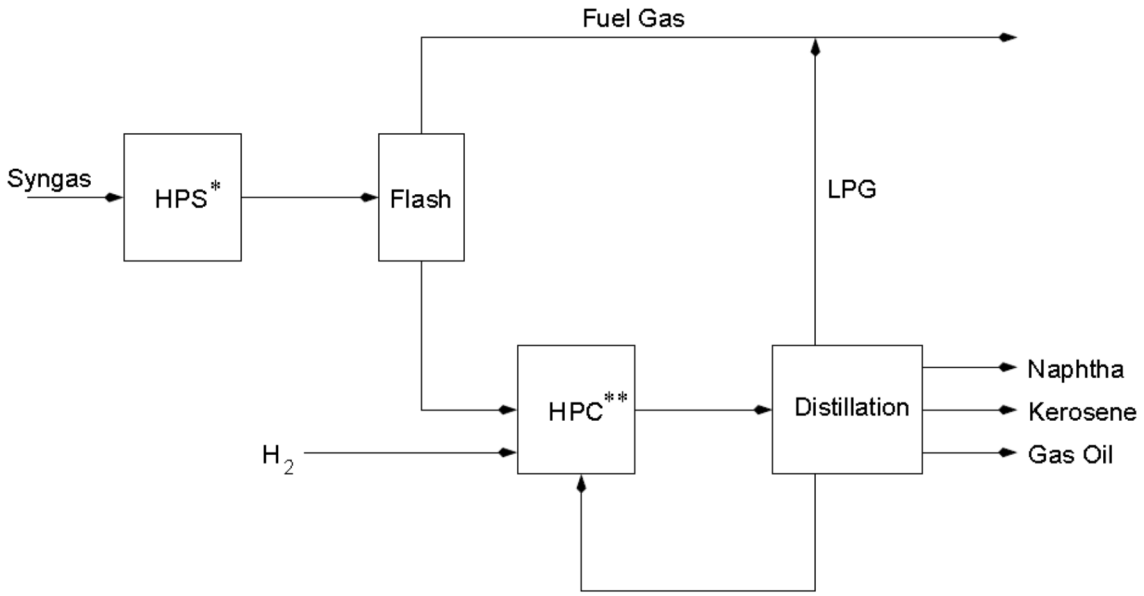

Figure 2.5: The Shell Middle Distillate Synthesis Process [* Heavy Paraffin synthesis; ** Heavy Paraffin Conversion]. Adapted from Sie et al. [1991]

2.2.2 Hydrocracking Mechanisms

A number of mechanisms have been proposed for the hydrocracking reactions. A hydrocracking mechanism, where the reactions occur on two separate and distinctly different sites via a series of intermediate diffusion and reaction steps between the metal and acid sites (Figure 2.6 - top row) was proposed by Mills et al. [1953] and Weisz and Swegler [1957]. This “classical” mechanism was generally accepted for several decades and is still generally considered to best represent the hydrocracking mechanism [Scherzer and Gruia,1996; Bouchy et al., 2009]. Kazanski et al. [1989] and Rigby et al. [1997] proposed a mechanism for the intermediate isomerization and cracking steps that involve surface silicon alkoxide type reaction intermediates instead of carbenium ions (Figure 2.6 - central box). The last two decades have seen the classical mechanism increasingly questioned and contested with a mechanism that avoids the fluid phase diffusion of intermediates. According to this new mechanism, all steps occur on the acid sites, triggered by activated hydrogen that spills over from the metal sites by surface diffusion. This route is indicated by the sequence of red arrows in Figure 2.6.

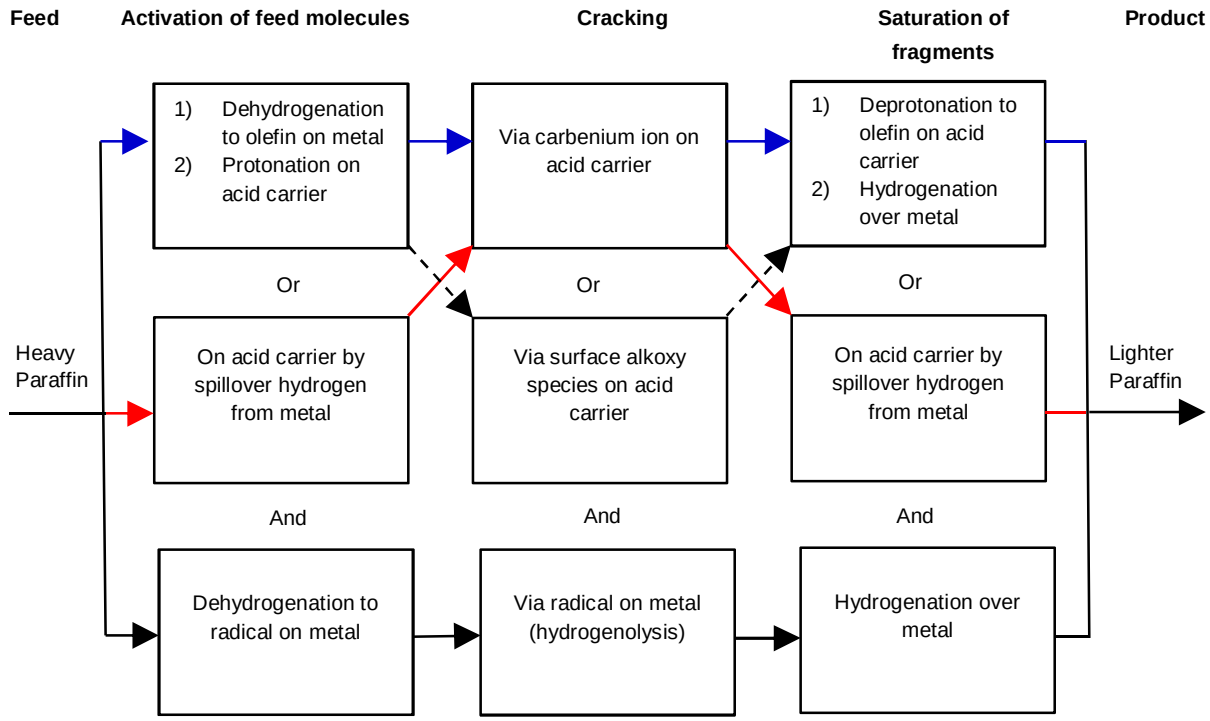

Figure 2.6: Reaction mechanisms occurring over bifunctional hydrocracking catalysts; here for a metal plus acid carrier.

However, detailed hydroisomerization and hydrocracking selectivity on Pt/H-USY zeolites with different Si/Al ratios were observed to be identical [Bouchy et al., 2009]. This important experimental evidence shows that alkylcarbenium chemistry best describes the cracking reactions for long chain hydrocarbons. If alkoxides were involved, differences in hydroisomerization and hydrocracking selectivity would have been observed as the Si/Al ratio was varied. Other reactions, in parallel to the acid catalyzed hydrocracking reactions, occur on the metal surface. These are the non-bond-specific hydrogenolysis and methane formation via selective cleavage of terminal carbon-carbon bonds, known as methanolysis (Figure 2.6 - bottom row).

2.2.2.1 The “Classical” Bifunctional Hydrocracking Mechanism

According to the “classical” mechanism, as illustrated in Figure 2.7, dehydrogenation of a paraffinic feed molecule takes place on the metal site resulting in the formation of an olefin. The olefin desorbs and migrates by diffusion through the fluid phase to an acid site where a carbenium ion forms by protonation of the olefin. The carbenium ion undergoes skeletal isomerisation and subsequent cracking. The carbenium ion fragment which results from cracking is deprotonated to an olefin, which desorbs from the acid site and migrates by fluid-

phase diffusion to a metal site where it is hydrogenated [Weisz and Swegler, 1957; Scherzer and Gruia, 1996].

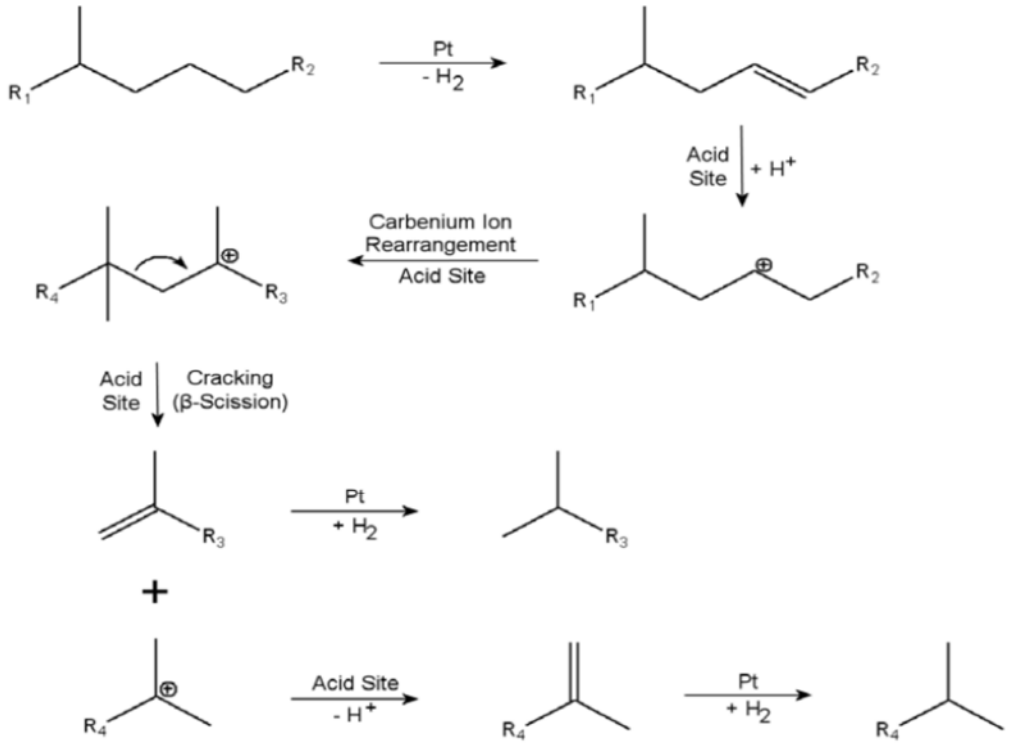

Figure 2.7: Classical bifunctional hydrocracking mechanism over Pt/acid catalyst [Weitkamp et al., 1983]

2.2.2.2 Carbenium Ion Isomerization and Cracking

There are two mechanisms by which isomerization can occur (once a first carbenium ion has formed), as follows

- Type A isomerization: side chain positional changes occur, via 1,2-alkyl hydride shift, while the degree of branching of the carbocation does not change [Marcilly, 2003]. For example [Bouchy et al., 2009],

- Type B isomerization: the degree of branching of the carbocation is increased via the formation of cyclic carbenium ion intermediate [Chevalier et al., 1977]. For example [Bouchy et al., 2009],

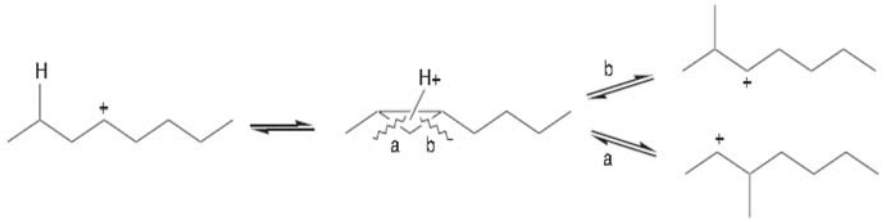

Several studies have shown that the type A isomerization occurs much faster than type B isomerization [Chevalier et al., 1977; Riberio et al., 1982].

Cracking of a carbenium ion occurs by scission of the C-C bond in the β position relative to the positively charged carbon atom of the carbocation [Bouchy et al., 2009] leaving an olefin and another carbenium ion (Figure 2.8). This process is called 'β scission'. The rate limiting step in the isomerization-cracking sequence is the β-scission of the carbon - carbon bond.

The rate at which cracking occurs decreases with decreasing stability of the reactant and product carbenium ions on the acid site. Stabilities of carbenium ions are generally ranked as follows:

Tertiary > secondary >> primary

Due to the very low stability of the primary carbenium ion, mechanisms proceeding via primary carbenium ions are considered to be negligible (as long as a route via secondary or tertiary carbenium ions is possible) [Martens and Jacobs, 1990]. Figure 2.8 shows examples of cracking via secondary and tertiary carbenium ions.

The relative rates of reactions that occur via the different types of carbenium ions can be ordered as follows:

$$A >> B_1, B_2 > C$$

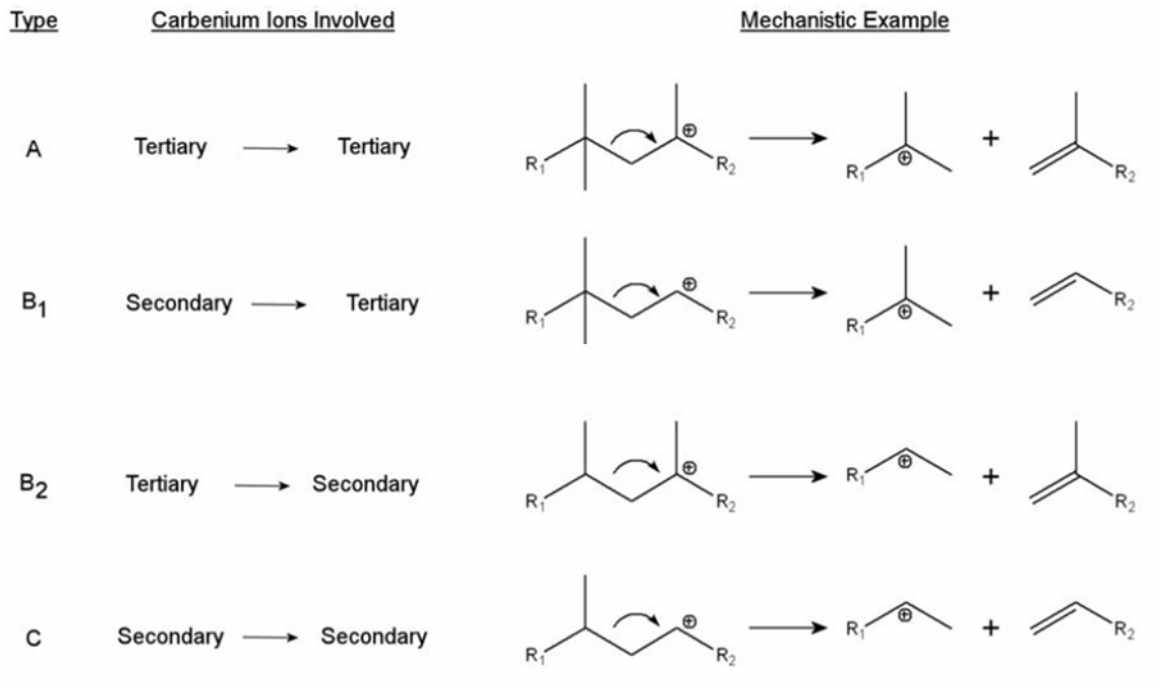

Figure 2.8: β-Scission reactions via secondary and tertiary carbenium ions [Weitkamp et al., 1983]

It follows that tertiary–tertiary cracking (A) will occur most rapidly because of the stability of the tertiary carbenium ions, but it will only proceed when a quaternary carbon is located in the β-position of a tertiary carbenium ion. Therefor the tertiary–tertiary β-scission is only feasible on central C-C bonds i.e., from the fourth carbon atom onwards, though with equal probability [Dry, 2003]. This will result in a product that exhibits a relatively equal molar distribution from C_4 onwards up to fragments with a carbon number lower than that of the feed molecule. This is known as ideal primary hydrocracking. Whether or not primary cracking occurs partly depends on the formulation of the hydrocracking catalyst and partly on the reaction conditions applied, e.g. hydrogen availability, since secondary cracking must be supressed. Carbenium ion chemistry is of particular importance for the hydrocracking of FT wax to diesel because the products formed will be branched, thus inherently the products exhibit improved cold flow properties versus the feed [Bouchy et al., 2009], fulfilling one of the key requirements for diesel coming from a wax hydrocracking stage outlined in the introduction to (section 2.2.1).

The relative reactivity of n-paraffins towards hydrocracking has been the subject of numerous publications. Pellegrini et al. [2004, 2007] developed a kinetic model of the hydrocracking of n-paraffins. They based the model on hydrocracking a model mixture of C_4 – C_{70} compounds and a Pt/amorphous-silica-alumina catalyst. They found that the reactivity of the n-paraffins on an acid catalyst increases with increasing chain length, that is, with increasing number of bonds

available for possible scission reactions. Figure 2.9 show that, for instance, C_{17} has a relative reactivity 90 times that of C_{10}. However, it must be understood that the reaction mechanism and the number of bonds available for type A β-scission are not the only factors responsible for this difference, different process conditions are another contributing factor.

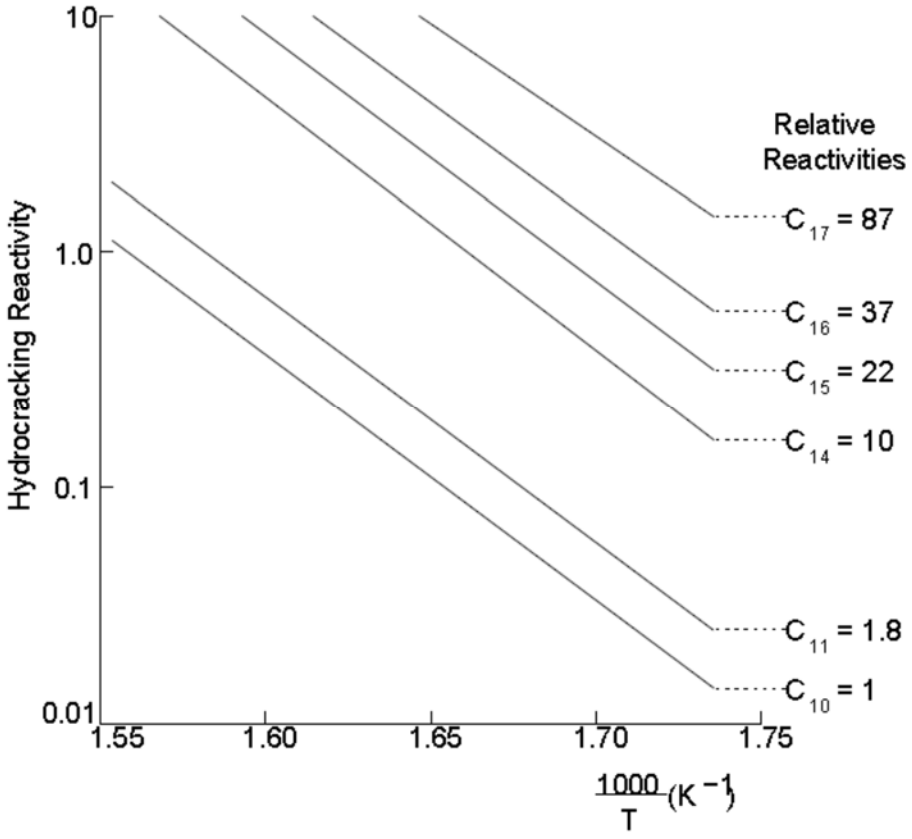

Figure 2.9: Relative reactivity of n-paraffins on a bifunctional catalyst [Sie et al., 1991]

2.2.2.3 Surface Alkoxyde Cracking

As an alternative to the classical mechanism, Kazanski et al. [1989] and Rigby et al. [1997] proposed a cracking mechanism that was based on results obtained from a computational study of small hydrocarbons, with cluster models representing zeolites and involving surface silicon alkoxy type intermediates. However, apparently due to computational limitations, the problem is that the simulations have never been done for long chain hydrocarbons such as LTFT wax.

2.2.2.4 The Weisz Intimacy Criterion

In the classical mechanism, which involves the diffusion of the olefin intermediates from the metal sites to the acid sites, the sites must be sufficiently close to each other [Weisz, 1962; Roessner and Roland, 1996]. To ensure that the two active sites of a bifunctional catalyst are sufficiently close to each other, bifunctional hydrocracking catalysts are usually prepared by impregnation of the metal component onto the support. This is done so as to obey the Weisz intimacy criterion, $y_{w\text{-}p}$, which is expressed mathematically as follows:

$$y_{w-p} = \frac{R_p^2 r}{C_s D_o} < 3\beta$$

where C_s, is the reactant concentration at the catalyst surface, r, is the reaction rate per volume of catalyst, R_p is the catalyst particle radius and D_o, is the effective diffusivity. The variable β, is defined For an effectiveness factor, η, and a reaction order, n, by the following equation:

$$\beta = \frac{4(1-\eta)}{n}$$

The Weisz intimacy criterion is a comparison of the diffusivity D_o and the reaction rate, r, to determine the maximum distance (in the order of a few micrometres) between the metal and the acid sites required to ensure that the diffusion steps in the classical hydrocracking sequence are not rate limiting [Böhringer et al., 2009].

2.2.2.5 Effect of Reactor Design and Conditions

The process conditions are tuned such that the lighter hydrocarbons, those boiling in the diesel range and below, are partially vaporized. This affords these light hydrocarbons (typically the desired products) a very much more limited catalyst contact time versus the heavier feed molecules, which is reflected also by their low reactivity in the hydrocracking process [Eilers et al., 1990] as shown in Figure 2.9. Consequently, this partial vaporization minimizes cracking of the lighter part of the feed and product (that is already boiling in the middle distillate range), thus achieving significant cracking only of the heavy part of the feed. As a result, the first, second and third requirement of hydrocracking to diesel, as outlined in section 2.2.1, can be met.

Calemma et al. [2005] reported the strong impact of temperature and the ratio of hydrogen/feedstock on the vapour/liquid distribution and phase composition in the reactor on hydrocracking. Table 2.2 shows that at a higher H_2/hydrocarbon ratio, for a given temperature and pressure, the liquid product is enriched in heavier fractions such as C_{22+}.

Table 2.2: Relative reactivity of n-paraffins on a bifunctional catalyst [Sie et al., 1991]

	Feedstock	Liquid Phase Product	
Pressure Bar	1	35	35
Temperature (C°)	Room Temperature	324	324
H_2/Hydrocarbon (wt/wt)	nil	0.06	0.15
Composition (wt/wt*)			
C_{9-}	0.037	0.001	0.001
$C_{16} - C_{14}$	0.176	0.055	0.026
$C_{15} - C_{22}$	0.301	0.264	0.202
C_{22+}	0.486	0.680	0.771

A boundary condition is that the trickle bed reactor applied must be operated such that the catalyst is covered entirely by the liquid fraction of the reaction mixture. This means that the reaction takes place entirely in the liquid phase. It is clear from Table 2.2 that at higher hydrogen/feedstock ratio, the liquid phase is enriched with heavier paraffins.

2.2.2.6 Results Not Readily Explained via the "Classical" Mechanism

Researchers investigating the effect of partially separating the metal and acid functions of hydrocracking and hydroisomeraztion catalysts discovered phenomena which are not readily explained by the classical hydrocracking mechanism. Steinberg et al. [1990] mimicked a bifuntional catalyst, a noble metal on inert carrier together with an acid zeolite, via combinations of individual catalysts kept in separate beds and beds arranged in different configurations as shown in Figure 2.10. The purpose of these experiments was to investigate the effect of the separation distance between the metal and the acid functions. The reactors were loaded as follows (referring to Figure 2.10):

(A) Metal co-catalyst directly above and in contact with the acid catalyst.

(B) Metal co-catalyst directly below and in contact with the acid catalyst.

(C) Metal co-catalyst above the acid catalyst but not in contact .

(D) Metal co-catalyst above the acid catalyst but separated by layer of inert material.

(E) Metal co-catalyst only, without acid co-catalyst (a 'blank' to investigate whether or not the metal itself was active).

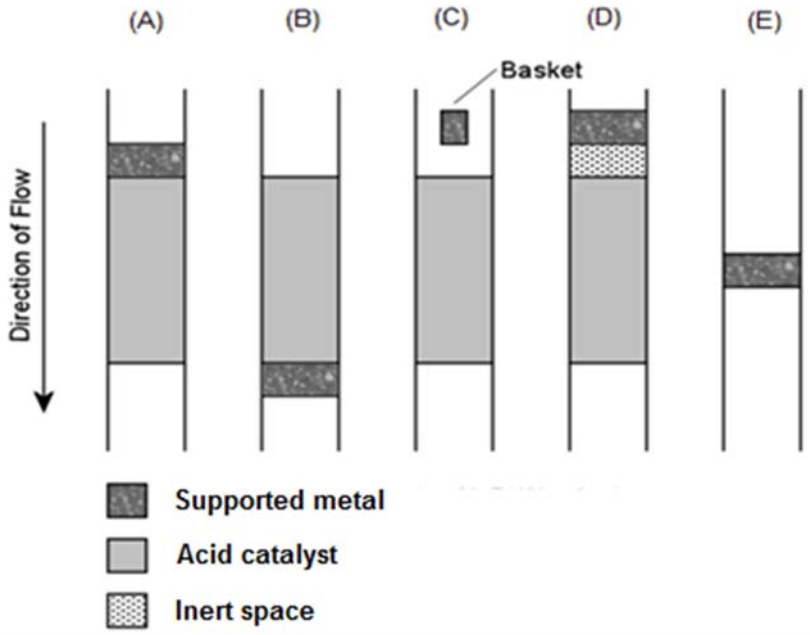

Figure 2.10: Different acid and metal site arrangments for hydrocracking [Steinberg et al., 1990]

It was noted in various hydroconversion experiments by Steinberg et al. [1990], Roland et al. [1997], Roessner et al. [1993] and others who worked with similar arrangements, that in three of the configurations (such as (A), (B) and (D) provided the barrier of space was rather thin), typical bifunctional conversion products were observed, i.e. hydroisomerisation and hydrocracking products. However, when the two functions had no physical contact or were separated by a thick layer of the inert spacer, (arrangements (C) an (D)), the products observed did not conform to those of typical bifunctional hydrocracking or hydroisomerization products. The products, rather, were consistent with those of catalytic cracking.

If the classical mechanism alone was occurring, which requires diffusion of the olefinic intermediates through the fluid phase (section 2.2.2.1), no hydrocracking or hydroisomerization products would be expected from bed arrangements (A), (B) and (D). This, is because according to the classical mechanism, the cracked olefins from bed arrangements (A) and (D) must diffuse from the acid sites, against the hydrodynamic flow, back to the metal sites to be hydrogenated. Vice versa, in arrangement (B) the intermediate olefins from feed dehydrogenation must diffuse back against the hydrodynamic flow, to the acid sites to be isomerized or cracked. This diffusion against the hydrodynamic flow is not considered probable [Steinberg et al., 1990; Roessner and Roland, 1996]. However, Steinberg et al. [1990] observed that the products from bed arrangements (A) and (B) all produced paraffin hydroisomerization

and hydrocracking products. To obtain such products according to the classical mechanism would require at least a well-mixed bed of the metal and acid co-catalyst particles.

A well-mixed catalyst bed would allow for transport of the olefins between the metal and the acid sites. Furthermore, if diffusion through the fluid phase were taking place, bed arrangements (C) and (D) (with a thick spacer layer) would also be expected to produce hydroisomerization/ hydrocracking products, since the extent of separation between the metal and acid co-catalysts is the same. This was not observed. Bed arrangements (C) and (D) (with a thick spacer layer) yielded a catalytic cracking product under the test conditions applied [Steinberg et al., 1990].

Based on these findings, it is likely that the classical mechanism was not the mechanism (or not the only mechanism) occurring [Steinberg et al., 1990]. It was thus suggested [Conner et al., 1995; Roessner and Roland, 1996] that the hydrogen itself is in some manner activated on the metal site and migrates to the acid sites where it interacts with the feed.

2.2.3 The Hydrogen Spillover Mechanism

The concept of the activation of hydrogen on metal sites and its surface migration from the metal to the acid sites is termed “hydrogen spillover”. The hydrocarbon feed activation, isomerization, cracking and the final saturation step in the hydrogen spillover mechanism all occur on the acid sites. Isomerization and cracking also follow a carbenium ion mechanism as described in section 2.2.2.2. Correspondingly, the products from reaction systems thought to require the hydrogen spillover mechanism exhibit the same degree of branching (provided the acid co-catalyst does not affect spatial restraints). The mechanistic scheme for hydrogen spillover mediated hydrocracking is shown in Figure 2.11.

Figure 2.11 indicates that the hydrogen, activated on the metal sites, aids the adsorption and activation of the paraffinic feed molecules on the acid sites (i.e. formation of a carbenium ion on the acid site). The deprotonating and desorption as paraffins, of the isomerized species and cracking fragments produced on the acid sites, is triggered by spillover hydrogen.

To-date, attempts at identifying the exact nature of the spillover hydrogen species have met with little success. Various possibilities have been proposed such as H^+/H^- ion pairs, paramagnetic H radicals [Roland et al., 1997] and H_3 species [Bianchi et al., 1981].

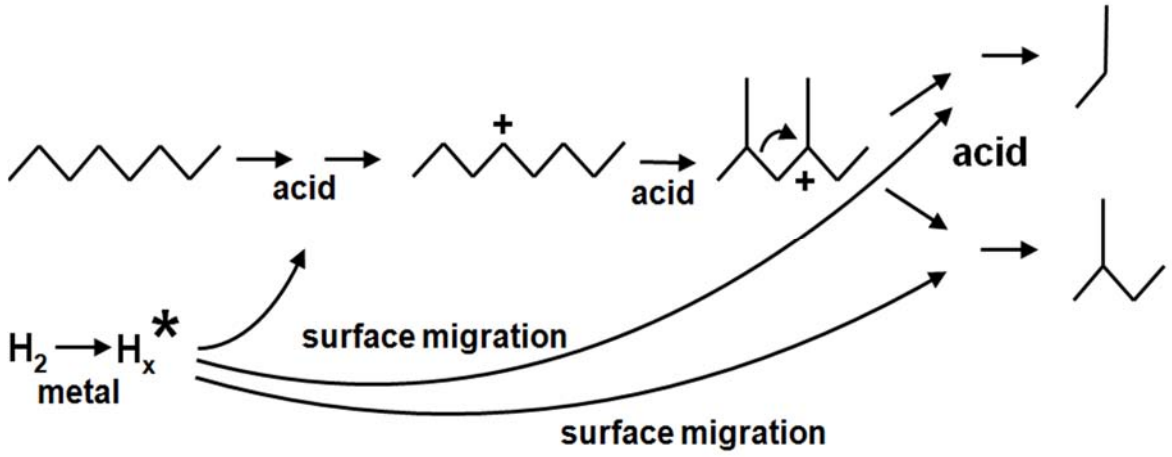

Figure 2.11: The hydrogen spillover mechanism (H_X* represents the migrating activated hydrogen) [Böhringer et al., 2009]

The hydrogen spillover mechanism may not be fully understood and widely accepted yet, nonetheless it does offer an explanation for experimental results such as those of Steinberg et al. [1990]. The hydrogen spillover mechanism suggests that the metal need not necessarily be loaded directly on the acid co-catalyst. The metal can also be loaded on an inert support and physically mixed with the acid. If prepared as a single batch, it would be possible to compare acid co-catalysts, knowing that the metal function is always exactly the same. On the other hand, for industrial application, it is best to have the metal impregnated in the acid co-catalyst because a decline in the overall performance with increasing distance of the two functions has been reported [Roessner and Roland, 1996] and which confirms hydrogen spillover to be a diffusion process. Therefore, segregating the metal and acid functions may only be of interest for laboratory investigations.

2.2.4 The Ideal Hydrocracking Catalyst

A specific formulation of the hydrocracking catalyst is important for the hydrocracking process to fulfill its requirements as outlined in section 2.2.1. Secondary cracking must be minimized in order to maximize yields of the target product (diesel). To meet these requirements, the catalyst must be formulated such that the cracking step is the rate limiting step in the hydrocracking sequence and, to achieve this, the two functions need to be at a short distance from each other, i.e to obey the Weisz intimacy criterion [Weisz, 1962]. This criterion, which compares the diffusivity of olefins in the fluid phase to the rate of reaction, states that the reaction should not

be limited by olefins transfer (in the case of the 'classical' mechanism). In the case of the hydrogen spillover mechanism, the overall rate must not be limited by the supply of activated hydrogen from the metal to the acid sites.

In the classical model, the hydrogenation/dehydrogenation function needs to be 'strong' enough to be able to adequately supply olefins to the acid sites as well as to quickly hydrogenate the cracked fragments. This is to ensure that the hydrogenation/dehydrogenation reactions on the metal co-catalyst are at quasi equilibrium and that the limiting step proceeds on the acid site [Bouchy et al., 2009]. For the case of hydrogen spillover, the hydrogen activation function must be 'strong' enough to provide sufficient hydrogen to activate and adsorb the feed molecules as well as to saturate the cracked fragments.

A hydrocracking catalyst, for which the limiting reaction step occurs on the acid sites, is considered an "ideal" hydrocracking catalyst [Weitkamp et al., 1983]. Ideal hydrocracking is understood as a special case of "classical" bifunctional catalysis with rapid desorption of the primary products formed on the acid sites and without subsequent secondary cracking occuring. Ideal hydrocracking of long chain n-paraffins is associated with the following [Weitkamp et al., 1975]:

- low temperature,
- the possibility for high selectivities for isomerization,
- the possibility of pure primary cracking.

Marcilly [2003] defined an "ideal" hydrocracking catalyst as one where ideal hydrocracking occurs to the highest possible conversion. Weitkamp et al. [1990] used an ideal (Pt/CaY) and a non-ideal (Co-Mo-S/SiO_2–Al_2O_3) catalyst to hydrocrack n-hexadecane. The product distributions for both catalysts were compared at 50% conversion (Figure 2.12). The ideal hydrocracking catalyst exhibited a molar product carbon number distribution that was fully symmetrical and centered at half the feed carbon number. The molar ratio of cracked products to cracked n-hexadecane was equal to 2, which is indicative of pure primary cracking [Bouchy et al., 2009]. On the non-ideal hydrocracking catalyst, secondary cracking occurred, as is evident from the skewed product carbon number distribution which peaks at around C_4-C_5 and where the cracking reactions of the primary cracked products are consecutive.

Operating conditions also influence the occurrence of ideal hydrocracking. Thybault et al. [2005] reported that for a given catalyst formulation (Pt/USY), decreasing molar hydrogen to hydrocarbon ratio, decreasing temperature and increasing total pressure favoured ideal

hydrocracking. High reactant carbon numbers were found to be detrimental to ideal hydrocracking.

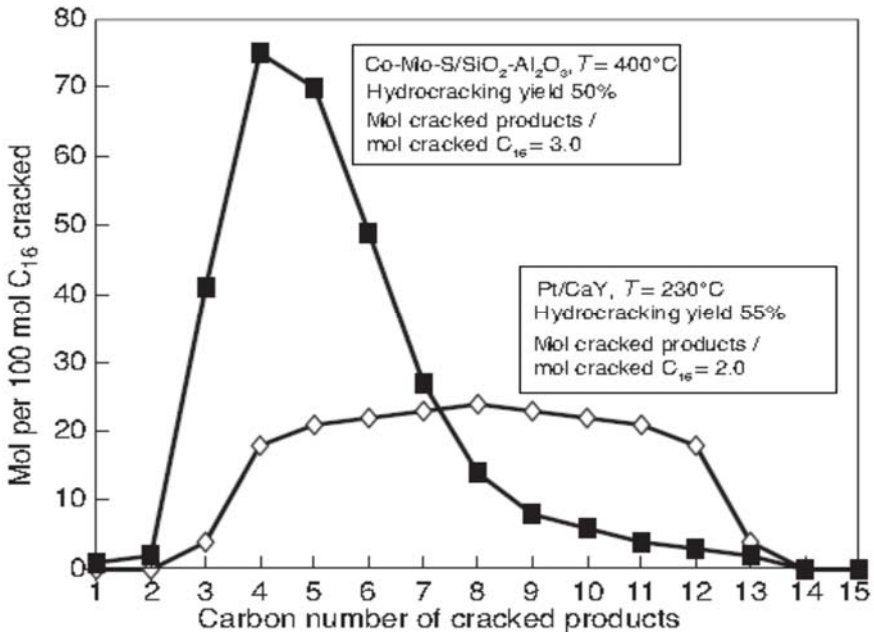

Figure 2.12: Molar carbon number distributions of n-hexadecane hydrocracking products over different catalysts at 50% conversion [adapted from Weitkamp et al., 1990]

In the case of crude oil derived hydrocracking, it is well known that the presence of organic nitrogen and sulfur compounds, ammonia and hydrogen sulfide can strongly influence the "ideality" of the hydrocracking catalyst/process [Dauns et al., 1986; Nat, 1988], since sulfur compounds poison the metal function and nitrogen compounds poison the acid function, leading to a change in the catalysts metal/acid balance.

Over an ideal hydrocracking catalyst and under appropriate conditions, the carbon number selectivities of an ideal long chain paraffin hydrocracking product can be predicted based on the ideal cracking hypothesis [Bouchy et al., 2009]. For instance, with tricosane the following can be exected:

- Only pure primary cracking,
- C_1 and C_2 cannot be formed,
- Equimolar amounts of fragments between C_4 and C_{19} are formed,
- C_3 and C_{20} fragments, although formed, are half of the molar amounts of fragments between C_4 and C_{19} [Bouchy et al., 2009].

It should, however, be noted that the quantities of C_4 and C_{19} fragments claimed above, are not substantiated by experimental results as can be seen by comparing the ideal product carbon number distribution obtained from hydrocracking of n-hexadecane over Pt/CaY in Figure 2.12. This is so, since the relative rates of type B cracking, from which the C_3/C_{20} cracking products originate, are much higher than the rate of type A cracking that produces the C_4 to C_{19} product range (see Figure 2.8 and related text).

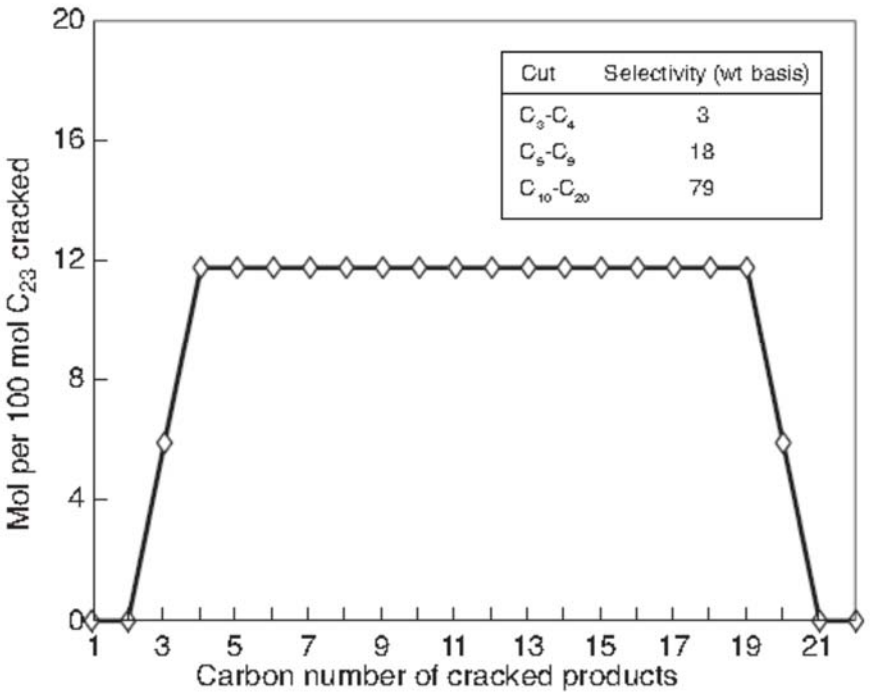

Figure 2.13: Theoretical carbon number distribution of cracked products for the ideal hydrocracking of tricosane [Bouchy et al., 2009]

It appears that, on a weight basis, typical middle distillate selectivites of up to 79% can be obtained [Bouchy et al., 2009]. Therefore, a combination of wax production via the LTFT process and ideal hydrocracking of the wax so produced could increase middle distillate yields up to 80%, such as from the Shell SMDS process. It is interesting to note that this value is twice that of the maximum possible, straight run middle distillate yield from a Fischer-Tropsch unit [Bouchy et al., 2009].

2.2.5 Hydrogenolysis and Methanolysis

A further route to 'hydrogen-mediated' carbon chain length reduction is shown in Figure 2.6 (bottom row) which is generally termed hydrogenolysis. All of the individual steps in the

hydrogenolysis mechanism occur via intermediates adsorbed on the metal co-catalyst (noble metals or base metal sulfides or oxides). The acid sites do not take part in the hydrogenolysis reaction. The term 'hydrogenolysis' refers to the unselective scission of any C-C bond of the adsorbed hydrocarbon, while methanolysis, which is a special case of hydrogenolysis, refers to the preferential cleavage of the terminal C-C bonds of the adsorbed hydrocarbon molecules. The product distribution of ideal hydrogenolysis exhibits equal selectivities for all hydrocarbons from the lowest possible fragment (C_1) as shown by the solid line in Figure 2.14.

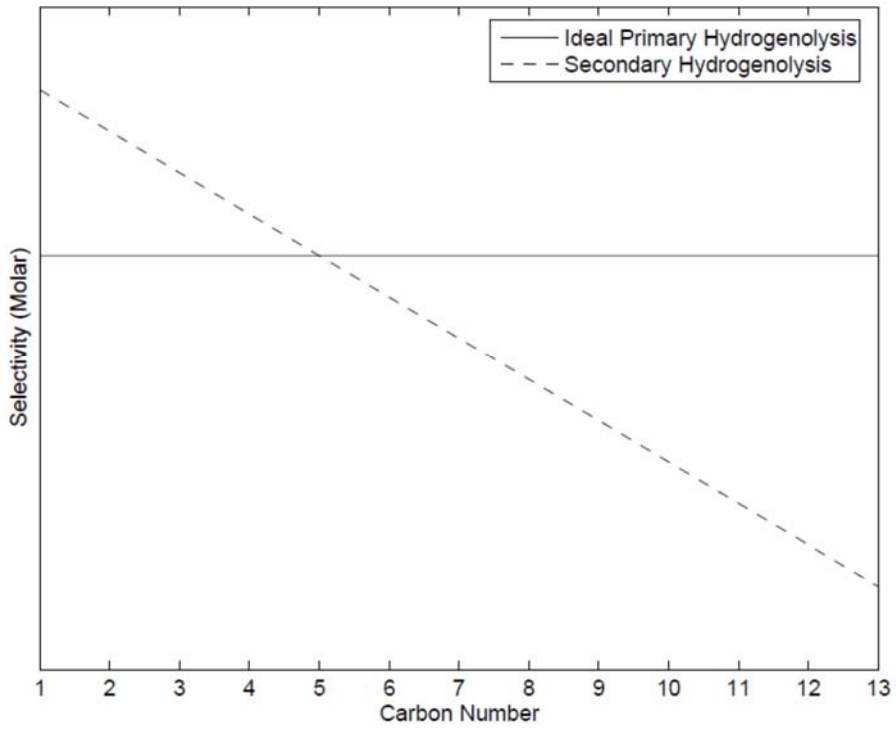

Figure 2.14: Theoretical carbon number distribution of products from hydrogenolysis of n-C_{14}. Redrawn from Böhringer et al. [2007]

Mechanistically, adsorption of a paraffinic hydrocarbon molecule on a metal surface is initiated with the cleavage of a carbon-hydrogen bond, since the reactivity of a carbon-hydrogen bond is much greater than the reactivity of a carbon-carbon bond. The resulting adsorbed alkyl radical can undergo homolytic scission of a carbon-carbon bond by β-scission, resulting in another adsorbed alkyl radical and an olefin [Kembal and Taylor, 1948; Cimino et al., 1954; Sinfelt, 1969]. The final step of the hydrogenolysis mechanism is the saturation and desorption of the adsorbed species [Sinfelt, 1973]. The products of hydrogenolysis show no branching [Sinfelt, 1973]. Since there exist only minor differences in stability of a secondary and tertiary radical. Unlike hydrogenolysis, which essentially non-bond specific, methanolysis is specific to the

terminal bonds in the molecule and may go on repeatedly, as shown in Figure 2.15. This results in the ideal methanolysis product distribution exhibiting more of the higher carbon number products and a high C_1 selectively as shown in Figure 2.16.

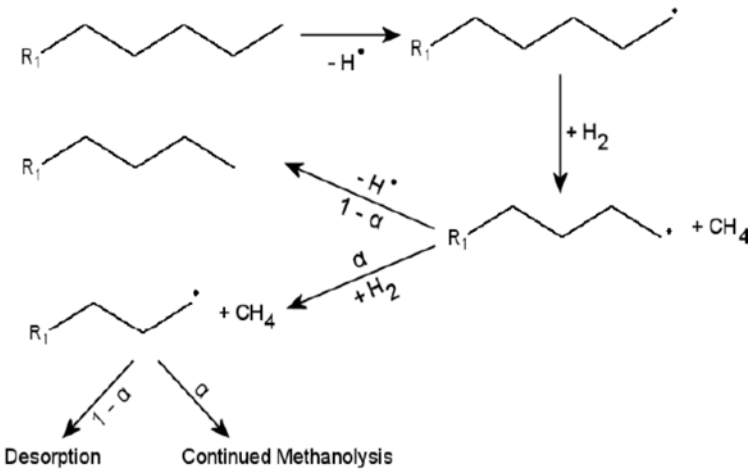

Figure 2.15: Mechanism of methanolysis. α is the probability for continuing demethylation. 1- α is correspondingly the probability of desorption of the large fragment [Böhringer et al., 2007]

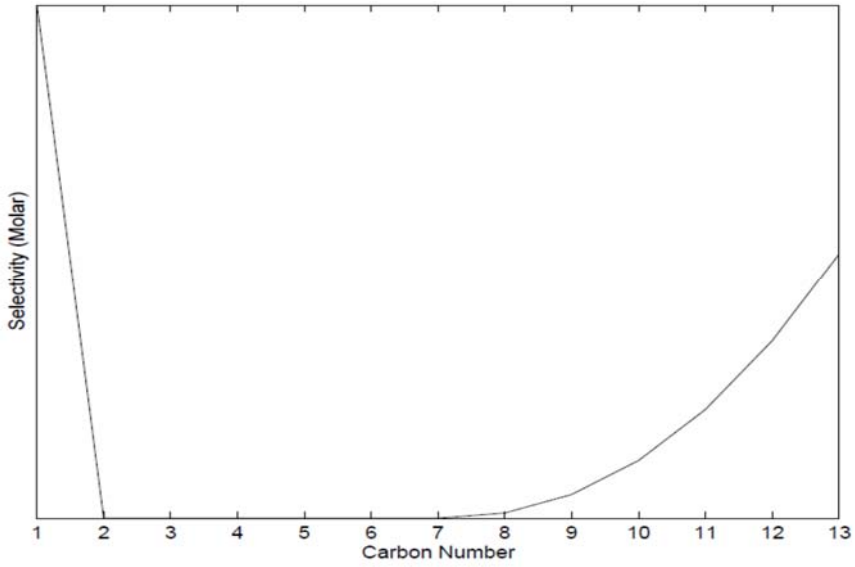

Figure 2.16: Theoretical carbon number distribution of products from methanolysis of n-C_{14} [Böhringer et al., 2007]

The type of metal co-catalyst used determines which of the two hydrogenolytic mechanisms is favoured. Metals such as Pt and Rh have been shown to favour unselective hydrogenolysis whereas Ni and Pd favour methanolysis [Sinfelt, 1973].

2.2.6 The Metal Co-catalyst

The activity of the metal co- catalyst (and its performance in effecting hydrogen spillover) is a function of the following factors [Scherzer and Gruia, 1996].

- Type of metal,
- Amount of metal and degree of dispersion of the metal,
- Metal-support interaction,
- Location of metal on support.

In a combined LTFT/hydrocracking system, compounds other than paraffinic hydrocarbons and hydrogen are present. In this environment the performance of the metallic co-catalyst is also a function of:

- The partial pressure of carbon monoxide,
- The partial pressure of water vapour.

2.2.6.1 Type of Metal

A great number of metals have been investigated as co-catalysts for hydrocracking, although almost exclusively, catalyst formulations have been developed and optimized for the crude oil environment. The choice of metal is determined by cost and technical constraints, operating conditions, properties of the feed such as the presence of sulfurous compounds and the target product [Böhringer et al., 2009]. Metals commercially used in crude oil refining are noble metals (Pt, Pd) and bimetallic combinations of base metals from groups VIA (Mo, W) and VIIIA (Co, Ni) [Bouchy et al., 2009]. For the hydrocracking of crude-derived feedstock, the base metals are usually applied as sulfides and noble metals are used only when sulfur levels are below 500ppm [Böhringer at al., 2009], implying in the latter case that the feed first has to be rather deeply desulphurised. Among noble metals, platinum has been shown to be more active than palladium. Overall hydrogenation activity decreases in the following order: noble metals > sulphided transition metals > sulphided noble metal [Scherzer and Gruia, 1996].

Conventional transition metal sulfides, oxides and combinations thereof, are not active in the low temperature FTS window of 200°C -240°C. They are therefore not suitable for a combined LTFT/hydrocracking application. Noble metal catalysts, however, have been found to be active in the FTS temperature window and suitable, since the FT wax feed-stock is virtually free of

sulfur compounds such that for the combination of low temperature FTS and hydrocracking, noble metals are the catalysts of choice.

2.2.6.2 Metal Site to Acid Site Ratio and Dispersion of the Metal

The amount and dispersion of the metal loaded i.e. the number of metal sites present, affects the activity and selectivity of the catalyst. Too little metal, in comparison to the amount of acid co-catalyst, results in secondary cracking and a consequent, loss of the target product. This is true, regardless whether the catalysts are segregated or the metal has been impregnated onto the acid carrier.

Alvarez et al. [1996] reported that ratios of exposed metal sites to exposed acid sites (metal/acid site ratios) higher than 0.3 (for a Pt/ HY catalyst) are required to ensure that the limiting reactions occur on the acid sites, as there would be sufficient hydrogenation activity to quench the reaction and inhibit secondary cracking, i.e this criterion is sufficient to ensure the occurrence of true or ideal hydrocracking.. Alvarez et al. [1996] went on to point out that at metal/acid site ratios less than 0.17, the metal sites are found to be limiting, i.e. resulting in non-ideal hydrocracking (secondary cracking).

The ratio of metal sites to acid sites was also shown by Wynne [2014], using a separated Pt/SiO_2 + H-ZSM-5 catalyst (a physical mixture of Pt on SiO_2 particles and commercial H-ZSM-5 zeolite extrudates) at LTFTS temperature conditions, to have an effect on conversion of n-C_{16}, as shown in Figure 2.17. For metal/acid site ratios less than 0.1, the metal function appears to limit the overall hydrocracking reaction. This was evident in that when metal loading was increased, the catalyst activity (total conversion) increased, until the metal/acid site ratio was above 0.1, at which point the activity of the catalyst did not increase further with increasing metal content and the metal function was no longer limiting the overall reaction. If the metal is no longer limiting, one would expect the acid function to be limiting, which is one of the defining characteristics of an ideal hydrocracking catalyst. However, Wynne [2014] observed that the molar product carbon number distribution was not ‘ideal’ but still showed strong evidence for secondary cracking, indicating that the acid function was not yet limiting. Since the acid catalyst and the metal co-catalyst were segregated, the other rate involved in the system, namely the rate of surface diffusion of the activated hydrogen (hydrogen spillover mechanism) or the rate of olefin fluid-diffusion (classical mechanism), was rate determining, and suggesting that segregating the two functions introduces diffusion limitations which effect control over the product distribution. In the classical model, this implies that the Weisz intimacy criterion (section 2.2.2.4) was not met in the experiments.

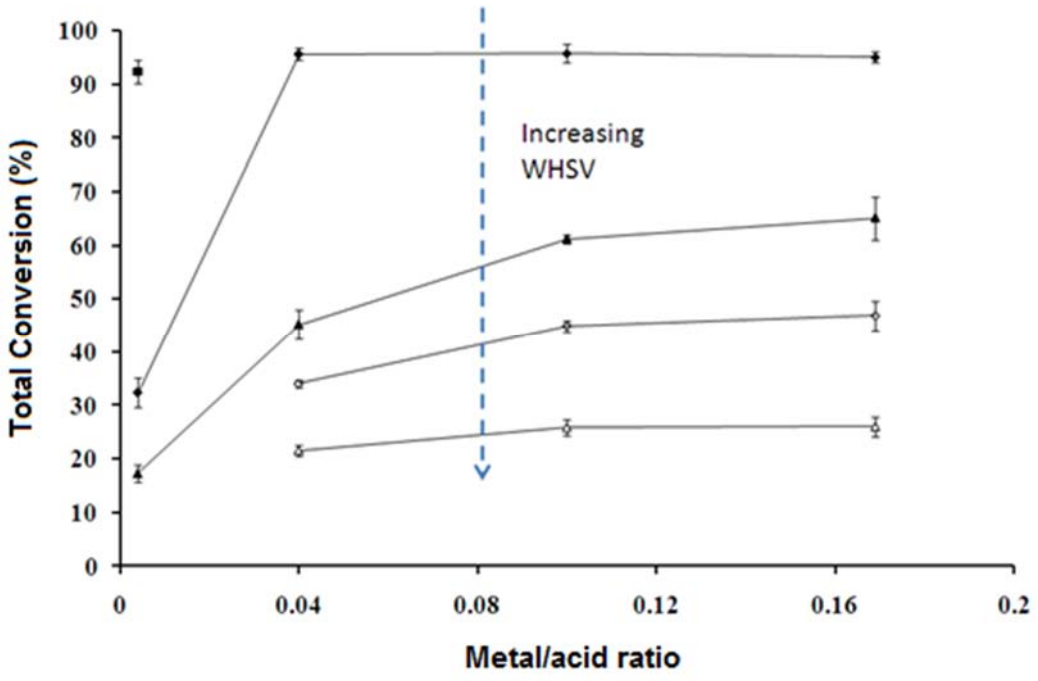

Figure 2.17: Effect of metal/acid ratio at varying WHSV on the total conversion of n-hexadecane over a physical mixture of Pt/SiO_2 +H-ZSM-5 catalysts. Temperature = 225°C, Pressure = 20 bar, $H_2/n\text{-}C_{16}$ =10 [Wynne, 2014]

Generally, patent literature suggests that the noble metal content of hydrocracking catalysts is around 1 wt % or less [Scherzer and Gruia, 1996].

2.2.6.3 Calcination and reduction

As outlined in section 2.2.6.2, key to determining the activity of the metal function of a hydrocracking catalyst is the metal dispersion. Ultimately, an increase in the metal surface area improves the activity of the metal function and this brings the catalyst closer to ideal properties and vice versa, a poorly dispersed metal will negatively affect the activity of the catalyst. The dispersion of the metal is dependent on the method of catalyst preparation. The metal loading technique and the conditions of reduction/activation are important factors influencing final metal dispersion.

The activation of a hydrocracking catalyst is a two-step process: calcination in air is followed by reduction in hydrogen [Gallezot, 1979]. Calcination ensures a well dispersed catalyst and also removes physisorbed water from the support. In cases where metal-organic complexes were used as the precursor, calcination decomposes and burns off the organic species. The severity

of the calcination, reduction process, i.e. the final reduction temperature and duration, controls the dispersion of the metal.

The reduction of platinum group metals has been the subject of numerous publications over the years [Scherzer and Gruia, 1996], although mostly focused on Pt/Y zeolite systems and less on Pd or other zeolite systems. Bergerat et al. [1981] studied the activation, reduction and reoxidation of Pd in zeolite-Y. They showed that in oxygen, calcination temperature affects the location of cations. At 97 – 147°C the $[PdNH_3O]^{2+}$ ions are located in the supercages, whereas at higher temperatures the ions move to smaller cages (sodalite units) where they displace the sodium ions. An explanation for this migration is the tendency of the transition metals to move to locations with high negative charge density, and the sodalite units, since they are smaller, have a higher negative charge density which offers greater charge stabilization for the metal ions. As a further consequence, the location of the metal ions affects the temperature required to reduce the metal, and ions in the sodalite units will reduce only at higher temperatures than those in the super cages [Park et al., 1986].

Okumura et al. [2004] studied the spontaneous metal dispersion and clustering process by means of the extended X-ray absorption fine structure (EXAFS) method. For the 0.4 wt% Pd/H-ZSM-5 system, in oxygen they observed the spontaneous dispersion of bulky metallic Pd into highly dispersed PdO such that agglomerated metal Pd migrates into the zeolite forming stable PdO. Stable Pd clusters are generated upon reduction in a stream of hydrogen, although the coordination number of these stable clusters depends upon the temperature of reduction as shown in Figure 2.18. At temperatures above 347°C Pd_6 clusters are formed.

It is known that in hydrocracking, the hydrogenation/dehydrogenation activity decreases with time-on-stream due in part to noble metal agglomeration or sintering, and that to restore hydrogenation activity, the metal must be oxidatively re-dispersed on the catalyst [Scherzer and Gruia, 1996].

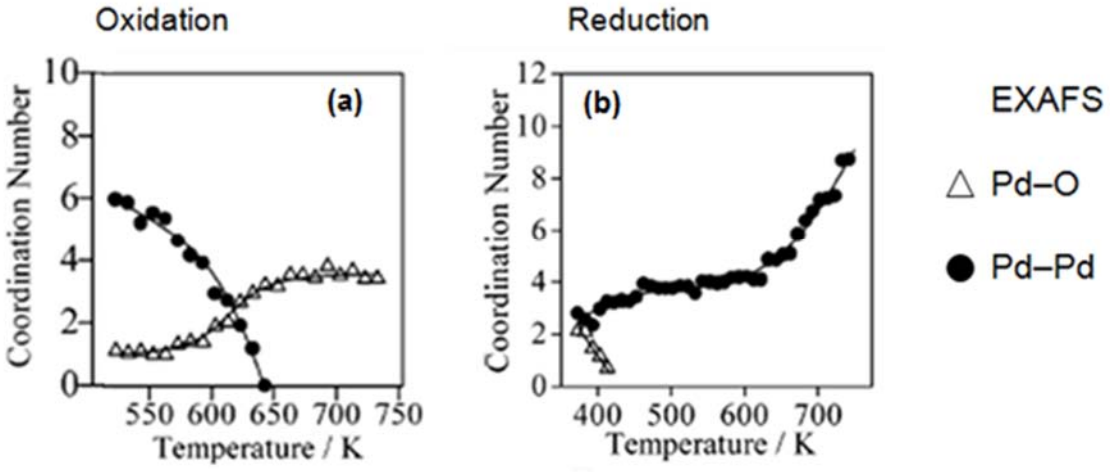

Figure 2.18: Dependence of coordination number on reduction temperature measured (a) in flowing O_2 (b) in flowing H_2 [Okumura et al., 2004]

2.2.6.4 Metal Support Interactions

When the metal is reduced to its zero-valent state, it has been shown to interact with the acid support, resulting in an electronic deficiency of the reduced noble metal. In cases where platinum is dispersed in Y zeolite, the resulting catalyst exhibits enhanced resistance to sulphur poisoning, such resistance being attributed to an electron deficiency in the small platinum particles in the zeolite caused by a strong metal-support interaction [Scherzer and Gruia, 1996].

2.2.6.5 Location of Metal on Support

Noble metals are usually added to the acid support by impregnation or ion exchange using an aqueous solution of a suitable compound, with final location of the metals being dependent upon the method used for catalyst preparation, as shown in Figure 2.19.

In the case of bifunctional hydrocracking catalysts, metal and acid sites are preferred in close proximity to minimize the diffusional distance of intermediate species allowing for rapid inter-diffusion in accordance with the Weisz intimacy rule. Thus, the metal should not be on the external surface of the acid support only such as in Figure 2.19 (a), or accumulated in certain spots, as in Figures 2.19 (b) and (d), but evenly distributed in the pores as in Figure 2.19 (c). A common technique for ensuring that the metal is well distributed, i.e. as close as possible to the acid sites, is incipient wetness impregnation, a method which also allows for the introduction of more metal into the zeolite than via the ion exchange method [Scherzer and Gruia, 1996].

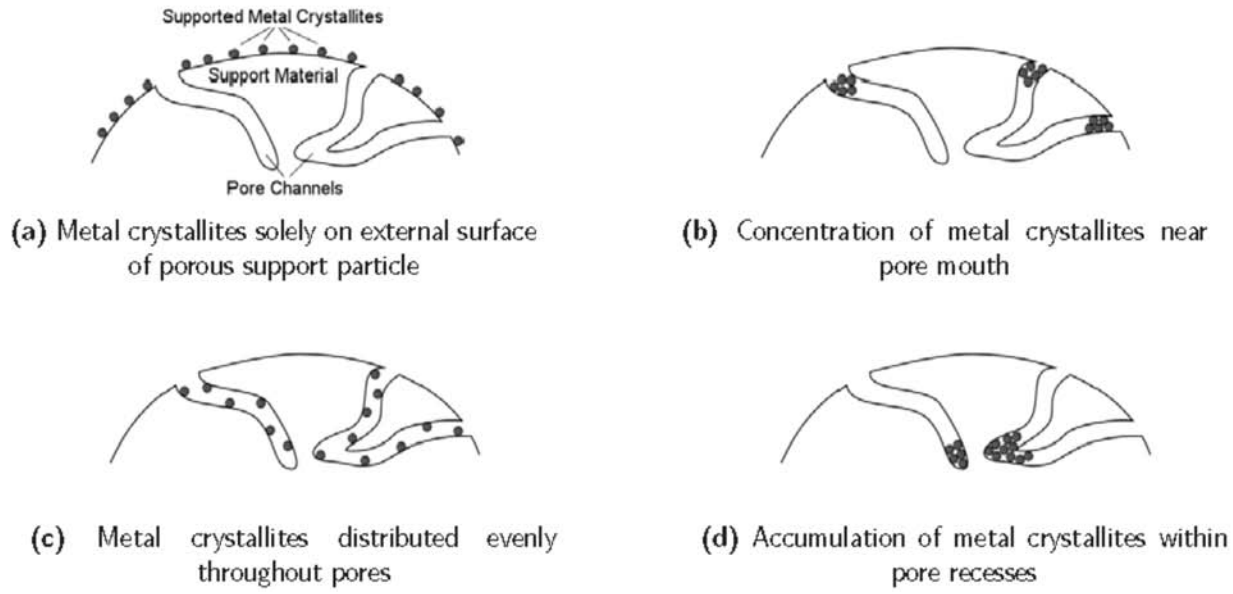

Figure 2.19: Possible metal crystallite distribution on porous support material [Kukard, 2008]

As a further example of the complexity of metal distribution, Scherzer and Gruia. [1996] report that for a zeolite with supercages, such as zeolite Y, there are five possible outcomes, as follows:

1. Metal atoms occupy the sites previously occupied by the exchange cations
2. Atoms remain in the same cage but form metal atom clusters
3. The atoms migrate from smaller cages to larger cages
4. The atoms agglomerate to form clusters in the larger cages
5. Atoms migrate outside of the zeolite crystals and sinter and form metal particles on the external surface of the zeolite

Generally, as the reaction conditions become more severe, the tendency of metal atoms to migrate and agglomerate increases, reducing both dispersion and the metal/acid ratio.

2.2.6.6 The Poisoning Effect of CO and H_2O on the Metal Co-catalyst

The integration of the FT wax synthesis and the hydrocracking process means that the hydrocracking catalyst will be exposed to CO which is a constituent of the feed of the FT process. It was found by Weiss et al. [1984], and interpreted in terms of the classical mechanism, that CO decreases the hydrogenation activity of noble metals. Al–Ammar et al.

[1978] and Arnold et al. [1997] came to the conclusion that CO competes with H_2 for adsorption on the metal surface. In the hydrogen spillover hydrocracking model, CO adsorption limits the supply of activated hydrogen to the acid sites, resulting in both reduced activation/adsorption of feed paraffins as carbenium ions on the acid sites and saturation of the cracking fragments prior to desorption from the acid sites.

Mena Subiranas and Schaub [2009] investigated the effect of CO on the hydrocracking catalyst (Pt/ZSM-5, Pt/Beta) under low temperature FT conditions using 1-octene as a model compound. They observed that, in the absence of CO, conversion was close to 100% and nearly all the 1-octene was hydrogenated to n-octane. Upon addition of CO, n-C_8 conversion was also close to 100%, however the yield of iso-C_8 was observed to be higher than in the case without CO (Figure 2.20). CO appears to suppress isomer cracking. It is clear from Figure 2.20 that an increase in temperature decreased the effect of CO on the cracking reactions.

Binneman [2012] studied the hydrocracking performance of a physically mixed Pd/SiO_2 + H-ZSM-5 catalyst with and without CO co-feeding, using n-hexadecane as a model compound and for which selected findings are shown in Table 2.3, Table 2.4 and Figure 2.21. A decrease in conversion was observed upon CO introduction, which was accompanied by an increase in the amount of unsaturated product. From their results it is apparent that CO seems to inhibit the dehydrogenation and hydrogenation reactions on the noble metal.

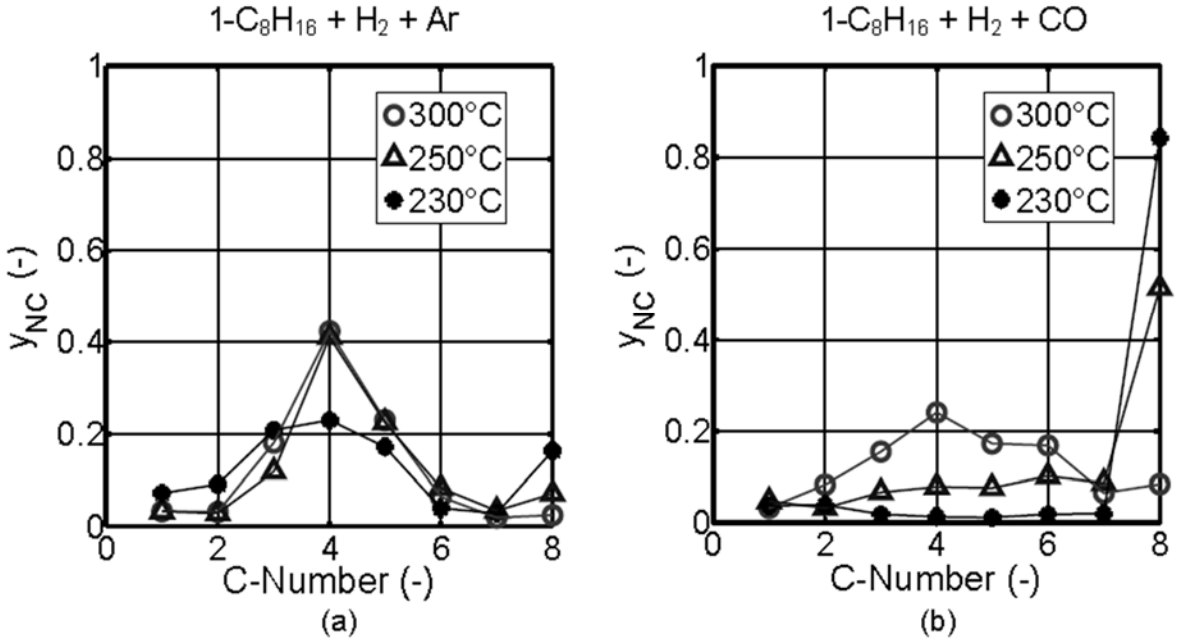

Figure 2.20: Effect of CO and temperature on gas phase hydrocracking of n-C_8H_{16} over Pt/ZSM-5. Adapted from Mena Subiranas and Schaub [2007]

Table 2.3: Conversion of n-hexadecane over 0.1 wt% Pd/SiO_2 + H-MFI. Reaction temperature = 225°C, pressure = 20 bar. Adapted from Binneman [2012]

Feed	Conversion, mean (μ) (%)	Standard deviation (σ) (%)
C_{16}: 0.03 ml/min, $H_2/N_2 = 2$	46.0	2.2
C_{16}: 0.03 ml/min, $H_2/CO = 2$	21.5	1.8
C_{16}: 0.03 ml/min, $H_2/CO = 2$, H_2O: 0,02 ml/min	9.1	1.3

Water, a product of the FTS, when administered at a partial pressure typical of FTS conditions, reduced the activity of the catalyst still further to less than 10%. Again it is apparent that co-feeding water results in an increase in the amount of unsaturated cracked product, such that H_2O also appears to limit the activity of the metal (in this case, Pd), to hydrogenate the cracked olefin fragments.

Table 2.4: The ratio of $C_i^=/C_i$ hydrocarbons in cracked product of n-C_{16} hydrocracking. Adapted from Binneman [2012]

Ratio	Standard	CO co-feeding	CO+H_2O co-feeding
$C_3^=/ C_3$	4.6	13.2	30.8
n-$C_4^=$/ n-C_4	6.0	18.8	41.8
n-$C_5^=$/ n-C_5	3.9	12.8	28.4
n-$C_6^=$/ n-C_6	5.0	14.3	28.3
n-$C_7^=$/ n-C_7	6.3	10.6	15.4
Iso-$C_4^=$/ iso-C_4	15.2	33.1	45.8
Iso-$C_5^=$/ iso-C_5	21.9	57.3	73.3
Iso-$C_6^=$/ iso-C_6	13.7	39.3	53.7
Iso-$C_7^=$/ iso-C_7	11.8	42.0	55.4
Iso-$C_8^=$/ iso-C_8	7.7	16.0	18.5

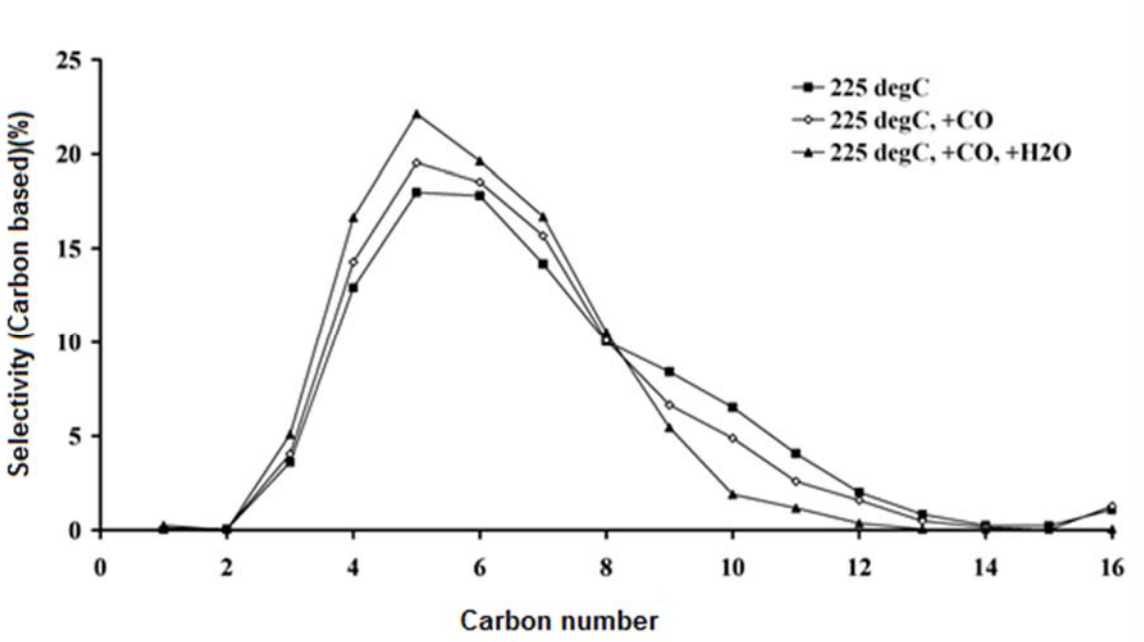

Figure 2.21: Effect of CO and H_2O on Pd/SiO_2 + ZSM-5 catalyst. Adapted from Binneman [2012]

2.2.7 The Acid Co-Catalyst

In the limited published findings concerning middle distillates production via LTFT wax hydrocracking, various acidic solids have been used to formulate hydrocracking catalysts, as compiled in Table 2.5.

Table 2.5: Acid catalysts used for hydroconversion of FT wax [Bouchy et al., 2009]

Acid	Reference
Amorphous silica-alumina	Böhringer et al. (2007), Calemma et al. (2000)
MoO_3 modified amorphous silica-alumina	Leckel et al. (2006)
Silicated alumina	De Haan et al. (2007)
Anion modified (tungstated, sulfated) zirconia	Zhang et al. (2001)
Tungstated zirconia & sulfated zirconia mixtures	Zhou et al. (2001)
Tungstated zirconia and zeolites (Y, beta, mordenite) mixtures	Zhou et al. (2001)
Microcrystalline USY zeolite	Seki et al. (2004)
Microcrystalline USY zeolite & silica-alumina mixtures	Aoki et al. (2004)
Polyoxocation-pillared montmorillonite	Liu et al. (2007)
Chlorinated alumina	Collins et al. (2006)

2.2.7.1 Zeoolites as the Acid Component

Crystalline aluminosilicates, also known as acid zeolites, have been in use as hydrocracking co-catalysts since the mid-1960s [Maxwell, 1991]. They have a well-defined and consistent porous structure and a well-defined and consistent intra-pore surface acidity. It is agreed that the surface acidity of these zeolites arises from bridging hydroxyl groups which link a silicon atom to an aluminium atom in the framework thus forming Brønsted acidity. Theoretical modelling suggests that there is in effect a bifunctional active site in the zeolite which comprises of a Brønsted acid and an adjacent Lewis base (Figure 2.20). The oxygen atom of the hydroxyl group interacts with the aluminium atom, weakening the hydrogen-oxygen bond, increasing the Brønsted acidity (Figure 2.20 a) and also weakening the aluminium-oxygen bonds (i.e increasing the basicity of the aluminium oxo ligands), thus creating adjacent Lewis sites (Figure 2.21 b).

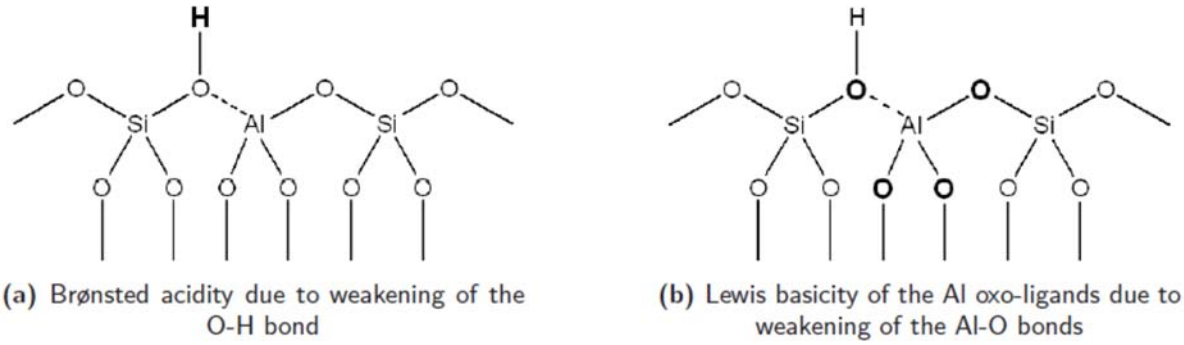

(a) Brønsted acidity due to weakening of the O-H bond

(b) Lewis basicity of the Al oxo-ligands due to weakening of the Al-O bonds

Figure 2.22: Active sites in Aluminosilicate Zeolites [Marterns and Jacobs, 2001]

The acidic properties of an H-zeolite give it the ability to act as the acid co-catalyst. The acid site catalytic turn over frequency is dependent on many parameters such as the crystallographic siting, zeolite structure type and the concentration and distribution of sites in the zeolite framework [Martens and Jacobs, 2001]

Having established what gives rise to the acidic properties of a zeolite, the overall acidity of a zeolite is related to the number (density) and strength of the acid sites on the surface of the zeolite. Rastelli et al. [1982] studied the activity of various acid zeolites with different Al content in n-butane hydrocracking. They reported that zeolites with a low SiO_2/Al_2O_3 ratio (i.e. high Al/(Al+Si)) have a high density of weak acid sites, resulting in a low overall acidity of the zeolite. The density of acid sites becomes low as SiO_2/Al_2O_3 increases. Concomitantly, the strength of the individual acid sites increases and so does the overall acidity of the zeolite and its observed activity. At very high SiO_2/Al_2O_3 ratios the individual acid sites are very strong, but because of their very low density, the overall acidity of the zeolite decreases and so does the observed activity.

Park and Ihm [2000] confirmed these findings when they studied the activity of zeolites with different SiO_2/Al_2O_3 ratios (as part of a bifunctional catalyst) in hydroisomerization and hydrocracking of n-hexadecane, and where ammonia temperature programmed desorption was used to characterize the acid strength of the zeolite co-catalyst. It was observed that zeolites with strong acid sites showed a greater overall conversion of n-hexadecane than those with weaker acid sites. However, in hydrocracking applications, primary cracking products tend to undergo secondary cracking at greater rates as the overall strength of the acid increases, and therefore, the ability of the metal function to supply the acid sites adequately with activated hydrogen, becomes very important.

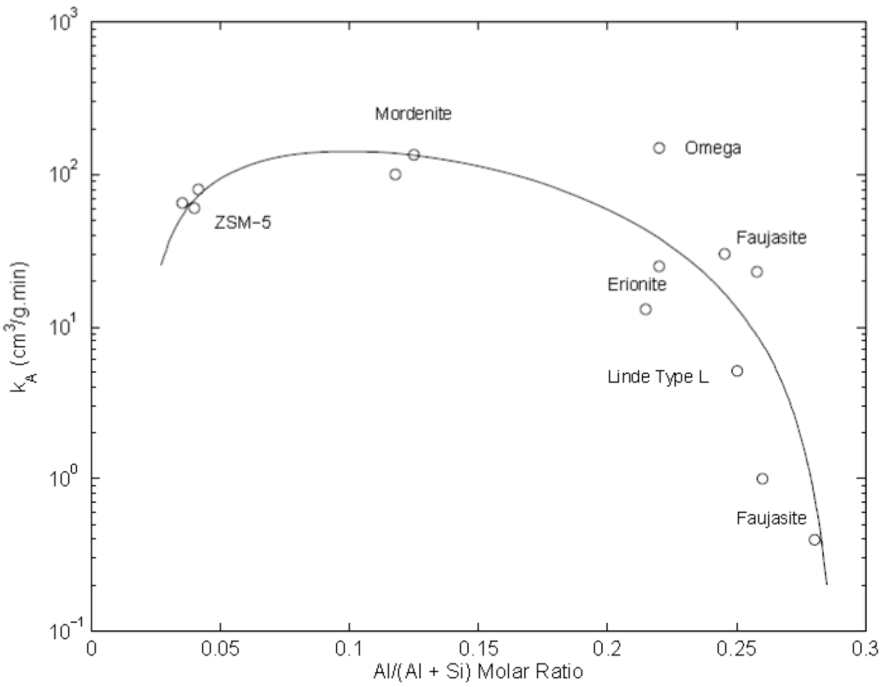

Figure 2.23: Zeolite acivity as a function of Si and Al content [Rastelli et al., 1982], redrawn from van Bekkum et al. [2001]

Secondary cracking can also become prevalent if the residence time of the primary cracking products in the zeolite pores or the shaped catalyst particle increases. This can happen if there exists a diffusional limitation in the catalyst system resulting in prolonged intraparticle residence time and re-adsorption of the primary cracking products. Therefore, the hydrocracking process must operate in the absence of diffusion limitations to minimize secondary cracking [Benazzi et al., 2003; Toulhoat et al., 2004].

2.2.7.2 Zeolite shape selectivity

Zeolites have well defined crystal structures and pore networks, the dimensions of which differ between zeolite types [van Bekkum et al., 2001]. Shape selectivity results from the confinement of molecules in the zeolite [Bouchey et al., 2009]. Shape selectivity was first described, by workers at the Mobil company in 1960 [Weisz et al., 1960], as phenomenon that typically occurs with medium pore zeolites and with molecules such as mono-aromatics and linear or slightly branched aliphatic hydrocarbons. Csicsery [1984] classified shape selectivity into three categorie; via reactant, product and transition state shape selectivity.

- Reactant shape selectivity occurs when the reactant molecules are too large to enter the zeolite pores (Figure 2.24), limiting the reaction of these molecules to only the active

sites on the external surface of the zeolites. Reactant shape selectivity is thus transport controlled, depending on the relative diffusion coefficients of the various reacting species. With respect to this study, reactant shape selective effects are not anticipated. The single n-C_{16} reactants can easily diffuse into the pores of the H-ZSM-5 acid co-catalyst.

- Product shape selectivity occurs when products that are too bulky to leave through the narrow channels, are formed in the zeolite (Figure 2.25). These products would either convert to less bulky molecules that are able to diffuse out or eventually deactivate the catalyst by filling and blocking the pores. Product shape selectivity is also transport controlled, depending on the relative diffusion coefficients of the products formed. With respect to this study, product shape selective effects are expected to limit the degree of product branching.
- Transition state shape selectivity occurs when certain conversion reactions are prevented due to the corresponding transition states requiring more space than is available within the zeolite cavities (Figure 2.26), and thus selectivity favouring reactions proceeding via smaller transition states. Transition state shape selectivity is governed by some form of spatial control, depending on the relative spatial demands of transition states. With respect to this study, transition shape selectivty would be expected to limit certain reactions, since rapid type A reactions were found to be limited over zeolite H-ZSM-5, while slower type B cracking is not (Figure 2.8). Consequently, the primary cracking product is expected to be less branched in the case of this study versus with large pore zeolites or amorphous silica-alumina supports.

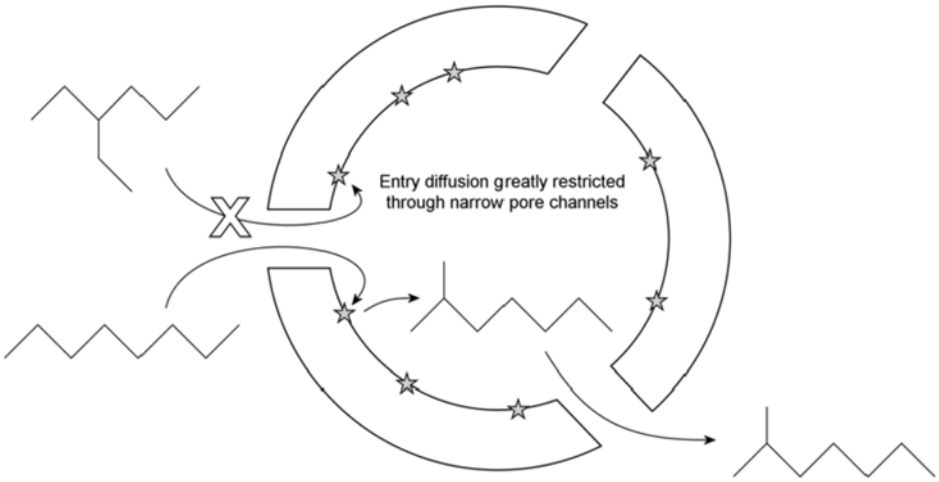

Figure 2.24: Reactant shape selectivity [Kukard, 2008]

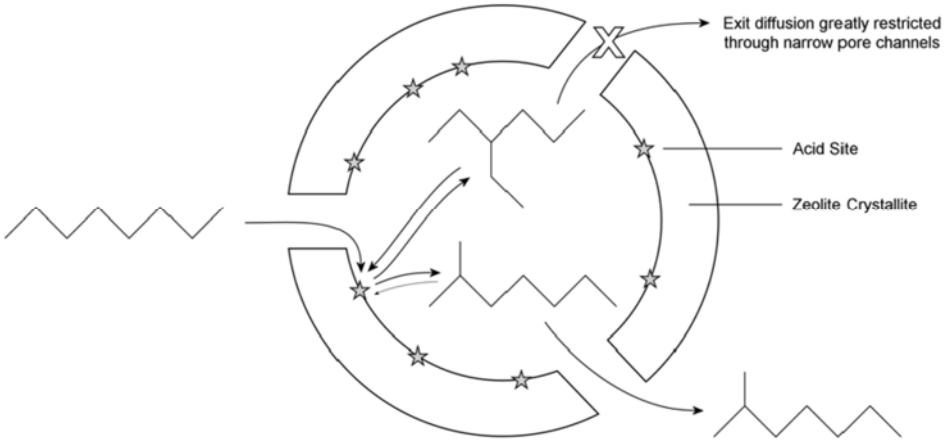

Figure 2.25: Product shape selectivity [Kukard, 2008]

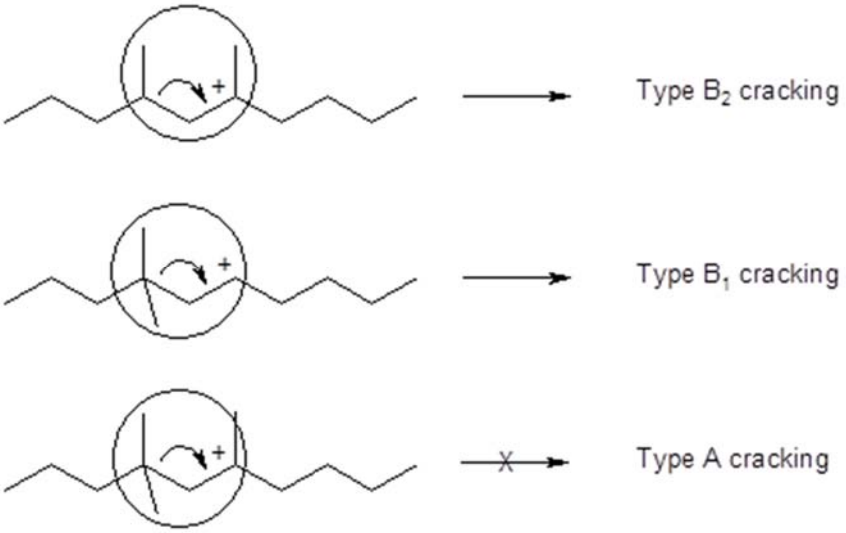

Figure 2.26: Spatial restrictions on type A cracking in medium pore environment

There exists a peculiar form of shape selectivity in medium pore zeolites called “pore mouth” and “key lock” catalysis that can have relevance in paraffin cracking. This may occur when the paraffin molecule penetrates the zeolite pore only with its end, in particular so, when deeper penetration of the molecule is hindered by a side chain. Consequently, preferential cracking of the paraffin molecule occurs near the end of the hydrocarbon chain, such that reduced selectivity towards middle distillates may arise [Lawson et al., 2006]. Venuto [1977] first introduced the term “pore mouth” to indicate that the conversion takes place at the zeolite pore opening and not deeper inside the channel system. The definition of the pore mouth for long chain paraffin is the first nanometer inside the pore such that pore mouths present a particular

geometry which is different from that deeper inside the pores [Claude, 1999]. Figure 2.27 illustrates molecules positioned both in the pore mouth and inside the zeolite pore. The Figure indicates also, that pore mouths, as in ZSM-5, are often wider, i.e. they can accommodate larger molecules than the pores themselves.

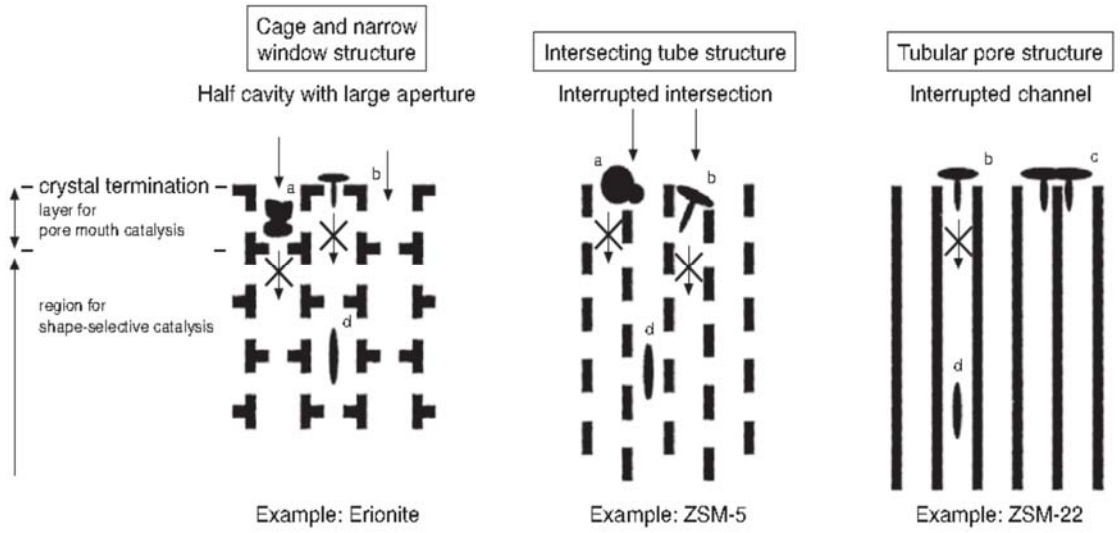

Figure 2.27: Adsorption of branched molecules at the pore mouths for different zeolites: a) molecules have access to open cavities or interrupted pore intersections, b) molecules are branched in pore openings, c) key-lock catalysis d) molecules have access to and are converted in intracrystalline space [Martens et al., 2001]

Another shape selective effect and a major advantage that comes with reactions over shape selective zeolites is the ability of the zeolite to inhibit coke formation in the zeolite pores. Rollman and Walsh (1979) noted a correlation between the reactant shape selectivity of different zeolites and the formation of coke. Medium pore zeolites, which exhibited all the three forms of shape selectivity, showed less coking than those with wider pores. The phenomenon was attributed to the increased spatial constraints that the medium pore zeolites impose on the formation of bulky coke precursors. Reducing overall coke formation in the catalyst increases the catalysts life-time.

3 Objectives

Hydrocracking LTFT wax will remain a crucial industrial reaction for middle distillate, namely diesel, production. The objective of this study is to investigate the possibility of integrating LTFT and the subsequent wax hydrocracking stages into a single process unit, and to develop an ideal hydrocracking catalyst to maximize middle distillate yields from such an integration of the two processes. The challenge such integration poses is twofold:

- Low temperatures at which the hydrocracking catalyst must be active
- Resistance of the hydrocracking catalyst to CO

Based on preceding literature, noble metals are known to be active in the LTFT temperature window. The activity of the noble metals Rh, Ru and Pd as co catalysts to H-MFI-90 for hydrocracking is evaluated. The test conditions used are LTFT conditions (20 bar, 225^{0}C, H_2/CO =2). The key questions this study purposes to answer are:

- Are the noble metals Rh, Ru and Pd as co-catalysts to H-MFI-90 active for hydrocracking at LTFT conditions?
- Is H-MFI-90, without the metal, active at LTFT conditions?
- What effect does the proximity of the metal and acid sites have on the activity and selectivity, i.e. ideal performance of the hydrocracking catalyst?
- What effect does metal loading have on the ideal performance of a hydrocracking catalyst
- What effect does CO have on the activity and selectivity of the hydrocracking catalyst?
- What effect does catalyst reduction temperature have on the activity and selectivity of the hydrocracking catalyst?

To answer these key questions, the reactions will be evaluated by observing the following:

- Selectivity of the reaction towards carbon number distribution;
- Conversion of the feed to both isomerization and cracking products;
- The n-paraffin and iso-paraffin content of the product.

4 Experimental

A flow sheet of the test unit used for the experiments is shown in Figure 4.1. The unit consisted of a trickle bed reactor with a subsequent vaporiser to ensure that the reactor products are in the vapour phase before being analysed by on-line gas chromatography. A description of each component of the test unit and the procedures applied are provided in the following sections.

Four of these units were operated in parallel with two of the reactors sharing a joint heating block furnace. All other parameters could be set and varied individually.

4.1 Nitrogen, Carbon Monoxide and Hydrogen Supply

Hydrogen, nitrogen and carbon monoxide were available from the main house lines at 100 bar supply pressure. The gases were passed through Tescom pressure regulators to step down pressure to 50 bar. Brooks thermal mass flow controllers were employed to meter the gases before they passed through one-way valves that protected the mass flow controllers against accidental back flow. The gases were combined and passed through a guard catch pot and supplied to the reactor. The guard catch pot serves as an additional means to prevent any back flow of liquid from the reactor to the mass flow controllers.

4.2 Liquid n-Hexadecane supply

Hexadecane was supplied to the reactor from a closed two litre metal feed vessel. Each metal feed vessel was placed on a separate A & D GX-4000 laboratory balance. A single piston Lab Alliance Series 1+ pump was used to pump the n-hexadecane to the reactor. The pump was equipped with a pulse dampener, to ensure smooth flow of liquid.

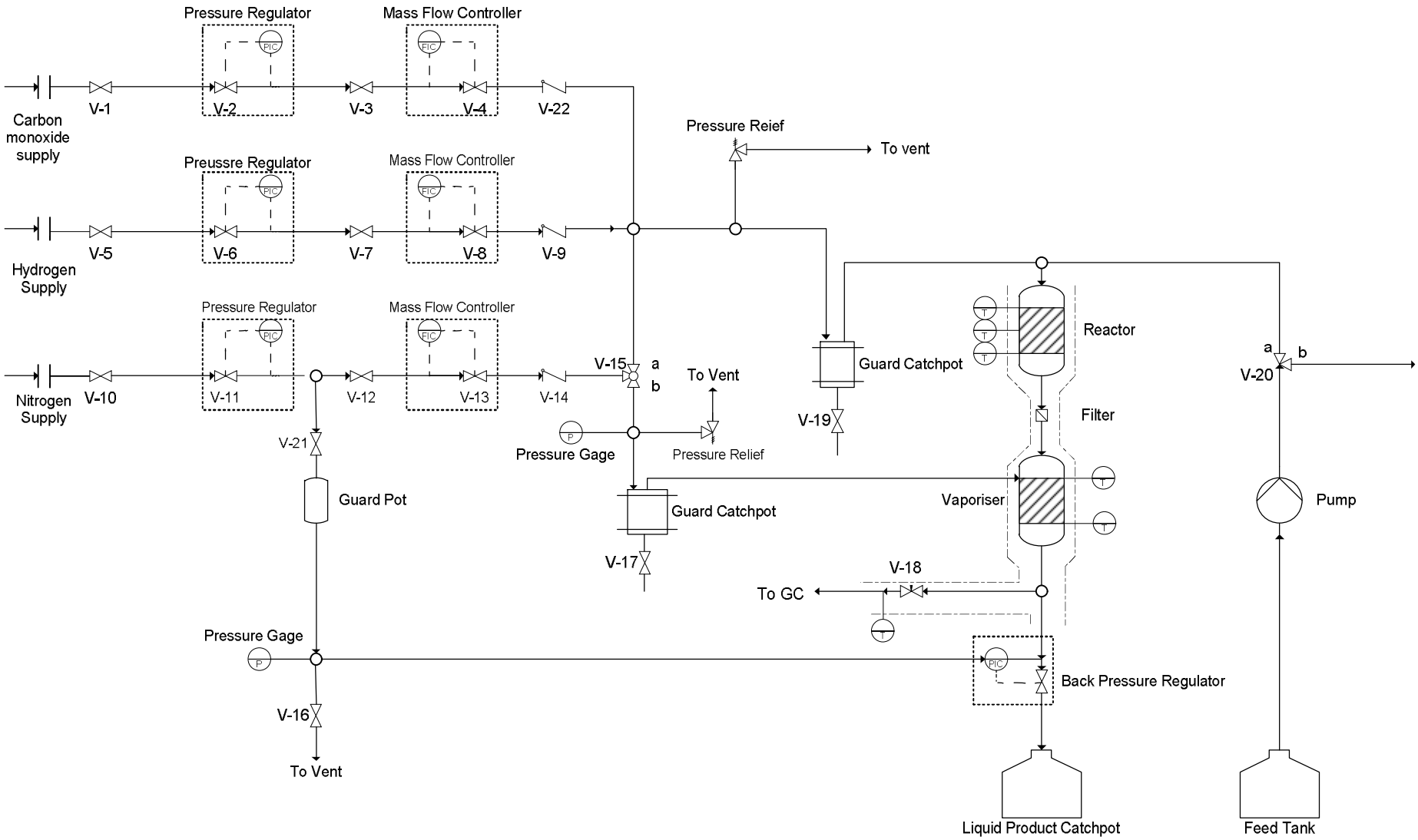

Figure 4.1: Flow sheet of the test unit

4.3 The Reactor

A photograph of the trickle phase reactor used for the experiments is shown in Figure 4.2. It comprised a 1/2" stainless steel tube with a central 1/8" thermowell and incorporates a removable head for ease of catalyst loading and removal. The reactor head includes two inlet ports, one for the gaseous feed and one for the liquid n-hexadecane, also as shown in Figure 4.3.

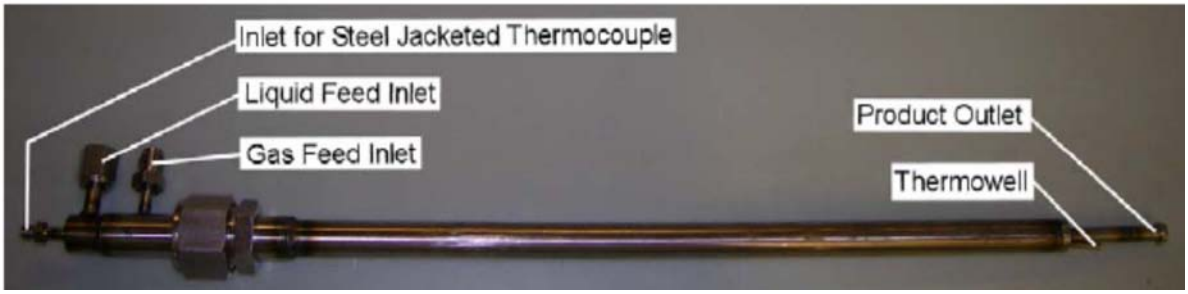

Figure 4.2: Reactor vessel [Kukard, 2008]

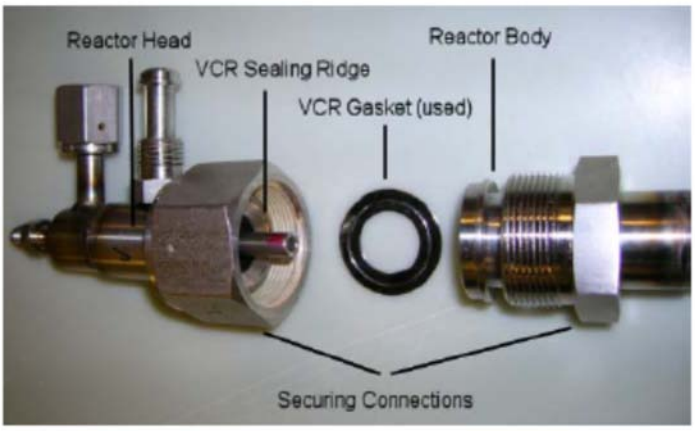

Figure 4.3: Reactor head [Kukard, 2008]

The reactor head (Figure 4.3) was connected to the reactor tube via a 1" Swagelok VCR fitting. The head is designed in such a manner that the outlets of the central tube for the liquid feed extended by about 1 cm into the reactor body and below the surface of the inert SiC reactor packing to ensure the liquid feed flows smoothly into the void spaces between the particles of the packing. The gases enter concentrically around the n-hexadecane feed tube.

A brass housing serves as a heating block such that the reactors could be placed inside during operation and removed after operation. The housing was heated by 4 individually controlled

temperature bands and well insulated. This enabled adjustment of an isothermal zone of between 44 cm to 26 cm from the top of the reactor body, to accommodate the catalyst bed. Each heating block carried two reactor tubes. The reactor was operated at 225°C in the isothermal catalyst bed zone. The reactor head was not heated. When the reactor volume was packed for operation it comprised of three zones:

- The bottom zone consisting of inert silicon carbide packing (400-600 µm) which supported the catalyst bed. Some glass wool at the bottom prevented the silicon carbide particles from falling out.
- The middle zone, which was composed of the catalyst bed.
- The upper zone consisting of inert silicon carbide packing, all the way to the upper edge of the reactor tube, so that the n-hexadecane feed entered the bed 5-10 mm below the packing upper surface. This silicon carbide packing served to preheat the feed and also to distribute the liquid and gas flow across the bed diameter.

After leaving the reactor effluent was allowed to cool to 175°C.

4.4 Product Vaporiser and Reactor Effluent Dilution

The vaporiser was designed to provide a slow temperature increase and a large heated surface area on which the liquid fraction of the reactor effluent was ‘smoothly’ vaporised. Nitrogen was also fed into the vaporizer so as to lower the partial hydrocarbon pressure reducing the temperature required to completely vaporise the reactor effluent. The vaporiser body was made of stainless steel and its dimensions are shown in Table 4.1.

Table 4.1: Vaporiser Dimensions

Length	500 mm
Internal diameter	10.2 mm
Wall thickness	1.25 mm

The vaporizer was housed in a metal conduit with a diameter of 25 mm and which was wrapped with a heating wire, wound such that the temperature along the vaporizer gradually increased from the reactor effluent temperature (175°C) to 250°C. The vaporizer was insulated and the entire temperature profile along the reactor and vaporizer is shown in Figure 4.4. The vaporiser was packed with silicon carbide, the purpose of which was threefold: firstly it served as an effective heat transfer medium for heat from the vaporizer wall; secondly, it provided void space

for the diluent gas and product vapours to flow through, and, thirdly, it provided a large surface on which the liquid reactor effluent could spread and smoothly evaporate. As the liquid fraction of the reactor effluent progressed down the vaporizer, over the increasingly hot surfaces, its vapour pressure increases until all the liquid is vaporized. Dilution gas flow rate and vaporizer bottom temperature were adjusted so that all feed n-hexadecane would be vaporized in the extreme case of no hexadecane conversion.

4.5 Product Analysis and Data Workup

The vaporized stream was analysed by gas chromatography. A side stream of the diluted vaporous effluent from the vaporiser was passed through a heated needle valve which lowered the pressure to atmospheric pressure for analysis (Figure 4.4). From the needle valve, the still gaseous/vapourous mixture passed to a heated (190°C) 6-port multi-switching valve which allowed for automatic sampling of one reactor (of four, connected) at a time while the effluents from the other reactors were directed to a common vent line.

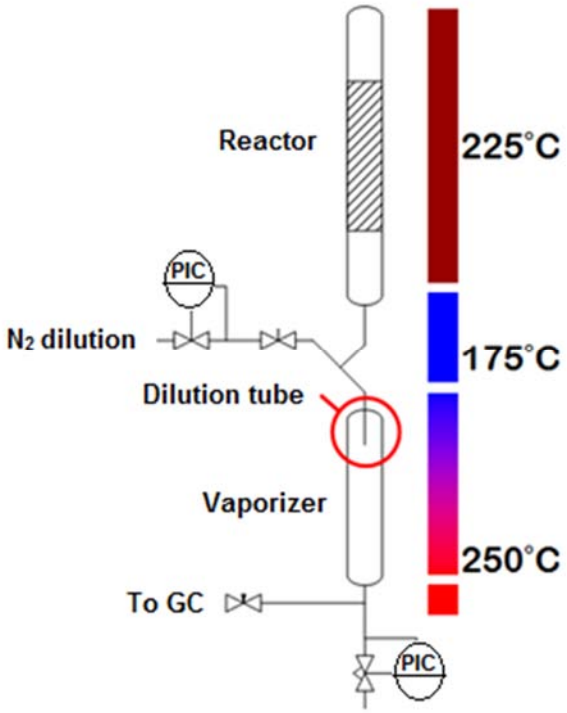

Figure 4.4: Temperature profile and dilution point

A Varian 3900 gas chromatograph was equipped with a non- polar GC column and a flame ionisation detector (FID), was employed for chromatographic analysis. Hydrogen was used as a

carrier gas and also a fuel for the FID. Pressurised synthetic air was used for operating the automatic selection valve and as the oxidant source for the FID flame.

For hydrocarbons, the FID current proportional to the number of carbon atoms that are being eluted at a certain time. Moreover, the detector sensitivity is almost independent of the molecular chain length, differing slightly for chain lengths between 1 and 4, such that for this study the carbon response factors were taken as unity for all molecular chain lengths. Consequently, all results presented in this study are on a carbon basis.

Total conversion, X was calculated as follows;

$$X=\left[1-\frac{A_{n-C_{16}}}{\sum_{i=C_1}^{n-C_{16}} A_{C_i}}\right]$$

Equation I

where $A_{n\text{-}C16}$ = Area of the peak of unconverted feed (n-hexadecane). Thus, the total n-hexadecane conversion value, X, includes conversion via cracking and via C_{16} isomerization.

The selectivity of each product species (i) detected by the FID was calculated, on a carbon basis, as follows:

$$S_i = \frac{A_i}{\sum_{i=C_1}^{iso-C_{16}} A_{C_i}}$$

Equation II

where A_i = peak area corresponding to species C_i

To determine the relative number of moles of a compound C_i, the peak area A_i is divided by the number of carbons in the compound (i). For example if the peak area of C_4 and C_{12} were to have the same value of 24, the relative number of moles of C_4 and C_{12} would be 6 and 2, respectively, i.e. the molar ratio C_4:C_{12} would be 3:1 for the same C_4 and C_{12} compound peak areas.

4.6 Catalyst Preparation

The acid catalyst of used was ZSM-5. The metals used were Pd, Rh and Ru. As mentioned earlier, the bifunctional catalyst was tested when the two functions were segregated and when they were in close proximity (metal impregnated on acid carrier).

4.6.1 Segregated Catalysts

The properties of the segregated catalyst are shown on the Tables 4.2 and 4.3 below. A range of metal to acid site ratios was evaluated. The supported metal catalyst was pelletized and physically mixed with the pelletized zeolite prior to loading into the reactor.s

Table 4.2: Metal Co-catalyst Properties

Metal	Wt% Metal loading	% dispersion (CO Chemisorption)	Reduction in hydrogen (°C)
Pd/SiO_2	5%	15.1	400
Rh/Al_2O_3	3%	98.8	400
Ru/Al_2O_3	3%	3.0	400

It should be noted that the metal dispersion on metal co-catalyst varied greatly - reasons for which are unclear.

Table 4.3: Zeolite Properties

Acid Co-catalyst	Code	SiO_2/Al_2O_3 (molar)	Acid site density (sites/g)
Zeolite H-ZSM-5	H-MFI	90	2.18×10^{20}

4.6.2 Impregnated Pd Catalyst

A palladium complex (tetramine palladium nitrate) was used to prepare the impregnated catalyst. The H-MFI-90 (supplied in powdered form) was the support. The pore volume of the H-MFI-90 was determined using 1 g of the zeolite and adding deionised water was added drop wise with mixing to determine the volume of liquid required to completely fill the pores of the zeolite. Consequently, the required amount of the metal complex is weighed out and mixed with an amount of water to ensure the solution volume is equal to the pore volume of the zeolite. The dry catalyst support is then added to the solution and mixed thoroughly. It was noticed that the mixture of zeolite and metal salt solution initially turned pink and with some mixing, turned yellow in colour. The impregnated zeolite was then dried at 120°C over night and pelletized in a pellet press at 147 KPa pressure.

The activities of the noble metal impregnated catalysts, was determined experimentally with the number of acid sites kept constant. That is, the amount of zeolite in the reactor, for a set of

experiments, is the same. The amount of metal, x (g), required to load the zeolite powder, W_z (g), to a desired degree (weight percentage: f) is calculated as follows.

$$W_z + x = W_{total}$$

Equation III

$$\frac{x}{W_{total}} = f$$

Equation IV

Solving for the unknown x, the weight of the noble metal gives;

$$x = \frac{fW_z}{(1-f)}$$

Equation V

For example, in order to load 2 g of zeolite H-MFI-90 with 0.9 wt% of noble metal, 0.0182 g of noble metal should be impregnated into the zeolite powder. The total catalyst weight of zeolite and noble metal combined is then 2.0182 g.

4.6.2.1 Pd Impregnated Catalyst loading

For simplicity's sake it was decided to load the same amount of catalyst, with different noble metal loadings, in the four reactors. So, for example, instead of loading 2.0182 g of catalyst with 0.9 wt.% of metal, 2.006 g of catalysts with 0.3 wt.% of metal, 2.0121 g of catalyst with 0.6 wt.% of metal and 2.0243 g of catalyst with 1.2 wt.% of metal, simply 2 g of all catalysts was loaded. Obviously, in this way, the amount of zeolite acid sites loaded in the various reactors is no longer the same. The error introduced this way is proportional to the difference between the zeolite mass within the total catalyst mass as calculated above (2 g within 2.0182 g) and the zeolite mass in the total catalyst mass of 2 g (1.982 g). This translates into the following formula, with its solution for the example cited;

$$e = \frac{W_z-(W_{total}-W_{total}f)}{W_z} = \frac{2-(2-2f)}{2} = f$$

Equation VI

In our example, with 2 g of zeolite and a noble metal loading of 0.9 wt.%, 0.018 g of noble metal, the difference between loading 2.0182 g of catalyst containing 2 g of zeolite and loading 2 g of catalyst containing 1.982 g of zeolite equals 0.018 g which amounts to an error of 0.9 %.

Thus the error introduced by simply loading a rounded off amount of catalysts in all reactors equals the numerical value of the weight loading percentage. In our experiments that is never more than 1.2 %. It was therefore decided to ignore this error and assume that the amount of zeolite acid sites loaded in each reactor is the same.

4.7 Reactor Loading and Catalyst Activation

To load the catalyst into the reactor, the reactor tube was placed in an upright position in a bench vice. Glass wool was placed at the bottom of the reactor to prevent any particles from leaving the reactor. The three layers mentioned in section 4.3, are then sequentially added to the reactor vessel. 20 cm^3 of (400-600 µm) SiC is loaded, using a funnel, into the reactor as a support packing for the catalyst bed, so that the subsequent catalyst layer was located in the isothermal zone of the reactor. Following the catalyst layer, the reactor was finally filled up to the top with SiC such that when the reactor head was mounted, the n-hexadecane inlet tube dipped into the top of this packing.

4.7.1 Catalyst Reduction

The reduction procedure is different for the segregated and the impregnated catalysts.

4.7.1.1 Segregated Catalyst Reduction

The segregated catalyst was reduced in hydrogen (50 ml/min). The temperature was ramped at 5°C/min up to 350°C and held at that temperature over-night. The temperature was then reduced to the reaction temperature.

4.7.1.2 Impregnated Catalyst Reduction

The impregnated catalyst was initially treated in air, prior to reduction, according to the procedure shown in Figure 4.8. After reduction, the catalyst bed temperature is reduced to the reaction temperature. The oxidative treatment served to fully disperse the metal in the zeolite.

4.8 Hydrocracking Operating Procedure

After catalyst loading, the normal operating procedure is as follows:

1. The four reactors were inserted into the brass housings and the liquid and gas inlet ports were connected. Care was taken to ensure that the gaskets of the VCR fittings were present and in good condition.
2. To ensure that all guard catch pots were empty, the drain valves to each pot were opened and subsequently closed.
3. N_2 was set to flow into the top of the reactors.
4. Back pressure regulators were set to the desired operating pressure (20 bar).
5. N_2 flow on the MFC was set to 50 ml/min and reactors were left to pressurize.
6. The reduction procedure mentioned in section 4.7.1 was executed, depending on the kind of catalyst being tested.
7. After catalysts reduction, N_2 dilution gas flows to the vaporizer were set.
8. The desired H_2 flow rate was set on the MFC (for every 0.01 ml/min of C_{16} 8 ml/min H_2)
9. The n-hexadecane flow rates were set.

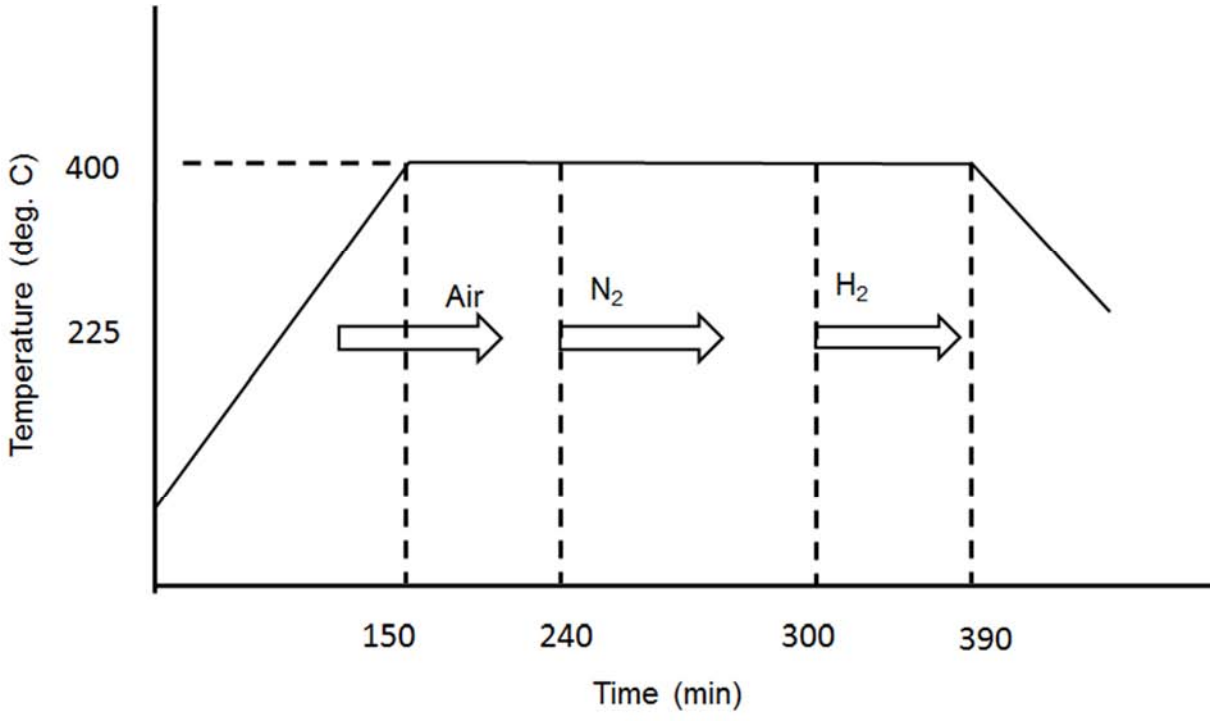

Figure 4.5: Activation of impregnated catalysts

A summary of the test conditions is provided in Table 4.4.

Table 4.4: Hydrocracking conditions

Temperature (°C)	**225**
Pressure (bar)	20
H_2/C_{16}	10
H_2/CO	2

4.8.1 Normal shut down Procedure

1. Shut off the C_{16} feed and allow it to evaporate out of the reactor under H_2 flow
2. Stop the sampling on the online GC
3. Switch off heating to the reactor.
4. Shut off N_2 and H_2 gas feeds

4.8.1.1 Emergency Shutdown Procedure

1. Turn off the illuminated main power switch on the front of the control panel, interrupting power supply to the test unit.
2. Turn off N_2 and H_2 supply lines to the test unit.

5 Results

5.1 Internal and External Mass Transfer Limitations

The objective of this work was to observe the intrinsic properties of the catalytic hydrocracking. Particles of Pd/SiO_2 + H-MFI-90 of different sizes (0.30 mm-0.85 mm) were prepared and loaded into four reactors. Each particle size was tested at 20 bar, 225°C. A plot of conversion versus inverse average pellet size is shown in Figure 5.1 and from which it can be seen that as the inverse of the pellet size increases, conversion increases to a certain point before levelling off. When the conversion is no longer dependant on the inverse of the pellet size, internal mass transfer limitations are absent, as indicated by a dotted line in Figure 5.1, which divides the regions with and without internal mass transfer limitations. The particle size range for which internal mass transfer limitations do not occur (0.3 mm – 0.4 mm) was selected for all subsequent experiments.

To evaluate external mass transfer limitations, the four parallel reactors were operated at different linear superficial velocities (the diameter of the reactors and reaction conditions were the same), concomitantly varying feed rate and catalyst mass such that the space velocity remained constant across all four reactors. A plot of the results is shown in Figure 5.2, and from which it can be seen that conversion does not change with increasing linear velocity (volumetric flow rate).

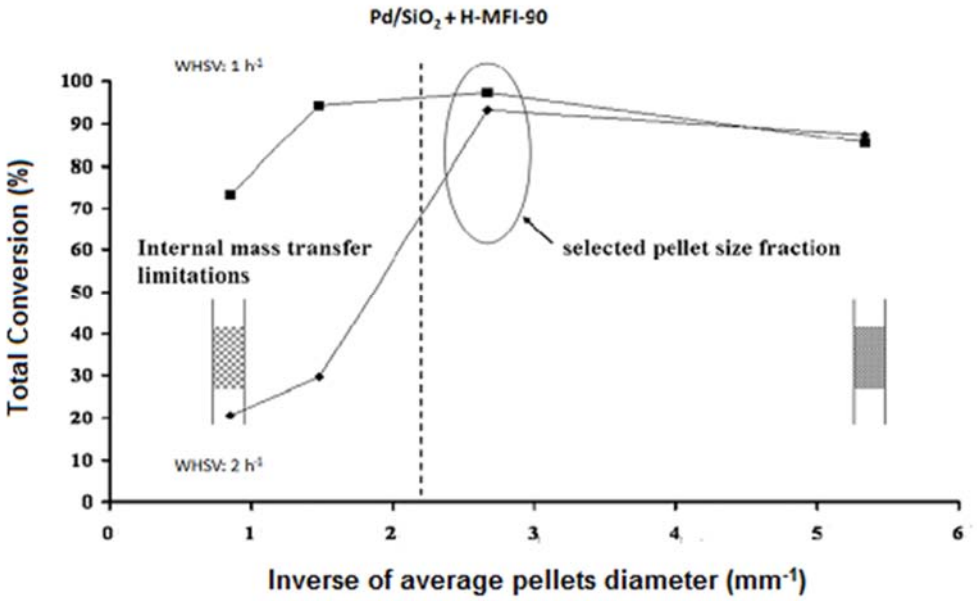

Figure 5.1: Internal mass transfer limitation test results. Temperature = 225°C, Pressure = 20 bar, H_2/n-C_{16} = 10

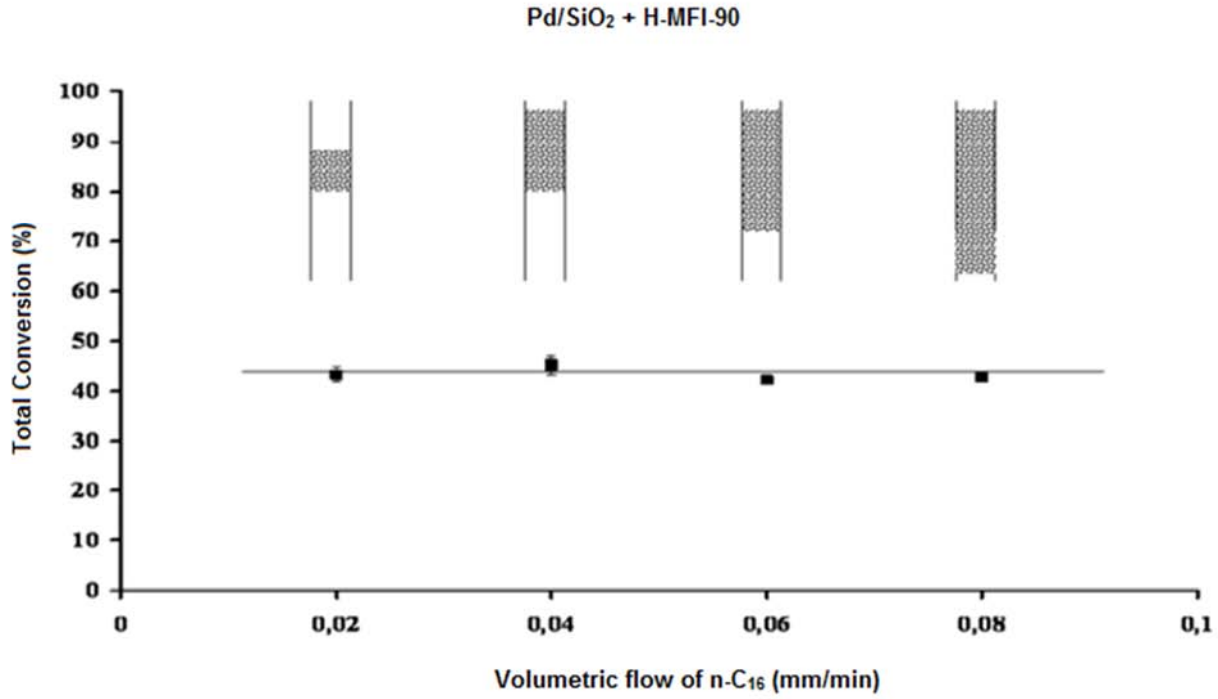

Figure 5.2: External mass transfer limitation test results. Temperature = 225°C, Pressure = 20 bar, H_2/n-C_{16} = 10, WHSV = 0.5

Consequently, external mass transfer limitations do not affect conversion and rate of reaction in the 0.02 ml/min-0.08 ml/min n-C_{16} flow range applicable to this study. In conclusion the test regime for this study is considered free from either internal or external mass transfer limitations.

5.2 Segregated Catalysts

The performance of each metal (Rh, Ru, Pd) was investigated at different metal loadings. In addition, the acid H-MFI-90 zeolite performance was evaluated in the absence of any metal co-catalyst. The performance of all catalysts was evaluated both in the presence and absence of CO.

5.2.1 Standard Hydrocracking

5.2.1.1 Rhodium/Alumina + H-MFI

Rhodium supported on alumina was tested at different metal/acid site ratios (0.01, 0.07, 0.18 and 0.30). The effect of metal loading and space velocity on conversion is shown in Figure 5.3, from which it can be see that the total conversion increases, with increasing metal loading, implying that under the conditions evaluated, metal content is limiting the reaction rate.

Product distributions are presented in Figure 5.4, where the values of all the bars on the chart are to be read off the Y axis. For example, for carbon number 6 on the plot for a Rh metal/acid site ratio of 0.07 (i.e the middle plot in Figure 5.4), the total iso-C_6 compounds, inclusive of the iso-$C_6^=$ have a selectivity of 10 %; 0.5% iso-$C_6^=$ and 9.5% iso-C_6. Similarly the bar representing the selectivity of the total n-C_6 compounds, inclusive of n-$C_6^=$ compounds reads 8.5%, the selectivity of the n-$C_6^=$ compounds, is low and not visible in the Figure.

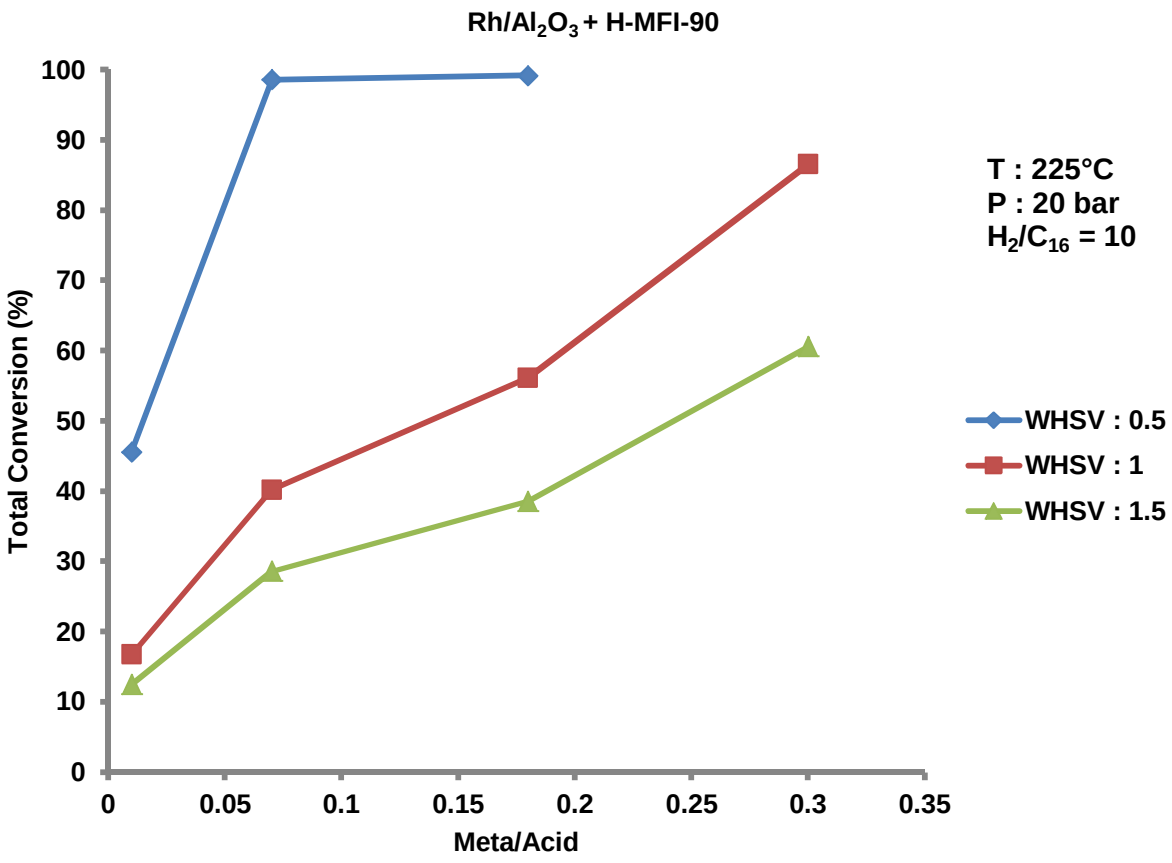

Figure 5.3: Conversion versus Rhodium loading shown at different weight hourly space velocities

The product distributions (carbon number distribution) are presented as a function of Rh metal/acid site ratio in Figure 5.5. There are no C_{14} and C_{15} compounds appearing in the product spectrum for all metal loadings. The C_1 selectivity is less than 0.5% and can be neglected, such that it can be concluded that the metal catalysed methanolysis and hydrogenolysis reactions are not prevalent. The lowest metal loading (metal/acid 0.01) exhibits a total olefin selectivity of 17%, whereas The higher metal loading (metal/acid 0.18) has a total olefin selectivity of 0.67% (Figure 5.4), indicating that as metal loading increases less olefins appear in the product spectrum.

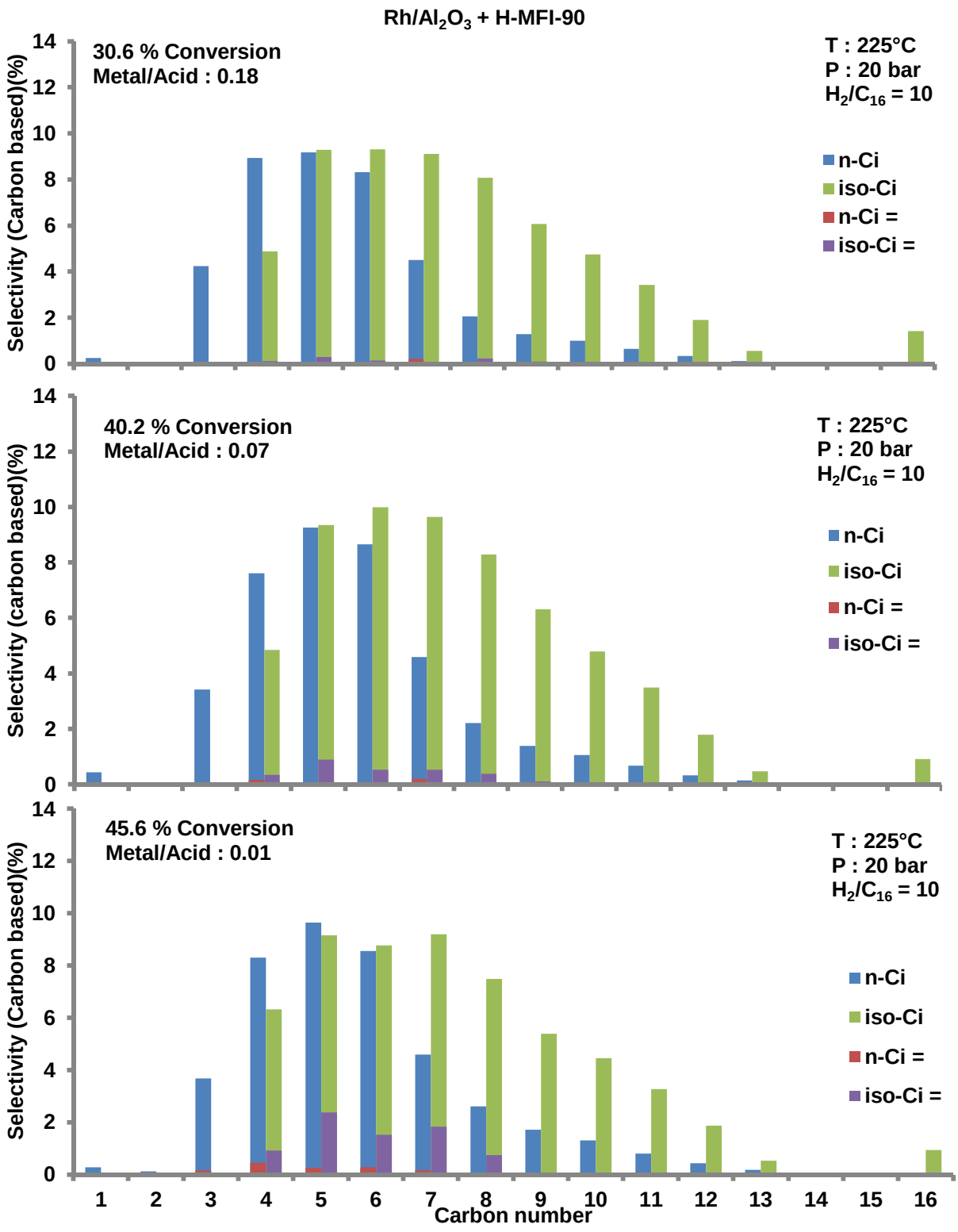

Figure 5.4: Selectivity as a function of Rhodium loading

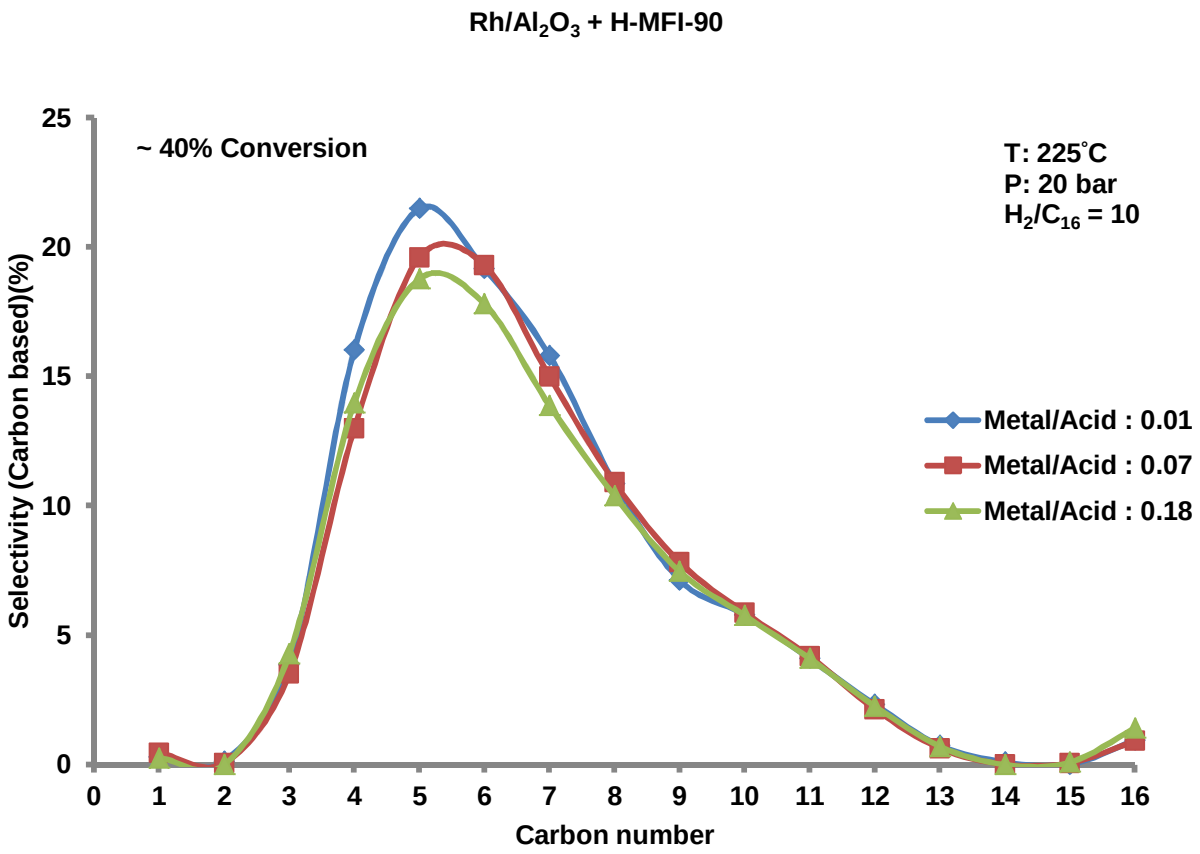

Figure 5.5: Total product distribution for Rh catalysts compared at similar conversion

Figure 5.5 shows clearly that the product distributions for all the metal loadings are peaking at low carbon numbers (C_4-C_6). C_4 selectivity is far greater than C_{12} selectivity, such that it is clear secondary cracking is occurring for all metal loadings. In the case of the n-C_{16} feed used in these experiments; an ideal hydrocracking product distribution will be characterised by equal molar selectivity toward the fragments between C_4 and C_{12}, and the ratio of the selectivity of C_4 and C_{12} is a good indicator of how much secondary cracking is occurring. When the C_4/C_{12} ratio is 1, ideal hydrocracking is occurring. When the ratio molar C_4/C_{12} is 1 ideal hydrocracking is occurring, whereas for a C_4/C_{12} molar ratio greater than 1secondary cracking is occurring.

It is important to note that since the data presented here is plotted on a carbon percent basis and not mole percent, a C_4/C_{12} ratio of 1 is not indicative of primary cracking since for true primary hydrocracking the C_4/C_{12} carbon ratio should be closer to 0.33 (i.e. ¼ divided by 1/12). It can further be seen that the C_4/C_{12} ratio changes only slightly with metal/acid site ratio such that, even at the highest metal loading, secondary cracking is prevalent

5.2.1.2 Ruthenium/alumina + H-MFI

Ruthenium was also tested at different metal to acid site ratios (0.0002, 0.0022, 0.006 and 0.009) A plot of conversion versus metal loading on the Ru catalyst is shown in Figure 5.6, and from which it can be seen that the total conversion increases with increasing metal loading.

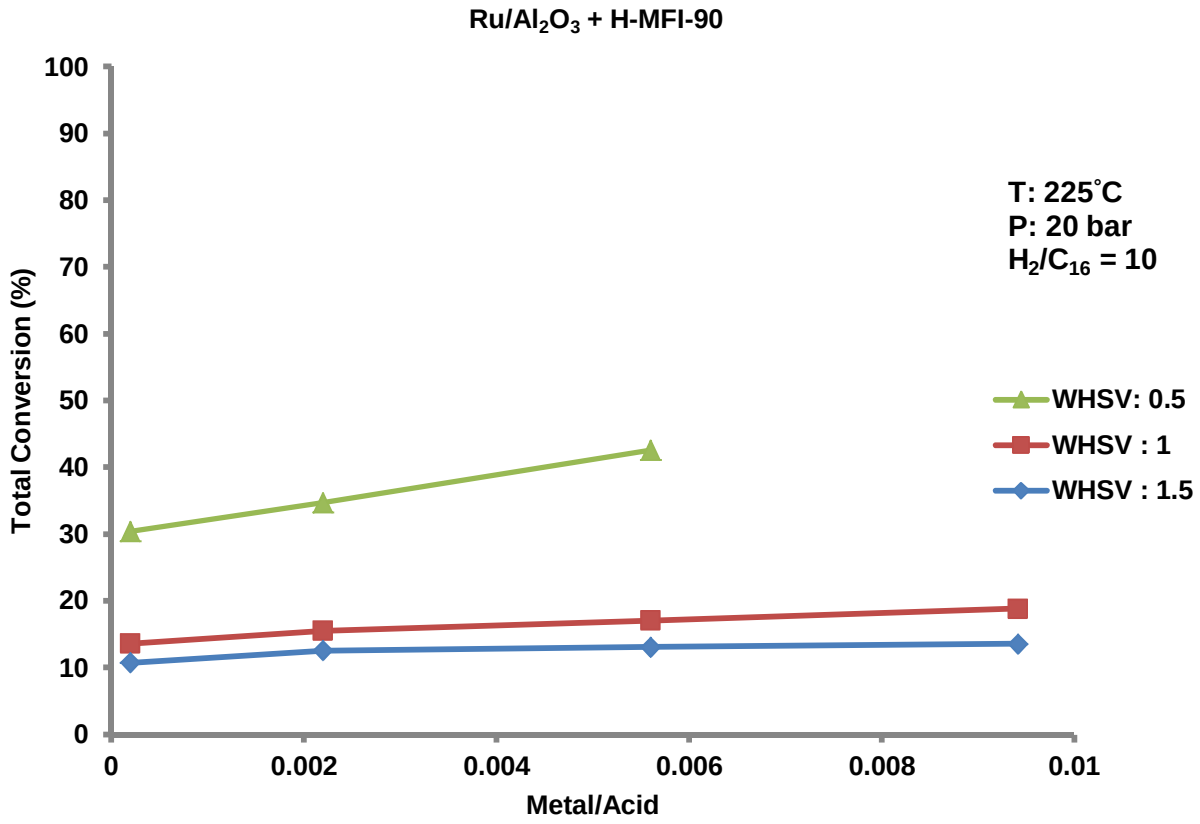

Figure 5.6: Conversion versus Ruthenium loading for different space velocities.

At low space velocities the increase in conversion with increasing metal loading is not very clear; at high space velocities the change is more apparent, such that as with Rhodium, the metal is reaction rate limiting. Figure 5.8 shows the product selectivies and carbon number distributions as a function of metal loading.

The product carbon number distributions for all metal loadings as shown in Figure 5.8 are similar, in the sense that they all show secondary cracking. The lowest metal loading (metal/acid 0.00022) exhibits a total olefin selectivity of 17%, whereas the higher metal loading (metal/acid 0.0056) has a total olefin selectivity of 0.67%, indicating that as metal loading increases less olefins appear in the product spectrum.

Figure 5.7 presents the total product distributions of the tested catalysts, clearly confirming that secondary cracking is occurring for all metal loadings. Likewise, C_4 selectivity is far greater then C_{12} selectivity for all metal loadings.

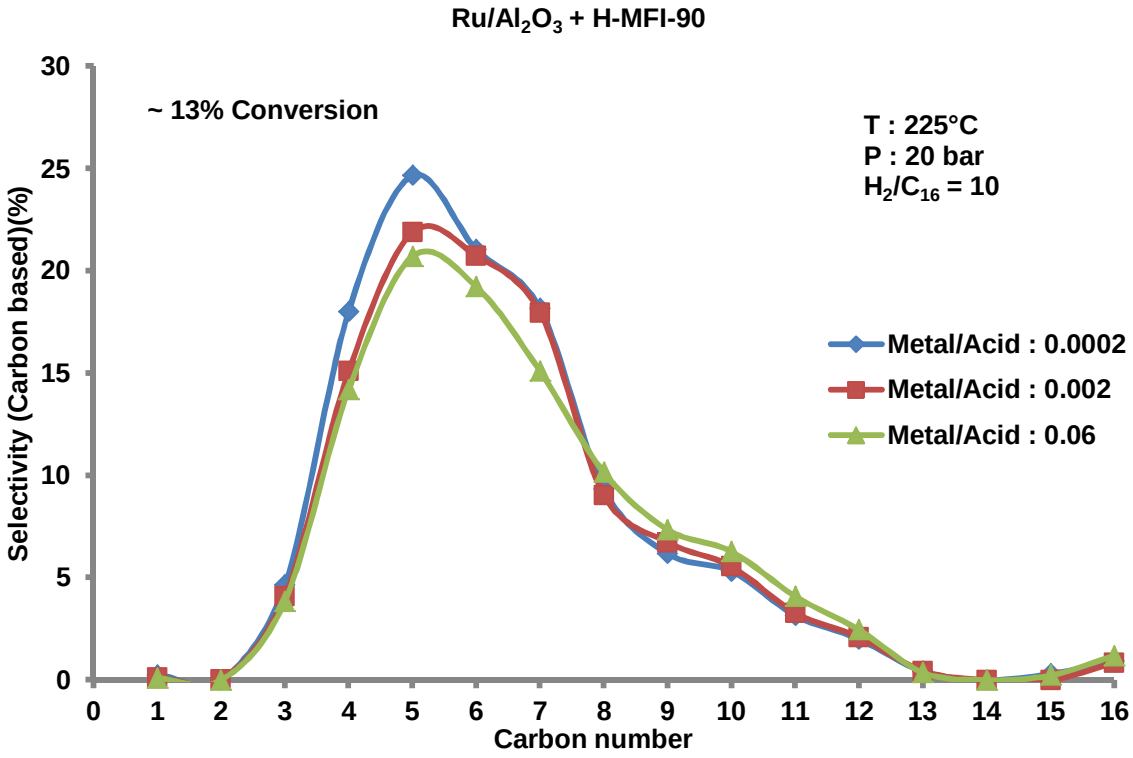

Figure 5.7: Total product distribution for Ruthenium catalyst at similar conversion

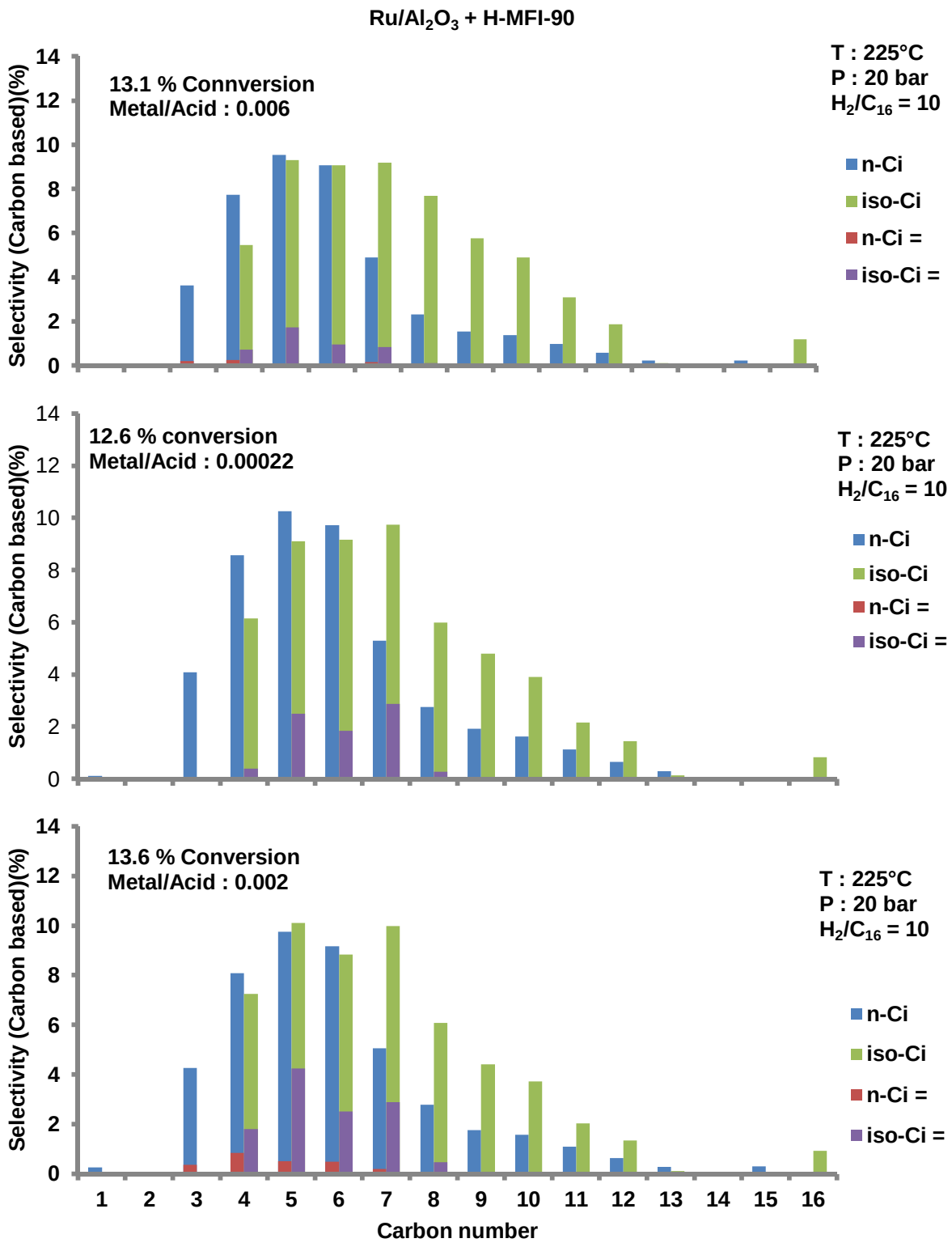

Figure 5.8: Selectivity as a function of Ruthenium loading

5.2.1.3 Palladium/alumina + H-MFI

Palladium performance was evaluated for metal/acid site ratios ranging from 0.0004 to 0.169. Figure 5.9 presents conversion data as a function of metal/acid site ratio and space velocity.

It is clear from Figure 5.9 that conversion increases as Pd loading increases. At metal/acid site ratios above 0.1, the conversion appears to level off, indicating a region in which the metal function does not limit the hydrocracking reaction. Under such conditions (metal/acid site ratio > 1) the rate limiting step is expected to be occurring on the acid sites. Even so, product distribution in Figures 5.10 and 5.11 clearly indicate secondary cracking. As per the case with the Rh and Ru, as metal loading increases less olefins appear in the product spectrum for the Pd catalyst.

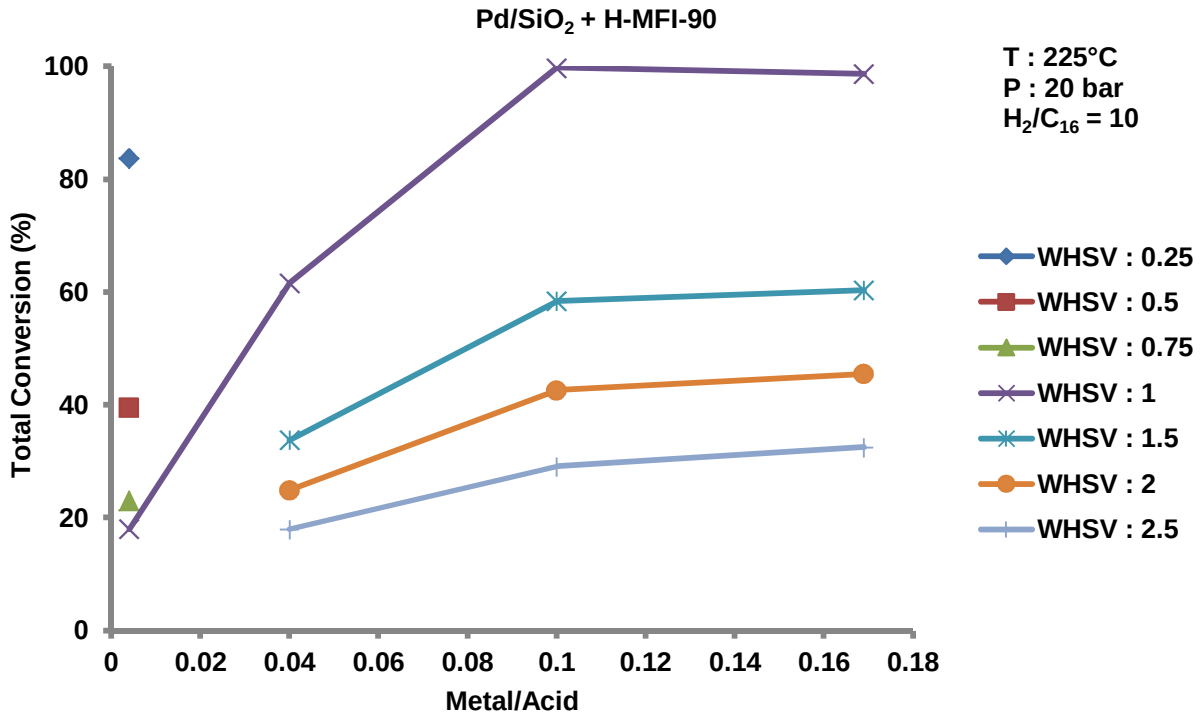

Figure 5.9: Conversion versus Palladium loading for different space velocities

From Figure 5.11, the selectivity towards C_4 is far greater than C_{12} selectivity for all metal loadings. At the highest metal loading the C_4/C_{12} ratio is 14 (i.e. the molar C_4/C_{12} ratio is 42) pointing to the fact that despite conversion 'saturation' at metal/acid site ratios greater than 1, secondary cracking is prevalent.

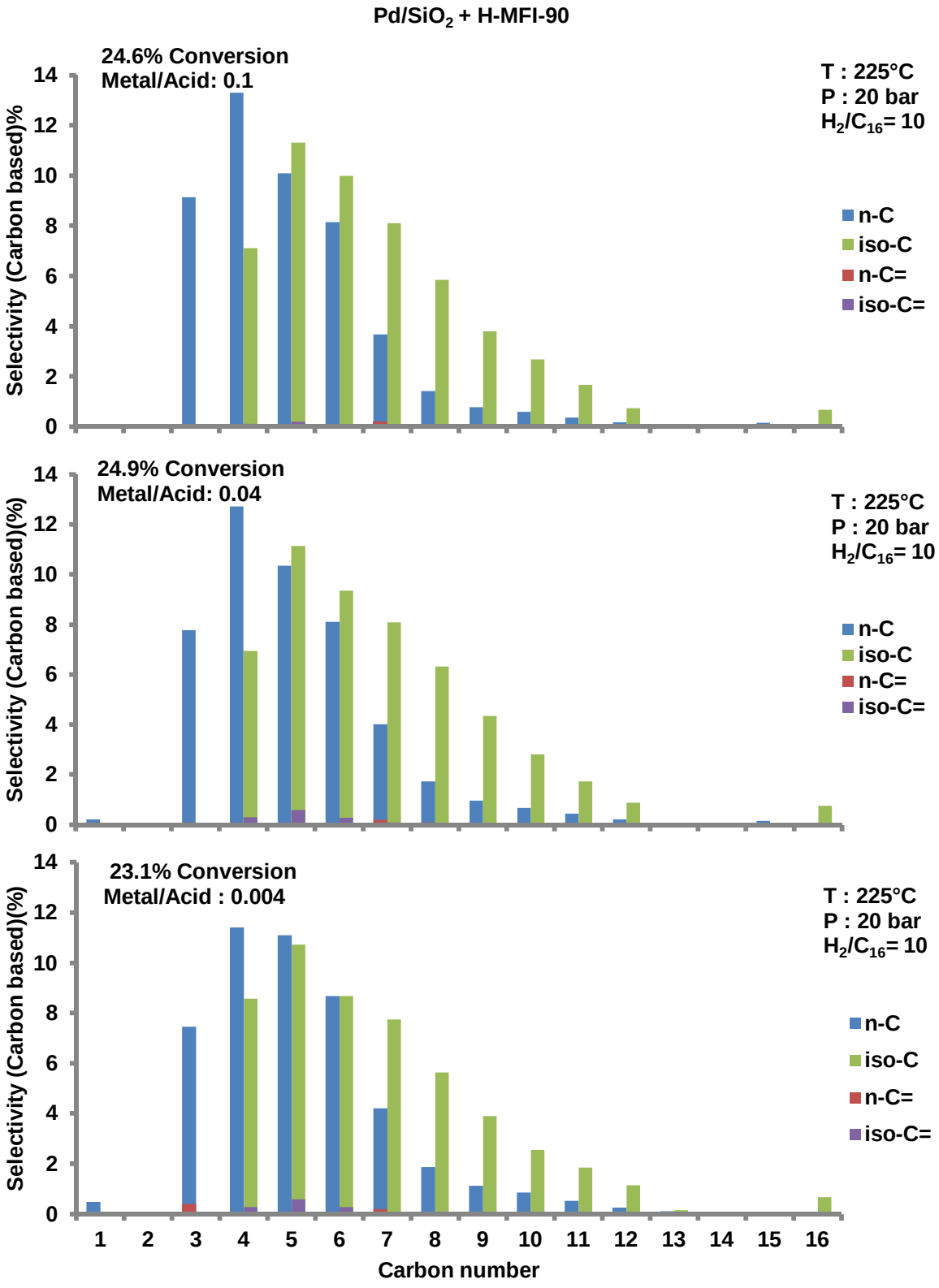

Figure 5.10: Selectivity as a function of Palladium loading

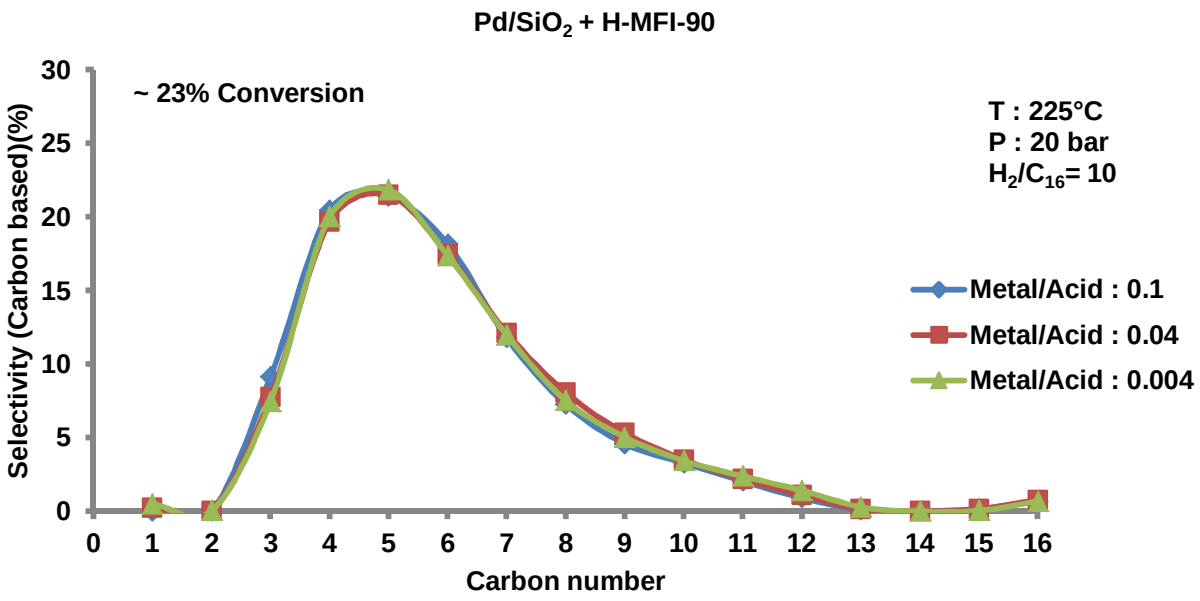

Figure 5.11: Total product distribution for Palladium catalysts at similar conversions

5.2.1.4 H-MFI-90 Zeolite without Metal Co-Catalyst

To establish the 'background' activity of the zeolite catalyst in the absence of the metal co-catalyst, a 0.5 – 0.85 mm granulate of H-MFI-90 was evaluated under the conditions relevant to this study (20 bar, 225°C and H_2/n-C_{16} = 10). Conversion data are presented in Table 5.1 and from which it is evident that the H-MFI-90 is capable of activating the paraffinic feed at conditions of this study.

Table 5.1: Conversion Results on H-MFI-90

Feed	Conversion, mean (μ) (%)	Standard deviation (σ) (%)
WHSV : 0.75 (C_{16}: 0.03 ml/min)	18.3	1.07
WHSV : 0.5 (C_{16}: 0.02 ml/min)	22.9	0.69
WHSV : 0.25 (C_{16}: 0.01 ml/min)	52.7	1.26

Figures 5.12 and 5.13 present product selectivity and carbon number distributions over H-MFI-90. The total olefins selectivity is 9% at 52.7% conversion. From Figure 5.13 it is clear that the total product distribution on the H-MFI-90 is peaking at low carbon numbers (C_4-C_6) indicating secondary cracking, as is to be expected in the absence of any metal co-catalyst. By comparison to the Pd/SiO_2 + H-MFI combination, the acid catalyst alone shows a C_4/C_{12} ratio of 6 versus that of 14 in the case of the Pd catalyst at similar conversions (~23%) such that the extent of overcracking is worse in the absence of metal.

Figure 5.14 shows that the metal containing catalysts have a higher activity compared to just the H-MFI-90 zeolite alone. A comparison of the product selectivity of the Pd containing catalyst and the H-MFI-90 without the metal function are shown in Fgure 5.15. There is however a noticeable difference between the product distributions of the H-MFI-90 without the metal function and the H-MFI-90 with the metal function. Total olefin selectivities on the H-MFI-90 and the Pd/SiO_2 + H-MFI-90 are 9% and 1%, respectively, confirming that the metal serves in part to hydrogenate the cracked olefinic fragments. Even so it is noticeable, that the vast majority of products from the H-MFI-90 test are paraffinic despite the absence of a metal function.

.

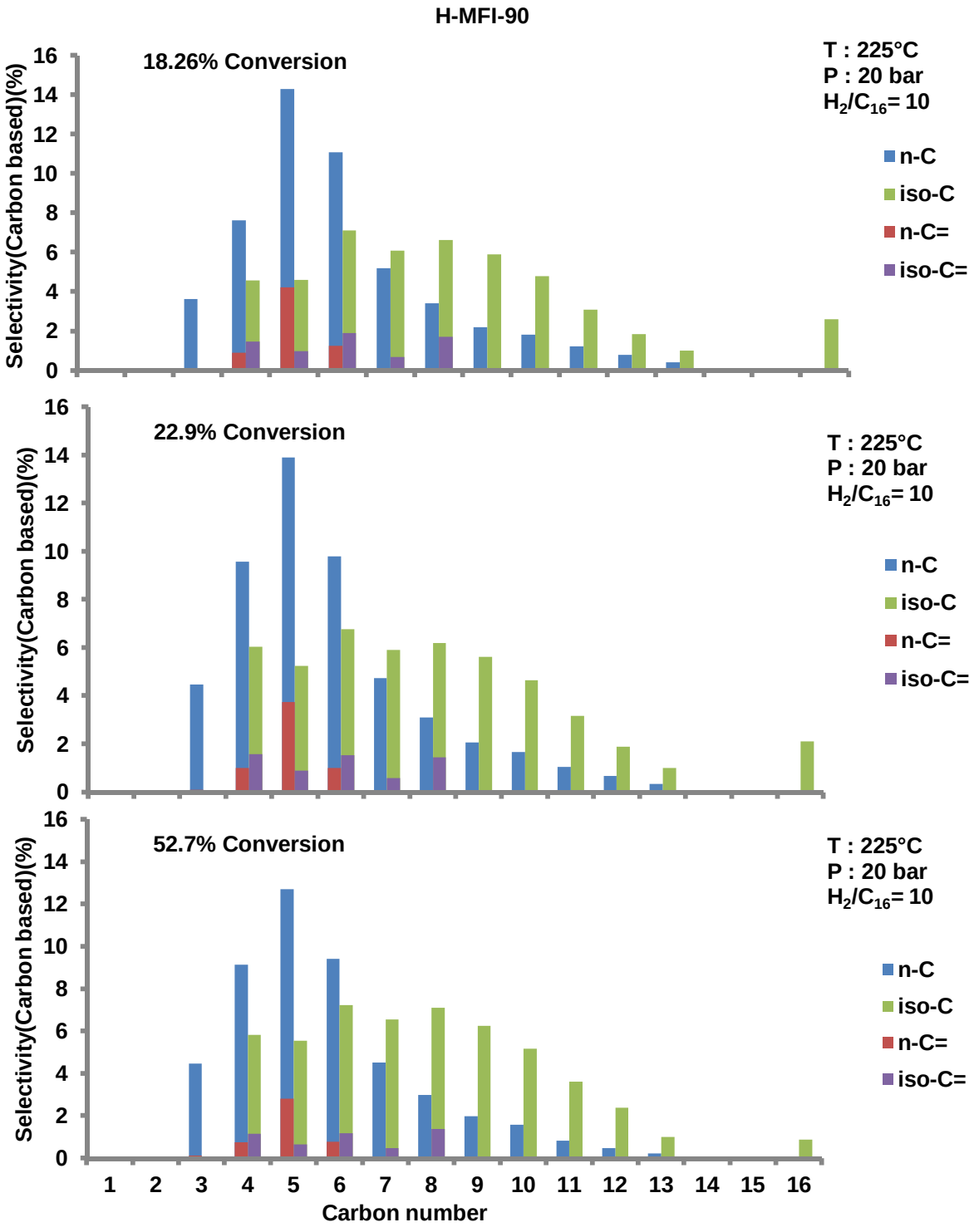

Figure 5.12: Selectivity as a function of space velocity (conversion)

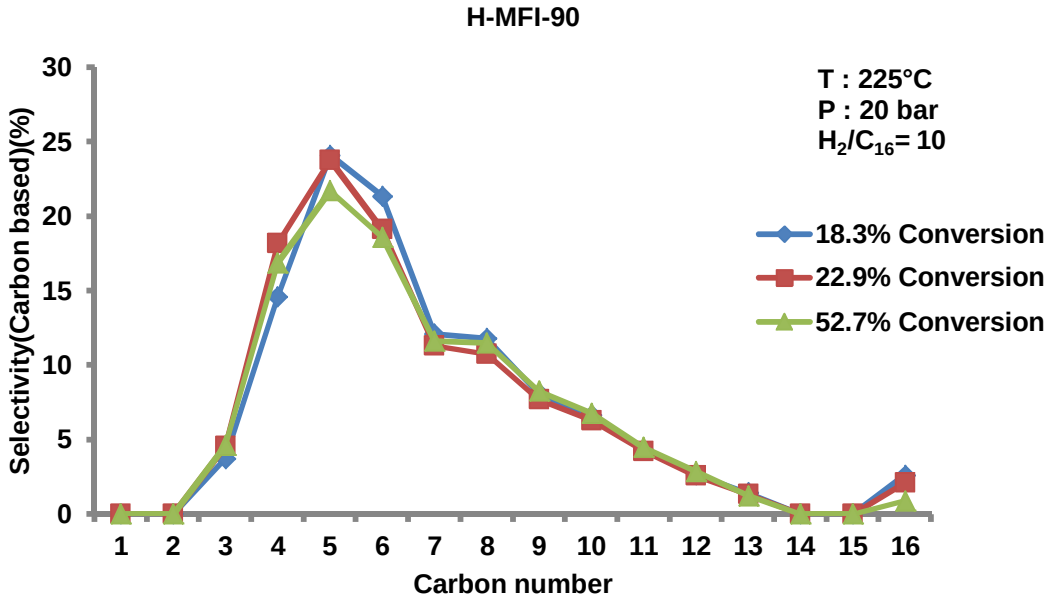

Figure 5.13: Total product distribution for H-MFI-90 as a function of conversion

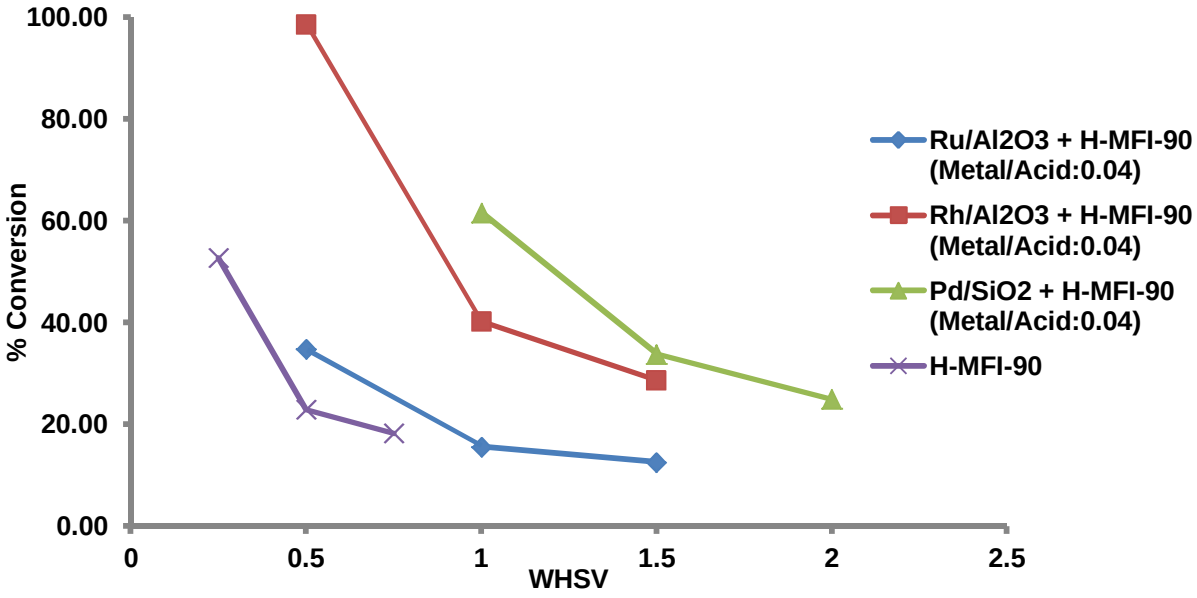

Figure 5.14: Comparison of H-MFI-90 with and without a metal function

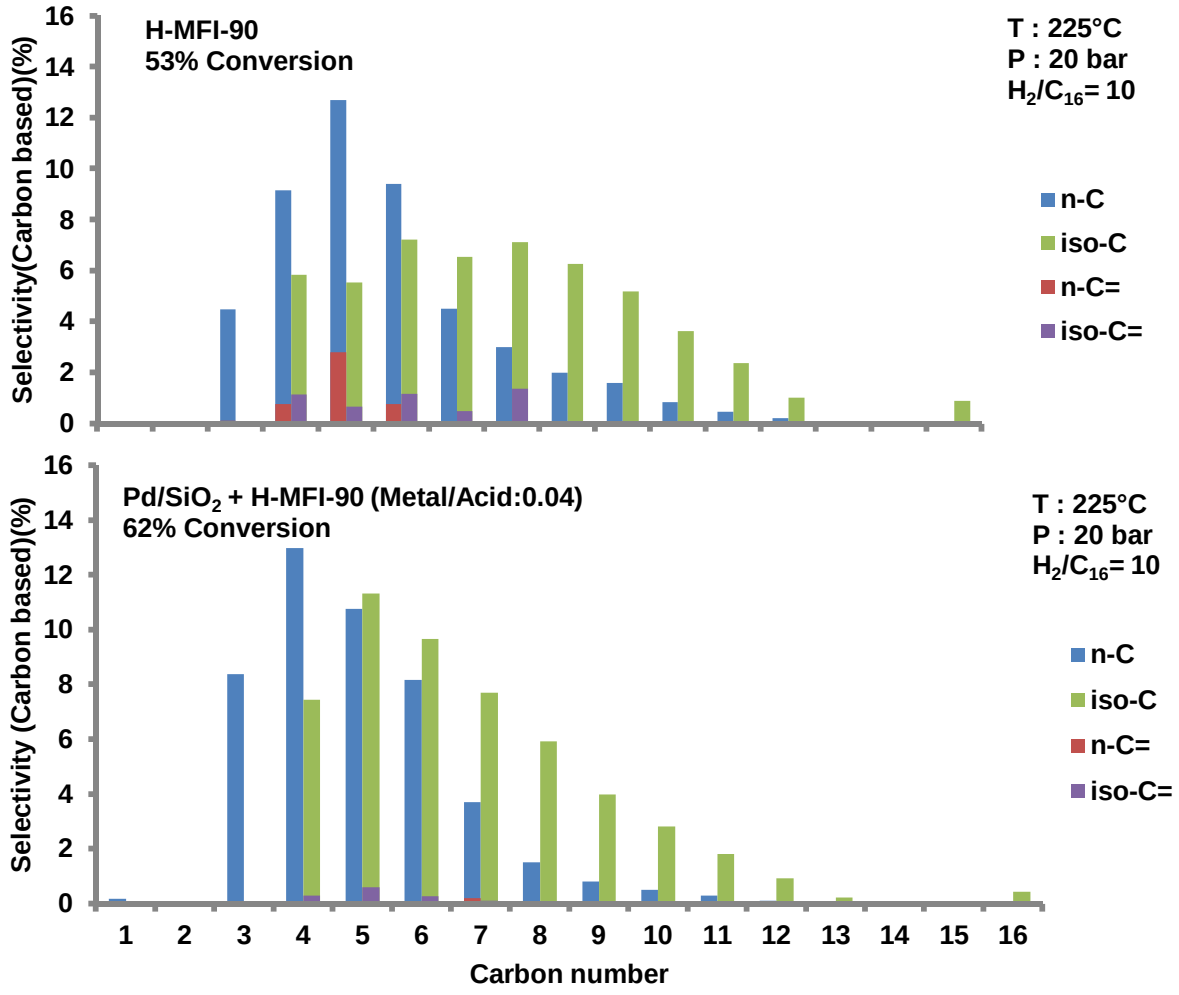

Figure 5.15: Comparison of product distribution over Pd/SiO_2 + H-MFI-90 and H-MFI-90

5.2.2 Hydrocracking In The Presence of CO

Since the overall objective is the integration of hydrocracking and LTFTS, The influence of CO on the performance of the Rh, Ru, Pd and H-MFI-90 catalysts of section 5.2.1, are presented below.

5.2.2.1 Rhodium/alumina + H-MFI

The effect of CO on the activity of the Rh catalyst (metal/acid site ratio 0.07) is presented in Table 5.2.

Table 5.2: Conversion over Rh/Al_2O_3 (metal/acid:0.07) + H-MFI at WHSV= 0.5, 20 bar and 225°C

Feed	Conversion, mean (μ) (%)	Standard deviation (σ) (%)
C_{16}: 0.01 ml/min	98.6	0.17
C_{16}: 0.01 ml/min, $H_2/CO = 2$	37.5	0.62
C_{16}: 0.01 ml/min , (after CO removal)	30.6	0.12

From Table 5.21 it is clear that n-C_{16} conversion decreases drastically upon addition of CO from 98.6% to 37.5%. Moreover, after CO removal the catalyst does not seem to regain its activity and conversion remains low at 31.6%. A comparison of the product distribution with and without CO is shown below is presented in Figure 5.16.

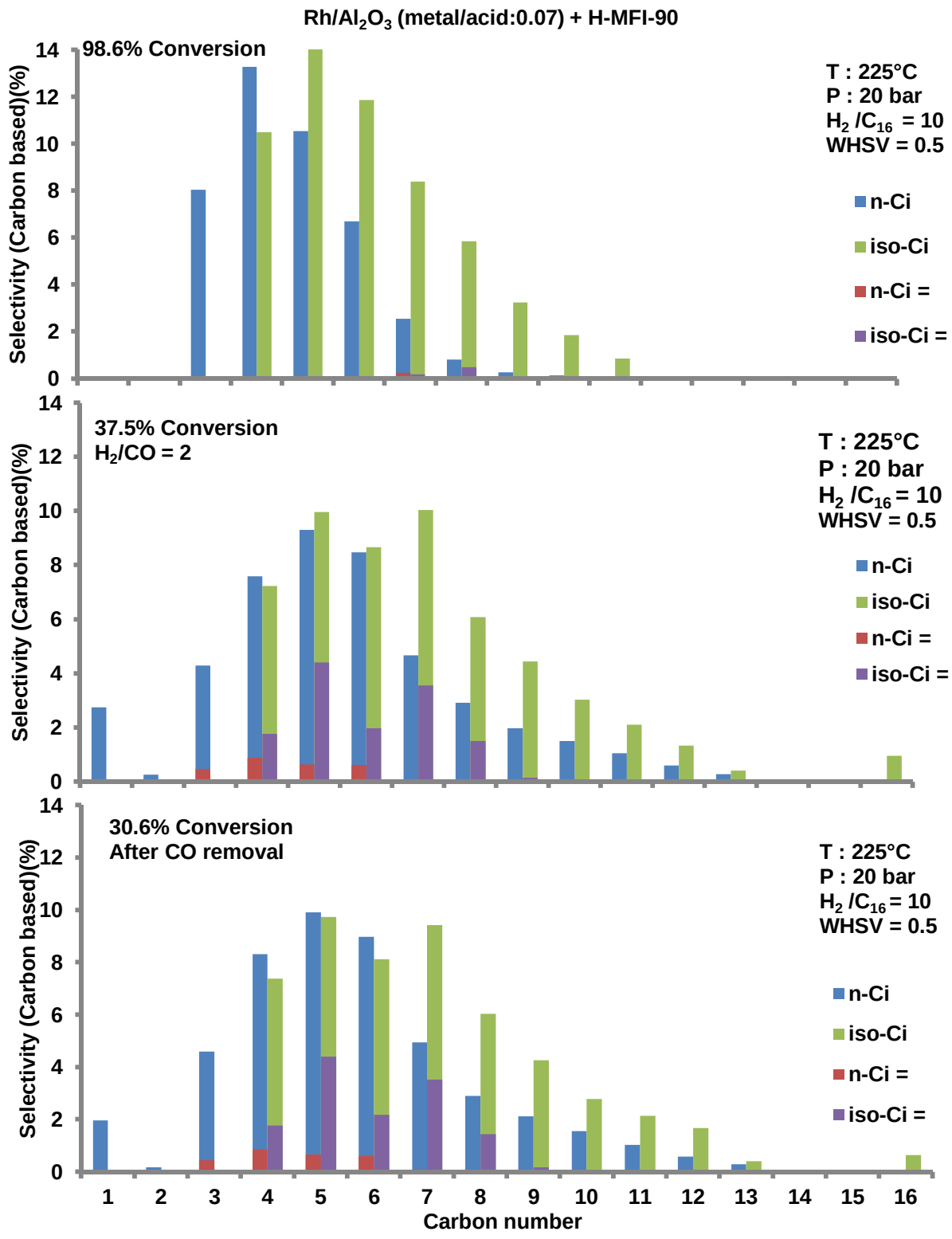

Figure 5.16: Selectivity as a function of CO introduction and removal for Rh/Al_2O_3 + H-MFI mixed catalyst.

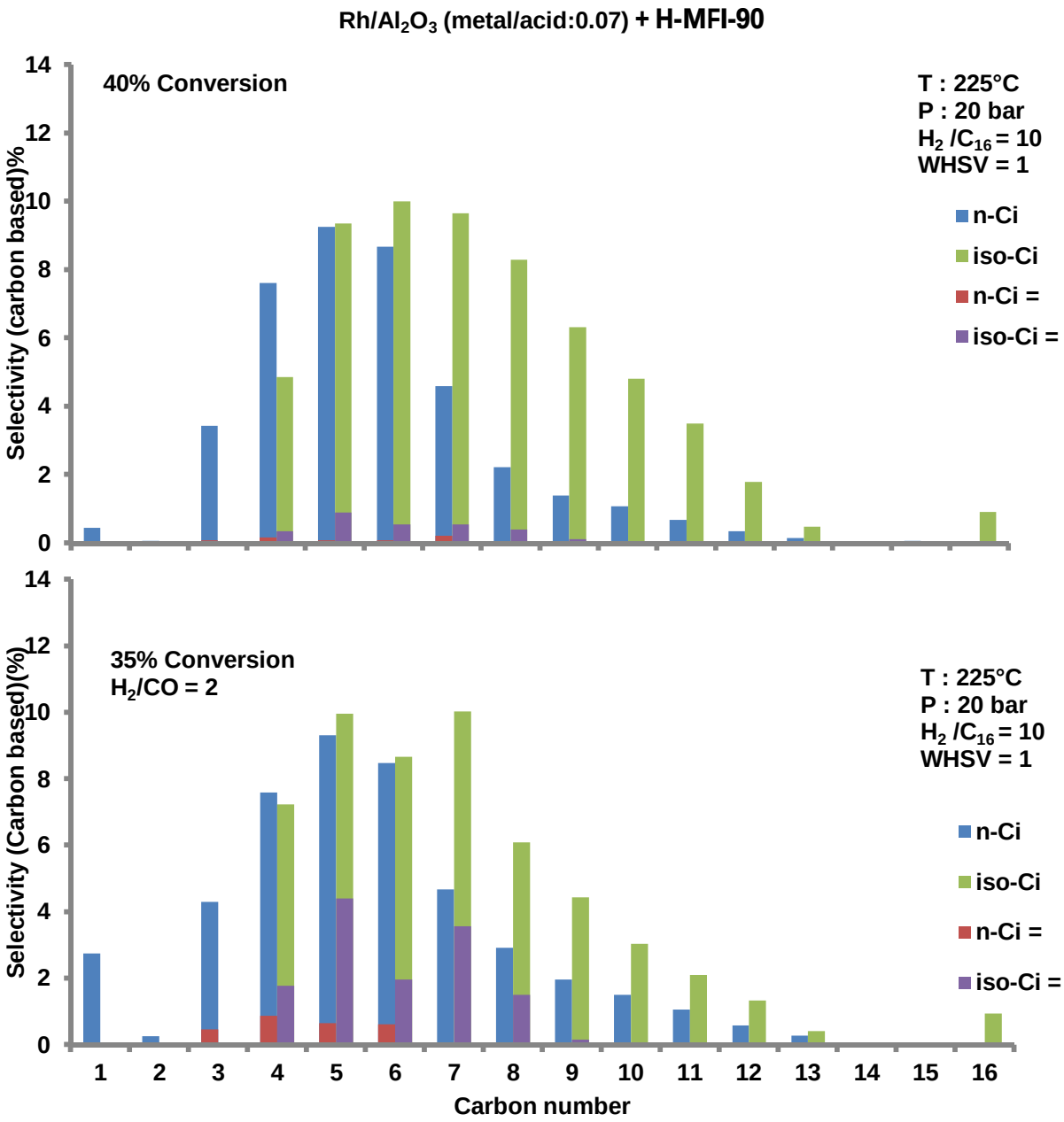

Figure 5.17: Product distributions in the presence and absence of CO compared at similar conversions

From Figure 5.16 it can be seen that secondary cracking is prevalent before, during and after CO introduction in the feed. Indeed, the general carbon number distribution is not altered by the presence of CO (see also Figure 5.18). Total olefin selectivity increases dramatically with CO addition from 3.2% to 14.6% respectively (Table 5.3) and remains high even after CO removal. Also striking, is the appearance of methane (and some ethane) in the product spectrum when CO is present, a feature which remains even after CO removal

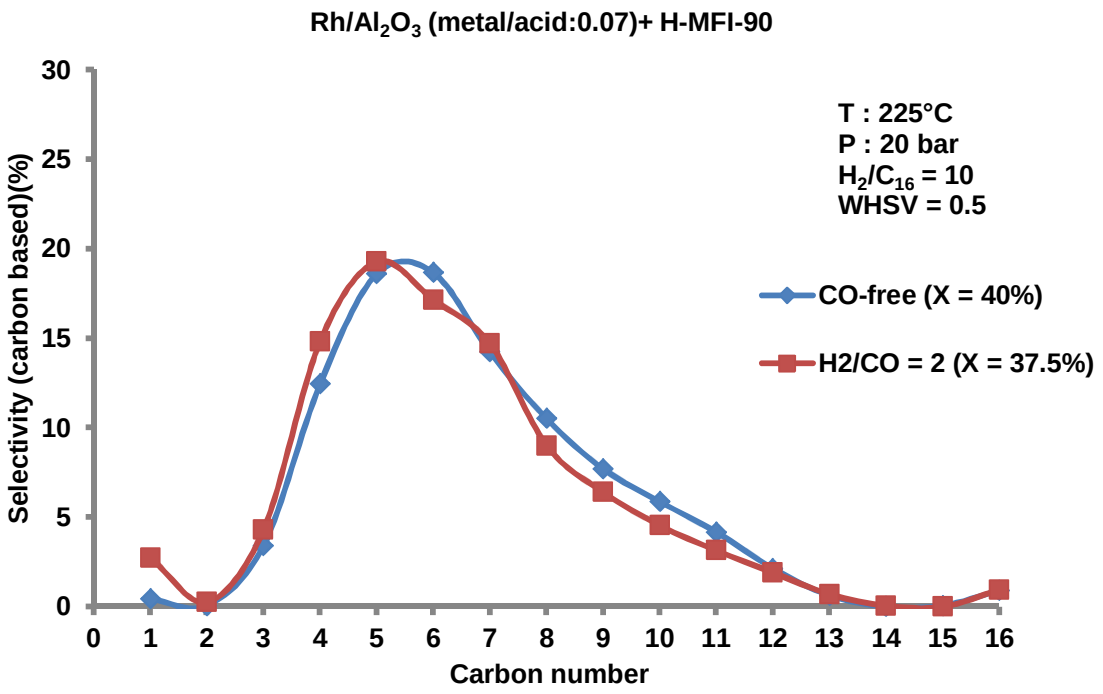

Figure 5.18: Effect of CO on total product distribution at equal conversion on Rh/Al_2O_3 (metal/acid:0.07) + H-MF-90

That CO has little effect on the extent of secondary cracking is further seen by the the C_4/C_{12} ratio before and during CO co-feeding, to be 8 and 7 respectively. In the presence of CO, selectivity toward the C_3 to C_4 fraction increases at the expense of the C_8 to C_{11} fraction.

Table 5.3: Effect of CO on Olefin Selectivity over Rh (225°C, 20 bar, H_2/C_{16} = 10, H_2/CO = 2, WHSV = 0.5)

Standard % Selectivity (at 98.6% Conversion)	% Selectivity with CO co-feed (at 37.5 % Conversion)
3.2	14.6

5.2.2.2 Ruthenium/alumina + H-MFI

The effect of CO on the activity and selectivity of the Ru catalyst with a metal/acid site ratio of 0.002 was determined. An over view of the experiment is presented in Table 5.4 and product selectivities and carbon number distributions are shown in Figures 5.19 and 5.20.

Table 5.4: Conversion over Ru/Al_2O_3 (metal/acid:0.002) + H-MFI at WHSV= 0.5, 20 bar and 225°C

Feed at	Conversion, mean (μ) (%)	Standard deviation (σ) (%)
C_{16}: 0.01 ml/min	34.7	1.04
C_{16}: 0.01 ml/min, $H_2/CO = 2$	33.1	1.33

Conversion over the Ru catalyst changes negligibly from 34.7% to 33.1% when CO is co-fed. Unlike in the case of Rh (section 5.2.2.1), no methane (or ethane) product is observed when CO is introduced. There is also little or no observable change to the product carbon number distribution (Figure 5.20) with CO introduction although olefin selectivity almost doubled in the presence of CO (Table 5.5)

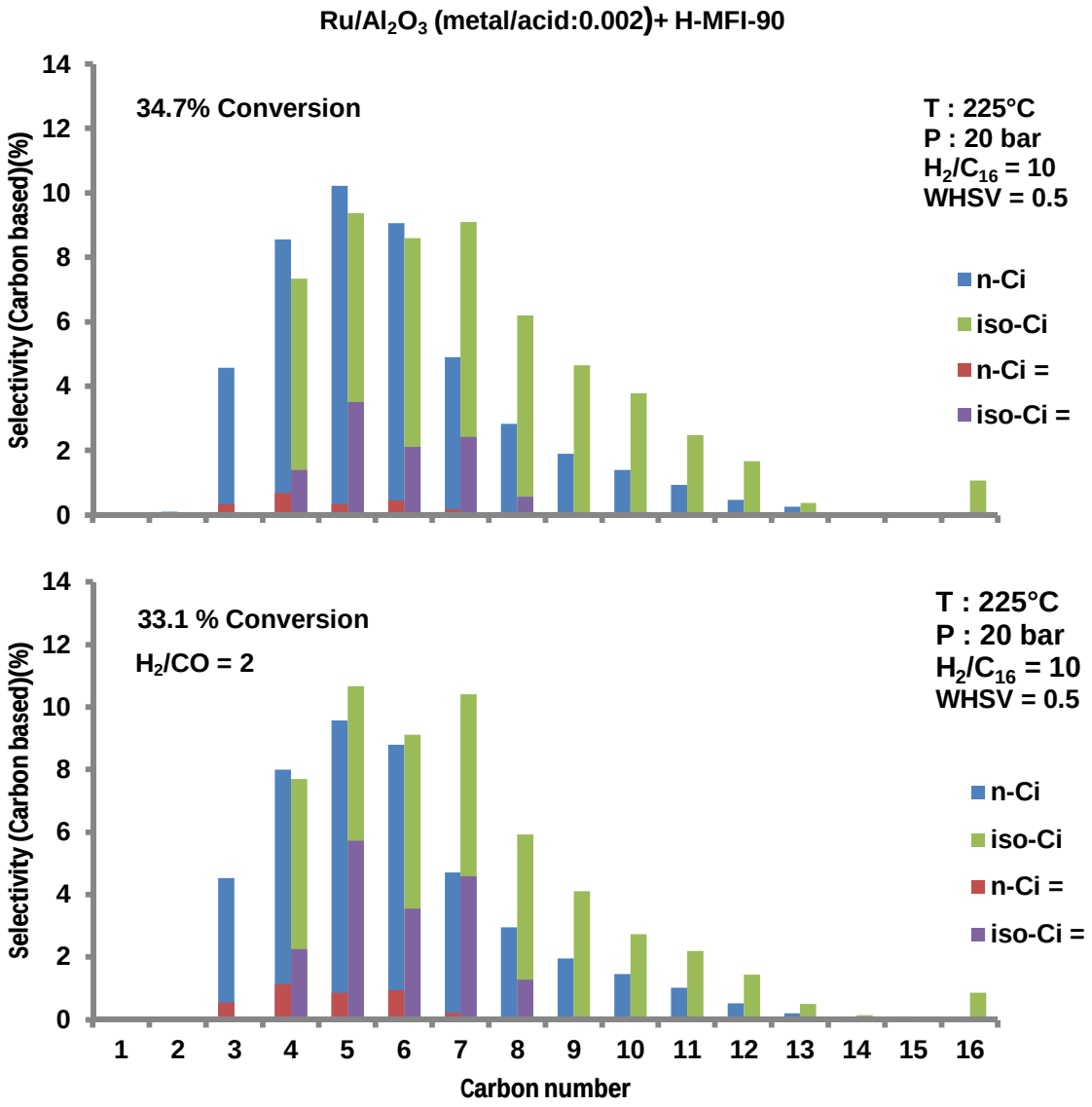

Figure 5.19: Effect of CO on Ru/Al_2O_3 (metal/acid:0.002) + H-MFI-90 catalyst

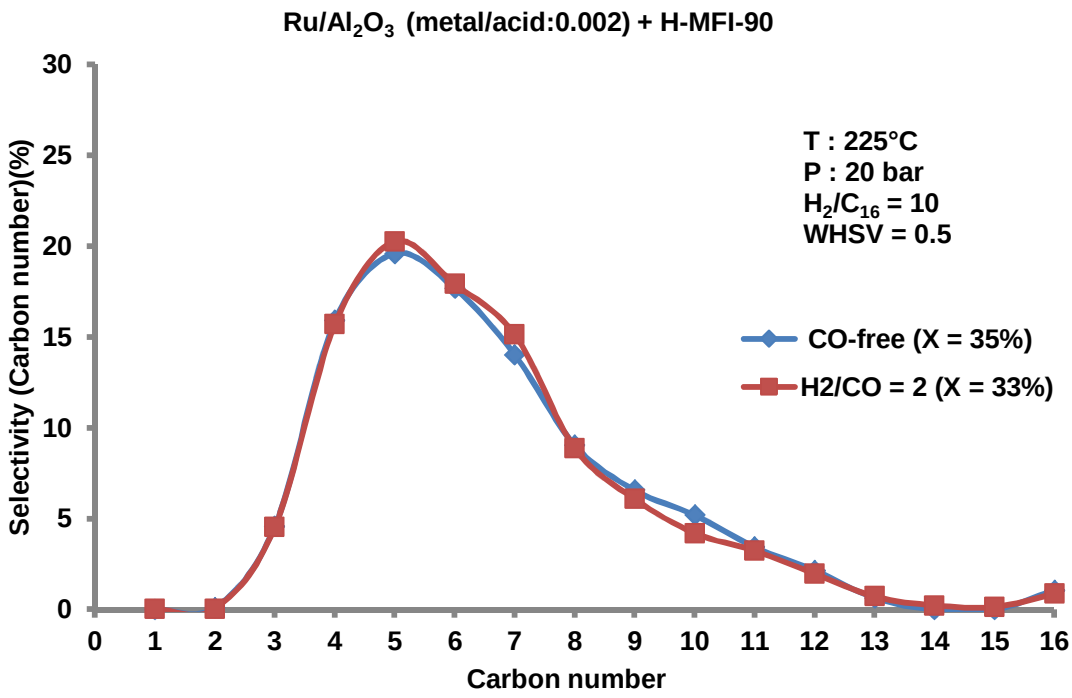

Figure 5.20: Effect of CO on product distribution at similar conversion over Ru/Al_2O_3 (Metal/Acid:0.002) + H-MFI.

Table 5.5: Effect of CO on Olefin Selectivity over Ru (225°C, 20 bar, H_2/C_{16} = 10, H_2/CO = 2, WHSV = 0.5)

Standard % Selectivity (at 35% Conversion)	% Selectivity with CO co-feed (at 33 % Conversion)
12.1	21.3

5.2.2.3 Palladium/silica + H-MFI

The effect of CO on the performance of mixed Pd/SiO_2 + H-MFI catalyst is presented in Table 5.6 (activity), and Figures 5.21 (product selectivity) and 5.22 (carbon number distribution).

Table 5.6: Conversion over Pd/SiO_2 (metal/acid:0.02) + H-MFI-90 at WHSV= 1, 20 bar and 225°C

Feed at	Conversion, mean (μ) (%)	Standard deviation (σ) (%)
C_{16}: 0.03 ml/min	46.0	2.16
C_{16}: 0.03 ml/min, $H_2/CO = 2$	21.5	1.77

CO introduction reduces the conversion over the Pd containing catalyst from 46% to 21.5%. In Figure 5.21 it can be seen that olefin selectivity increases when CO is introduced, indicating a decrease in catalyst hydrogenation activity. Secondary cracking prevails and is slightly enhanced in the presence of CO (despite the CO data in Figure 5.22 being at half the conversion level of the CO-free data). No methane is observed with CO introduction.

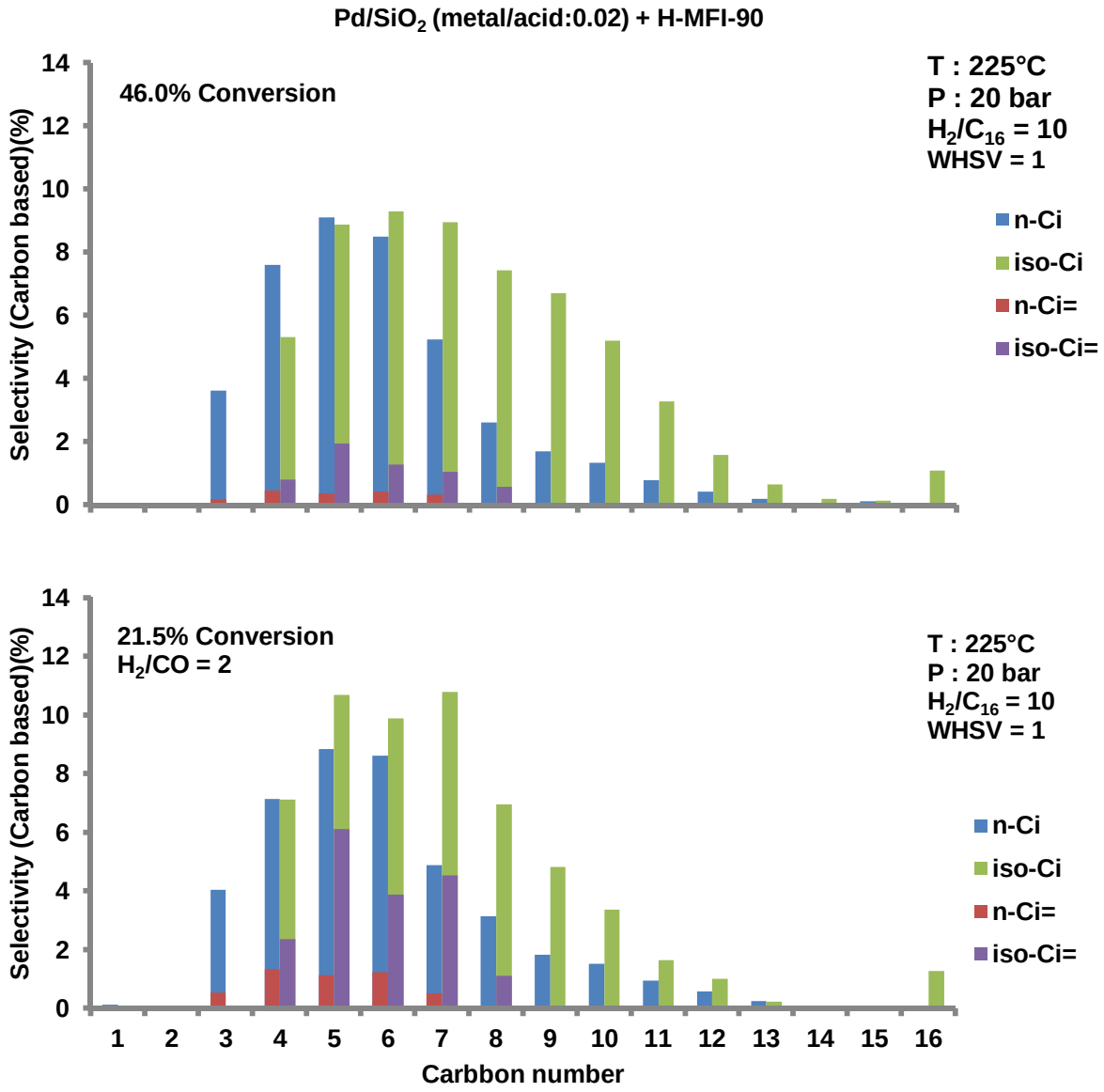

Figure 5.21: Effect of CO on product selectivities over Pd/SiO_2 (metal/acid:0.02)+ H-MFI-90 catalyst

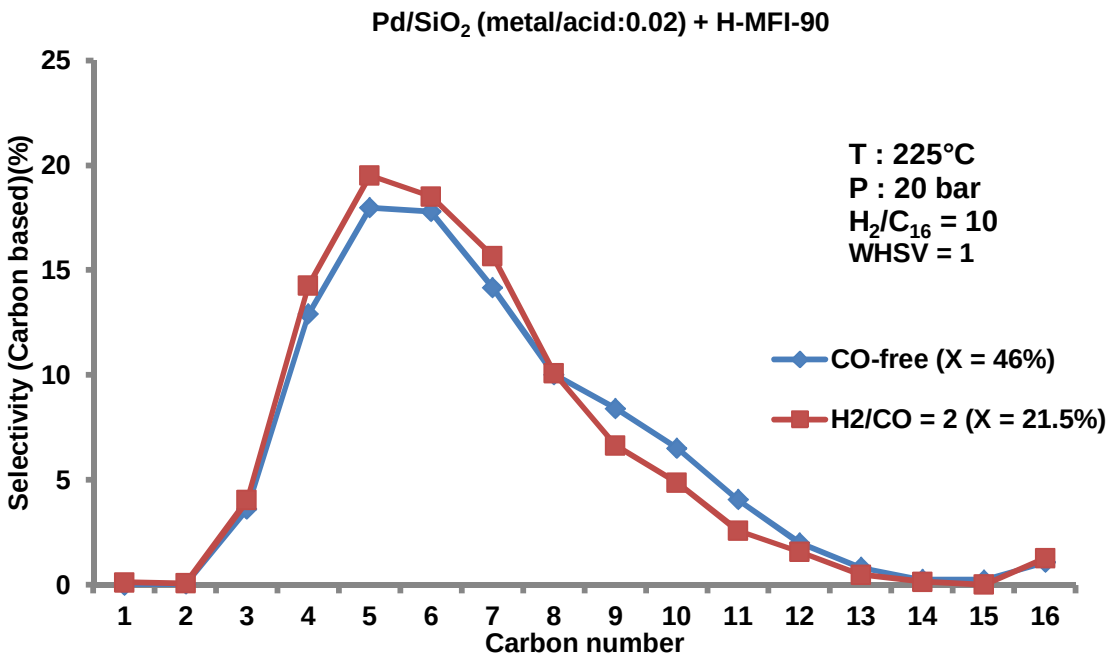

Figure 5.22: Effect of CO on Pd/SiO_2 (metal/acid:0.02) + H-MFI-90 product carbon number

.

Table 5.7: Effect of CO on Olefin Selectivity over Pd (225°C, 20 bar, H_2/C_{16} = 10, H_2/CO = 2, WHSV = 1)

Standard % Selectivity (46% Conversion)	% Selectivity with CO co-feed (21.5 % Conversion)
7.4	22.8

5.2.2.4 Effect of CO on H-MFI-90 Zeolite without Metal Co-Catalyst

The effect of CO on H-MFI-90 performance is presented in Table 5.8 and Figures 5.23 (product carbon number distribution) and 5.24 (product selectivity), respectively.

Table 5.8: Conversion over H-MFI-90 with CO co-feed (225°C, 20 bar, H_2/C_{16} = 10, H_2/CO = 2, WHSV = 0.25)

Feed	Conversion, mean (μ) (%)	Standard deviation (σ) (%)
C_{16}: 0.01 ml/min	53	1.26
C_{16}: 0.01 ml/min, H_2/CO = 2	58	0.75

The conversion over H-MFI-90 increases slightly upon the introduction of CO from about 53% to 58% as shown in Table 5.8. The product carbon number distribution (Figure 5.23) does not change noticeably with CO introduction. Even so, it is noticeable that over H-MFI-90 alone, there is a distinct enhancement of C_8 selectivity (Figures 5.13 and 5.23) versus all catalysts involving a metal co-catalyst (Figures 5.7, 5.8, 5.11, 5.18, 5.20 and 5.22).

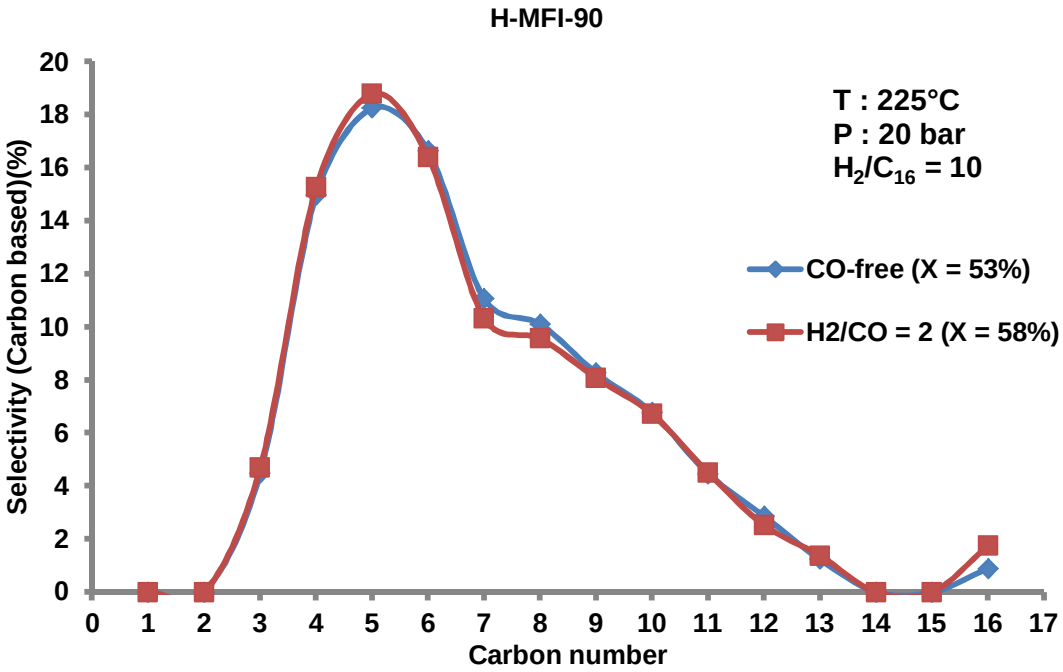

Figure 5.23: Effect of CO over H-MFI-90 product carbon number distribution

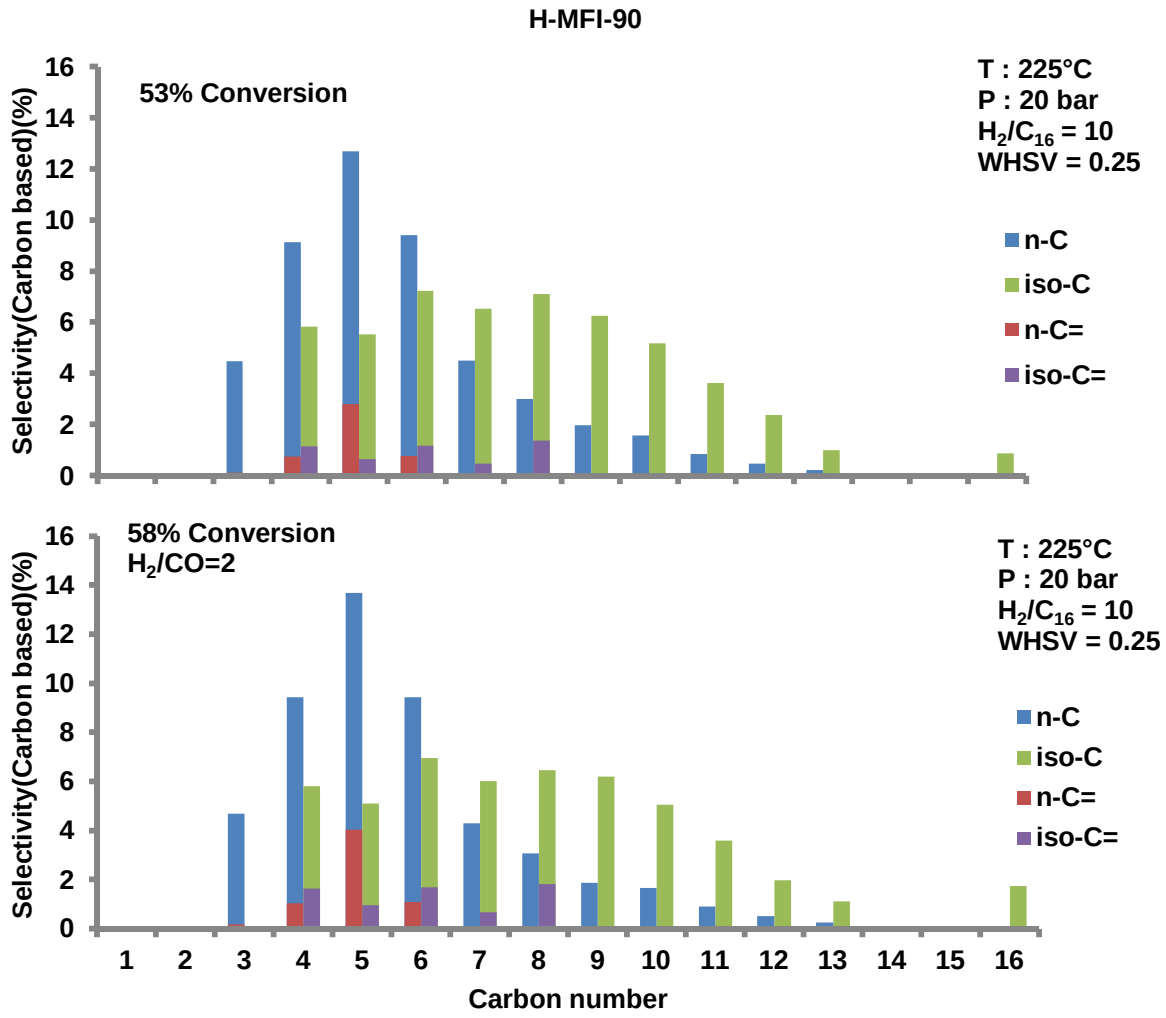

Figure 5.24: Effect of CO on product selectivities over H-MFI-90 catalyst

From Figure 5.24, total olefinicity of the product is clearly unaffected by CO introduction.

5.3 Impregnated Palladium Catalysts

Impregnated Pd/H-MFI catalysts were prepared via the incipient wetness method (section 4.6.2) at Pd loadings of 0.3 wt%, 0.6 wt%, 0.9 wt% and 1.2 wt%, and tested at the same conditions as applied for the segregated catalysts of section 5.2. Conversion versus space velocity findings are presented in Figure 5.25.

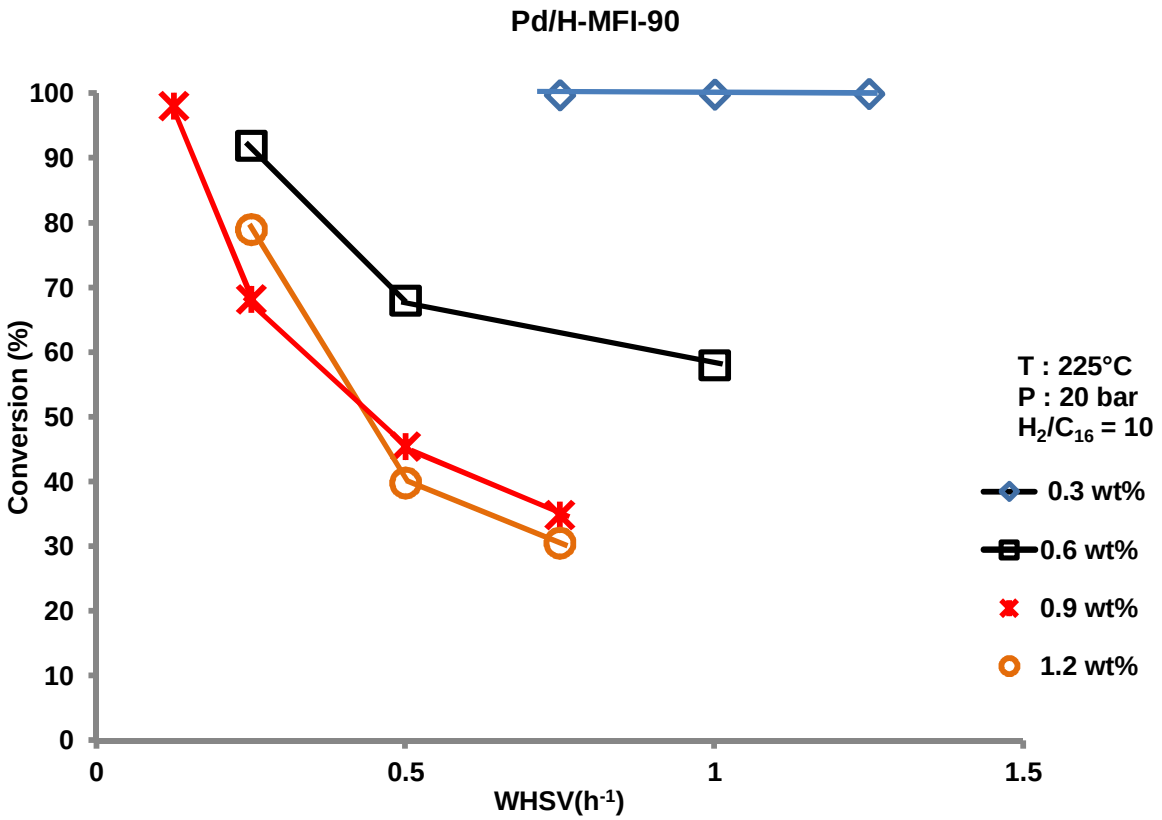

Figure 5.25: Conversion vs space velocity data for impregnated Pd/H-MFI-90 Catalysts

For the impregnated catalyst a decrease in conversion is observed as metal loading is increased. This is seen from Figure 5.25 and is completely contrary to what was observed for the segregated catalysts.

Detailed performance data for the 0.6 wt%, 0.9 wt% and 1.2 wt% Pd/H-MFI-90 catalysts, notably product selectivities and carbon number distributions, are presented for standard hydrocracking conditions and in the presence of CO, in sections 5.3.1 and 5.3.2 respectively.

5.3.1 Standard Hydrocracking

5.3.1.1 0.6 wt% Pd/H-MFI-90

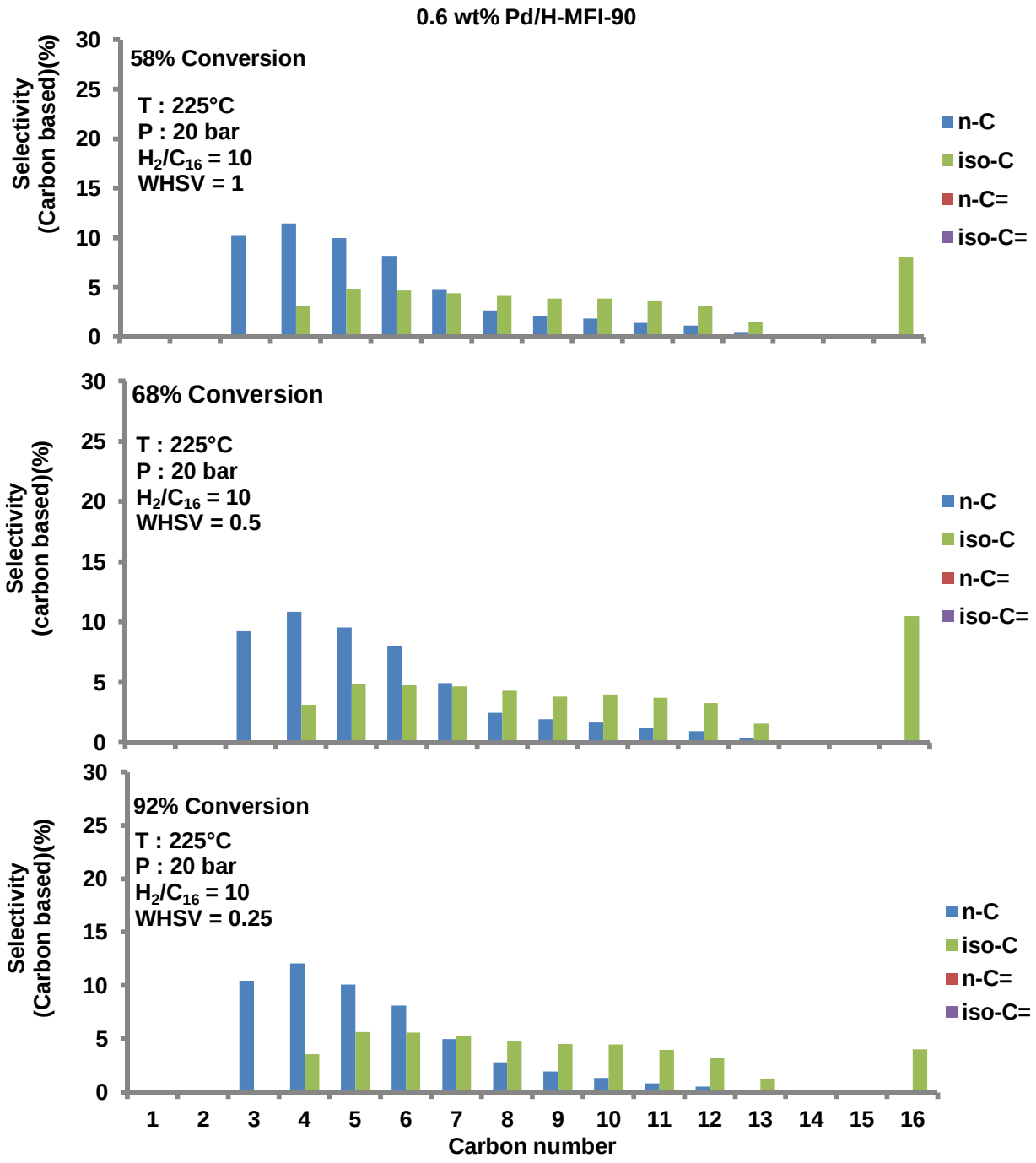

Figure 5.26: 0.6 wt% Pd/H-MFI-90 product selectivity at different space velocities (conversion level)

Figure 5.26 shows that there are no olefins in the product, i.e. all products are saturated. It can be seen from Figure 5.27 that total product distribution peaks at low carbon numbers (C_4-C_6), that secondary cracking is occurring, but that the C_4/C_{12} ratio is substantially lower than for the segregated Pd catalyst of section 5.2.1.3, even at high conversions. Also noticeable, are 'appreciable' amounts of iso-C_{16} in the product which is not the case for the segregated catalysts of section 5.2.1.3. As may be expected, secondary cracking increases as conversion increases, albeit only slightly.

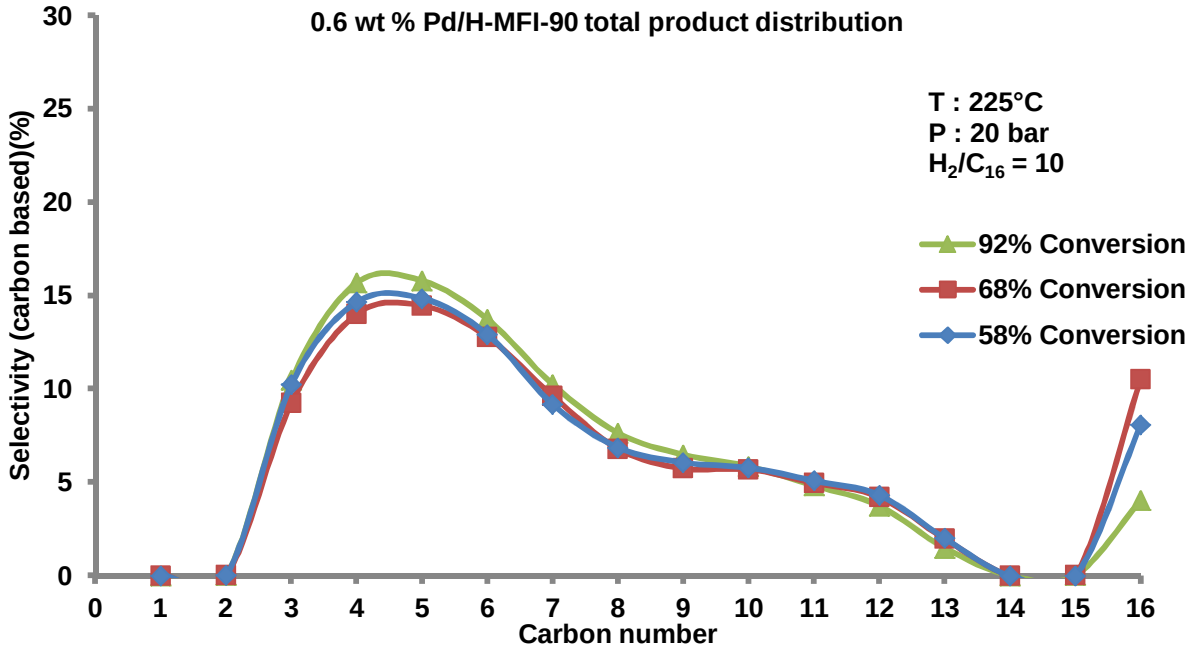

Figure 5.27: Total product carbon number distribution over 0.6 wt% Pd/H-MFI-90

5.3.1.2 0.9 wt% Pd/H-MFI-90

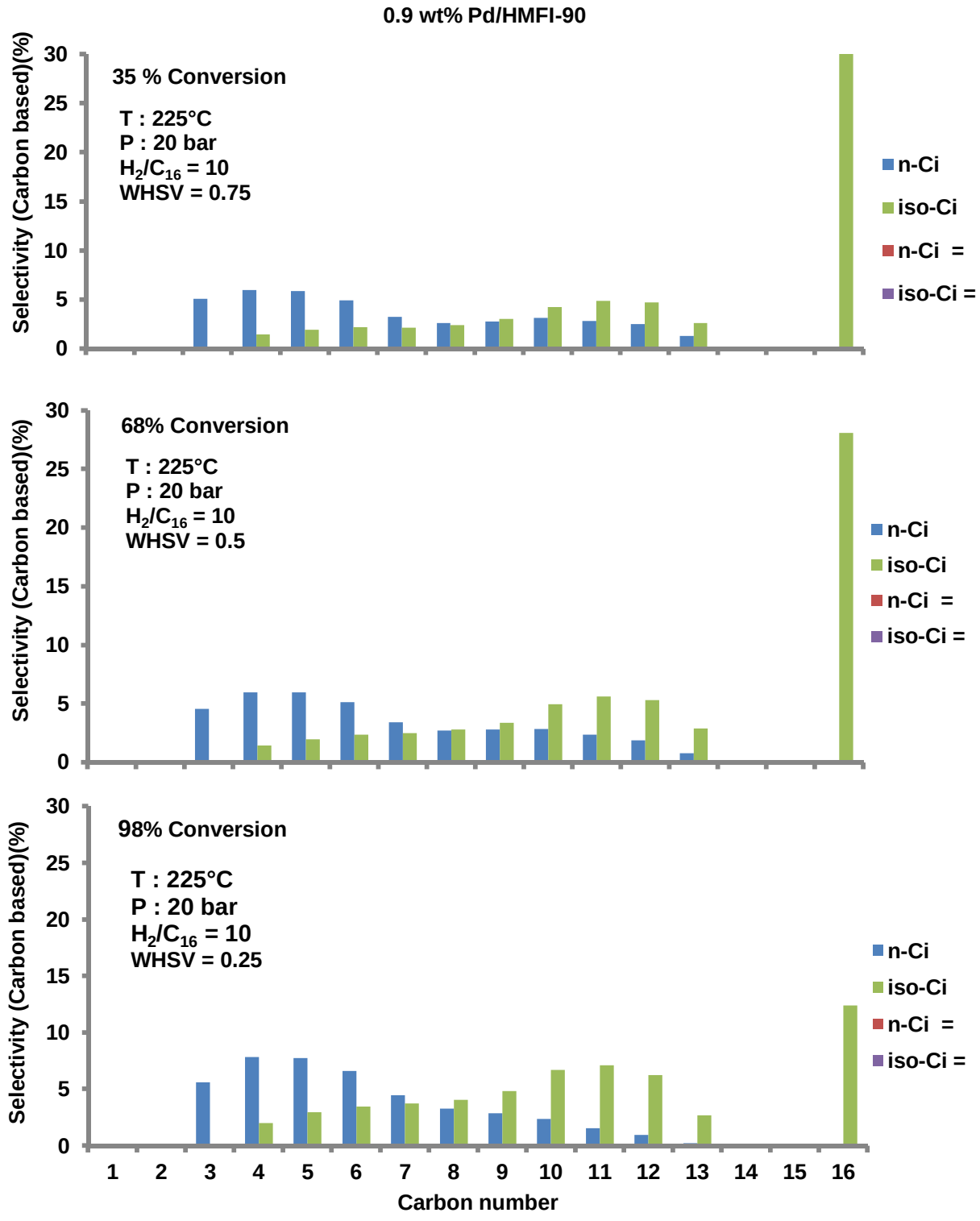

Figure 5.28: 0.9 wt% Pd/H-MFI-90 product selectivity at different space velocities (conversion level)

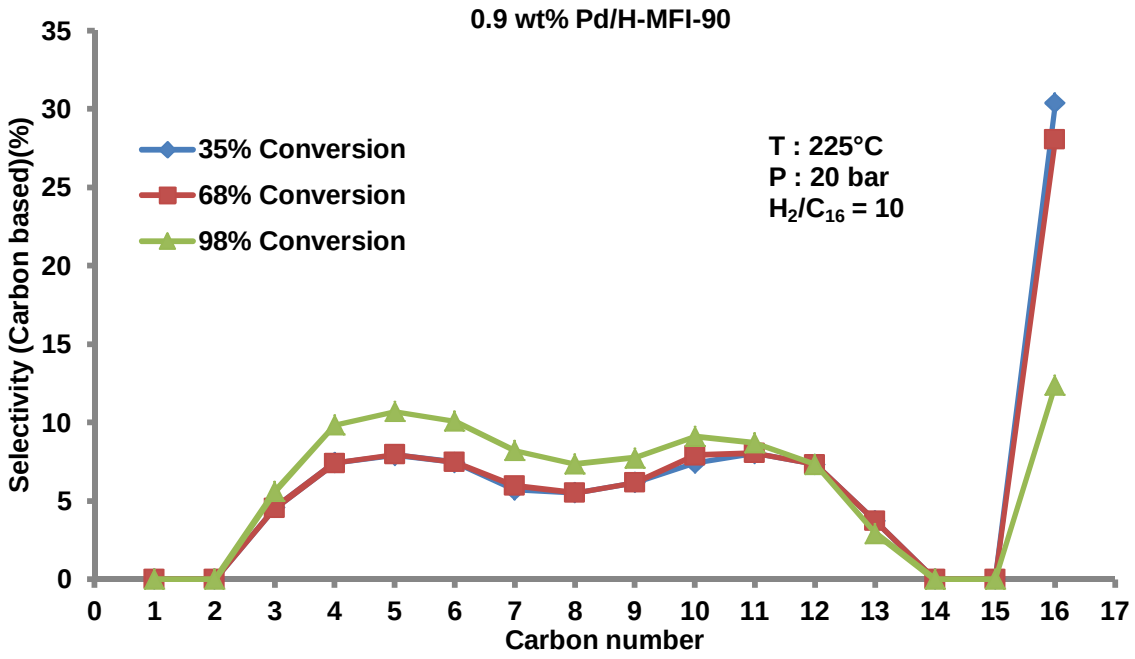

Figure 5.29: Total product carbon number distribution on 0.9 wt% Pd/H-MFI-90

As per the situation with the 0.6 wt% Pd/H-MFI-90 catalyst, no methane (or ethane) nor any olefins, are observed, and substantial amounts of iso-C_{16} appear in the products. At a metal loading of 0.9 wt%, the product distribution is almost uniform over the range C_4-C_{12}, with a C_4/C_{12} ratio of 1.3 at 98% conversion and 1 at 35% conversion. This uniform disitribution over the C_4-C_{12} occurs up to the highest conversion. Also noticeable is the distinct minimum occurring at C_8.

5.3.1.3 1.2 wt% Pd/H-HMFI-90 and comparison of Pd/H-MFI-90 catalysts

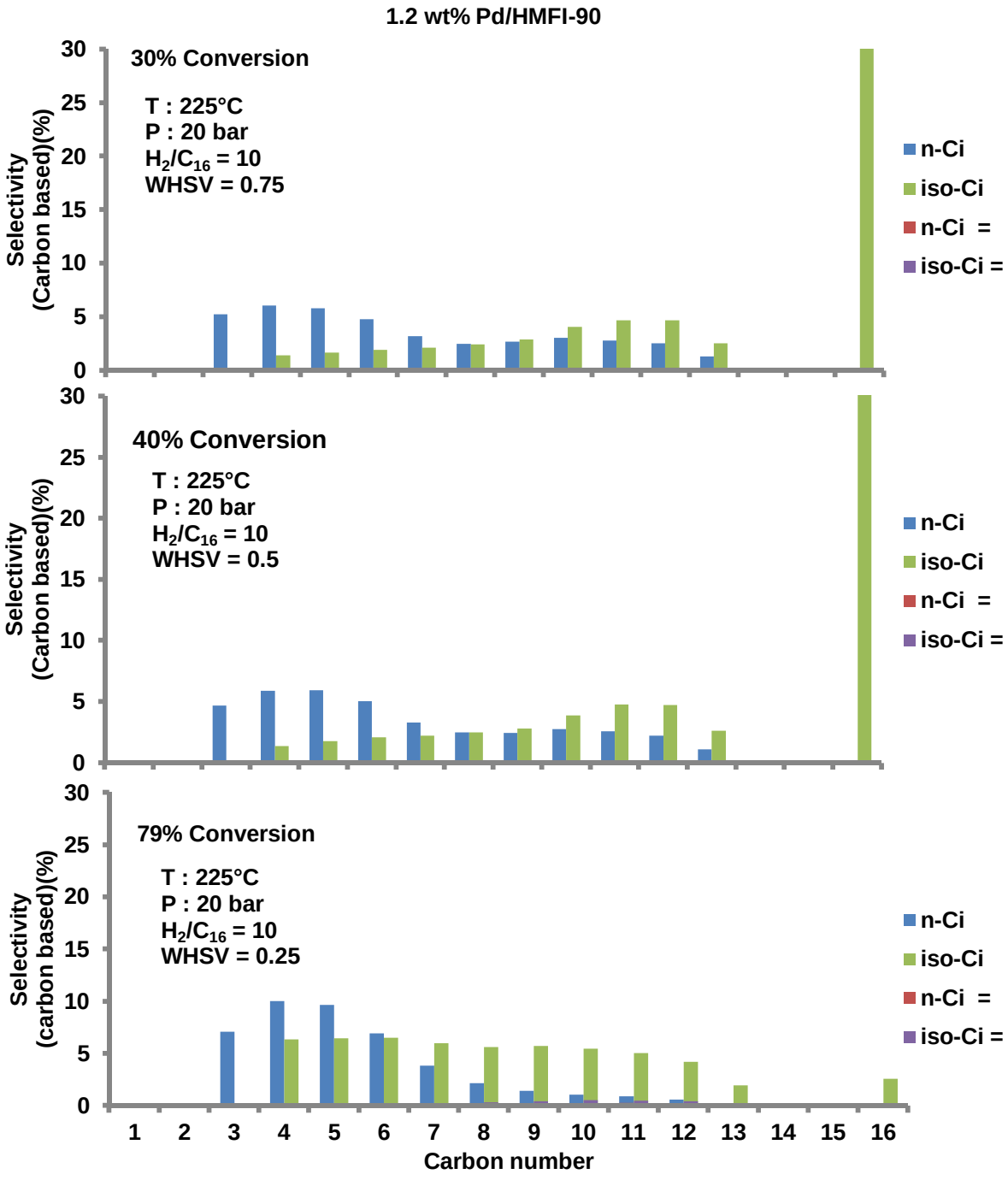

Figure 5.30: Product selectivity over 1.2 wt% Pd/H-MFI-90 at different space velocities (conversion levels)

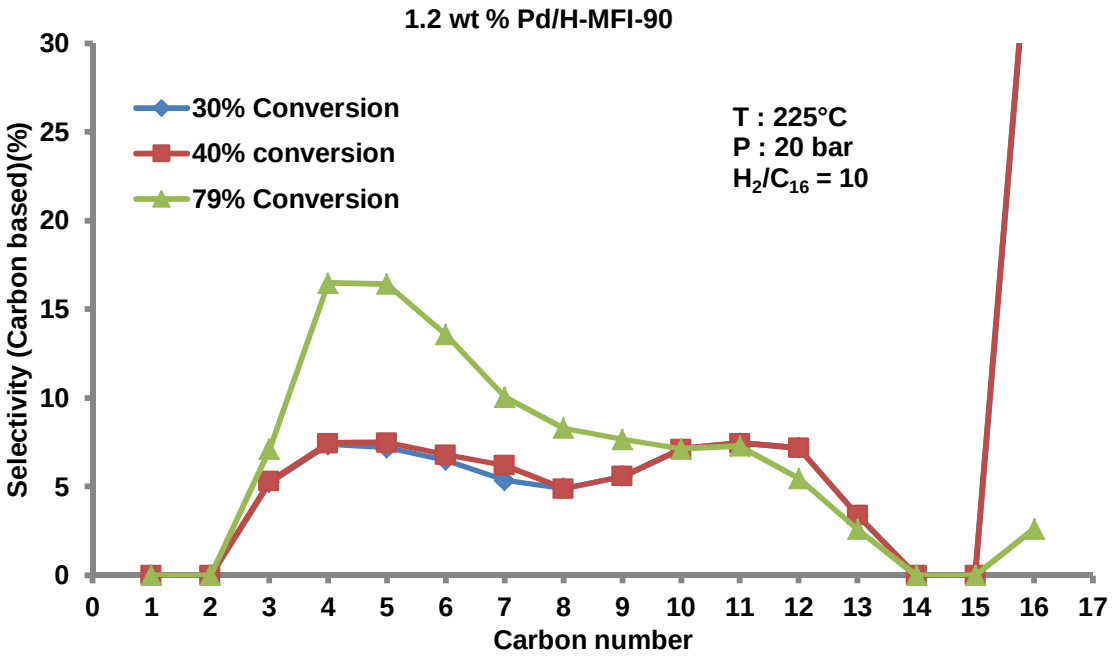

Figure 5.31: Total product carbon number distribution on 1.2 wt% Pd/H-MFI-90

At low conversions the total product carbon number distribution is almost uniform across the range C_4-C_{12} and roughly symmetrical about C_8 as can be seen from Figures 5.30 and 5.31. The C_4/C_{12} ratio at low conversions is 1. At 79% conversion significant secondary cracking sets in, with the C_4/C_{12} ratio equal to 3. The 1.2 wt% catalyst is not as ideal as the 0.9 wt% catalyst, since it is less stable to secondary cracking with increasing conversion. A plot of the Pd/H-MFI-90 catalyst product spectra at similar conversion is presented in Figure 5.32 and from which a plot of the the C_4/C_{12} ratio against metal loading is shown in Figure 5.33.

From Figure 5.33 it is clear that, up to a point, as metal loading increases, the catalyst behaviour moves closer to ideal behaviour producing a product distribution that becomes more symmetrical. When the metal loading was increased further, from 0.9 wt% to 1.2 wt%, additional secondary cracking is again observed. Figure 5.33 further illustrates that increasing metal loading decreases the C_4/C_{12} ratio, bringing the catalyst behaviour closer to ideal behaviour. In Figure 5.33, the C_4/C_{12} ratio data point of the 0.3 wt% catalyst corresponds to a conversion 99.83% and not the 70% conversion at which others are compared. On an ideal hydrocracking catalyst, the C_4/C_{12} ratio is 1 even at high conversions. On a non-ideal catalyst such as the 0.3 wt% Pd/H-MFI-90, the C_4/C_{12} ratio increases with increasing conversion. The C_4/C_{12} ratio of the 0.3 wt% catalyst at 99% conversion represents the upper limit of secondary cracking on the catalyst; it would have been slightly lower at 70% conversion but still significantly higher than 1.

Despite the fact that it is not compared at 70% conversion, this data point cannot be discarded because the trend is still apparent.

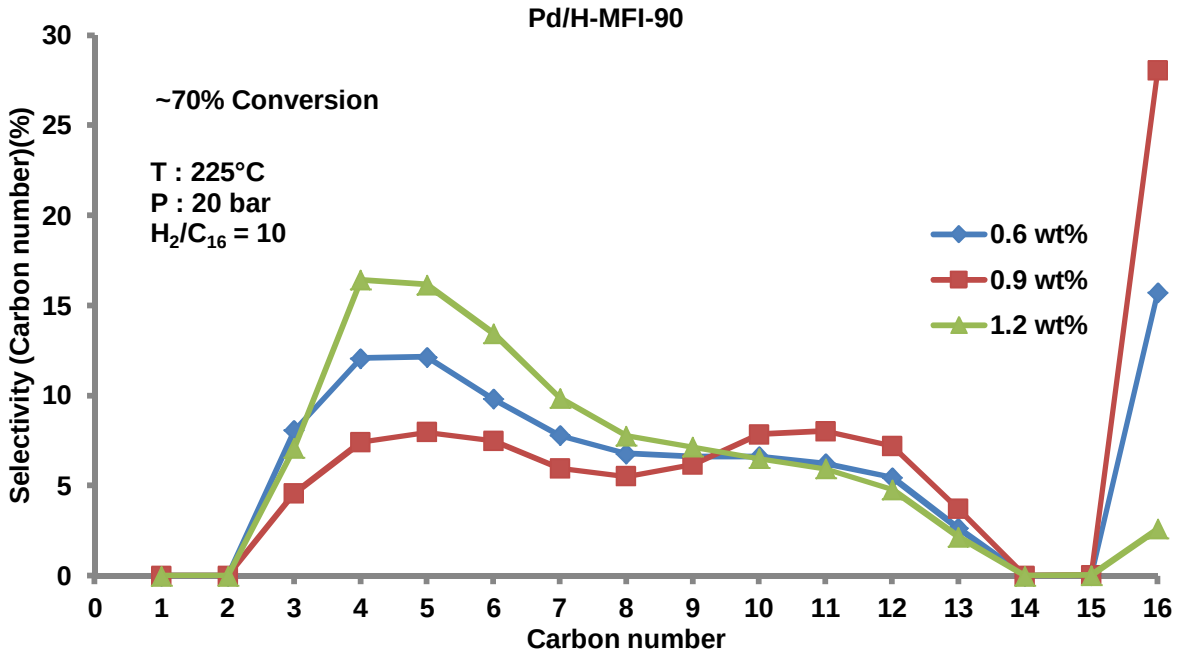

Figure 5.32: Pd/H-MFI-90 catalsys product carbon number distribution compared at equal conversion (~70%)

Figure 5.33 shows that the C_4/C_{12} ratio of the 0.3 wt%, and the 1.2 wt% catalysts is higher than 1, whereas on the 0.9 wt% catalyst the C_4/C_{12} was about 1 up to the highest conversion. This indicates that the 0.9 wt% catalyst best fits the description of an ideal hydrocracking catalyst by Marcilly [2003].

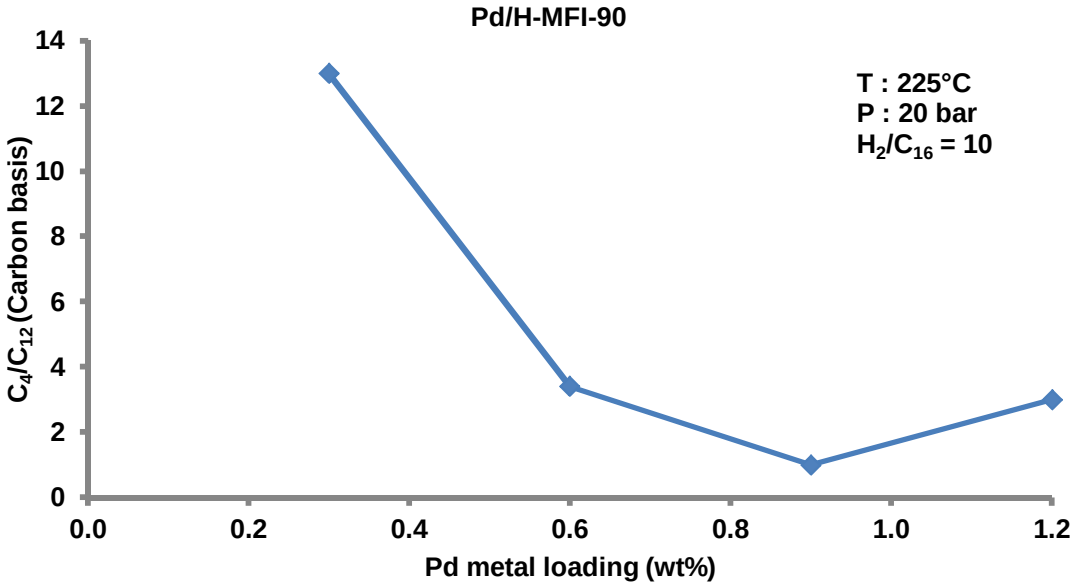

Figure 5.33: Effect of metal loading on Pd/H-MFI-90 catalyst C_4/C_{12} carbon ratio at approximately 70% conversion

5.3.2 Hydrocracking over Impregnated Pd/H-MFI-90 Catalysts in the Presence of CO

Of particular interest is the effect of CO on the performance of the 0.9 wt% catalyst which shows an even product carbon number distribution. Nonetheless, results of the 0.6 wt%, 0.9 wt% and the 1.2 wt% catalysts are presented. The 0.3 wt% catalyst was not evaluated since conversions obtained on that catalyst in the absence of CO were almost 100% as shown in Figure 5.25. The 0.6 wt% catalyst was reduced at 225°C whereas the rest of the catalysts were reduced at 400°C.

5.3.2.1 0.6 wt% Pd/H-MFI-90

Performance data for the 0.6 wt% Pd/H-MFI-90 catalyst in the presence of CO are presented in Table 5.9 (conversion), and Figure 5.34 (product carbon number distribution).

Table 5.9: Conversion over 0.6 wt% Pd/H-MFI-90 in the presence of CO (225°C, 20 bar, H_2/C_{16} = 10, WHSV = 1)[Reduced ad 225°C]

Feed	Conversion, mean (μ) (%)	Standard deviation (σ) (%)
C_{16}: 0.05 ml/min	49	1.5
C_{16}: 0.05 ml/min, H_2/CO = 2	95	0.7

Upon the introduction of CO to the impregnated 0.6 wt% Pd/H-MFI-90 catalyst, conversion increases from 49% to 95% (Table 5.9).

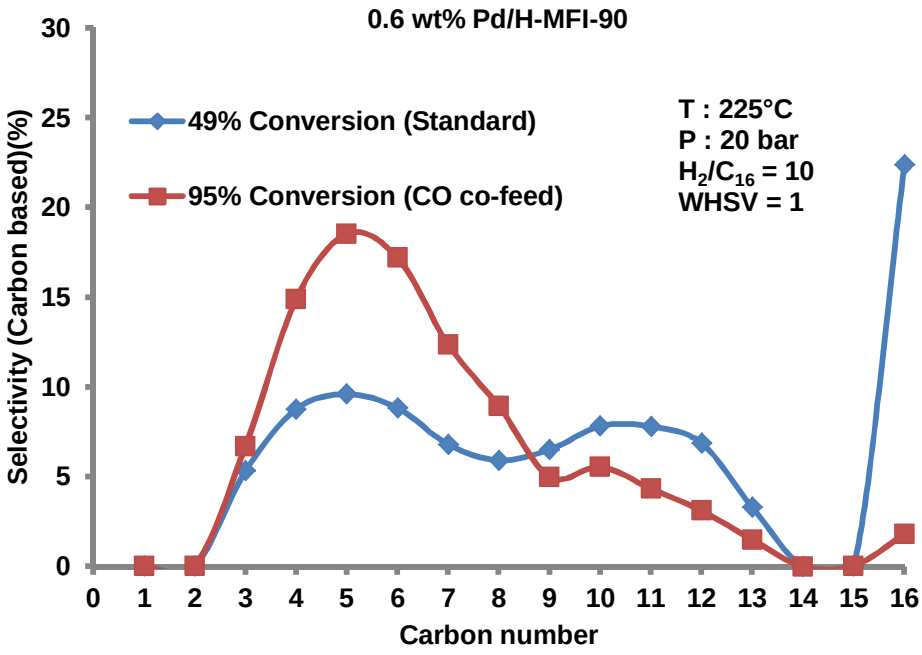

Figure 5.34: Effect of CO on 0.6 wt% Pd/H-MFI-90 total product distribution

It can be seen from Figure 5.34 that introduction of CO also has a dramatic effect on the product distribution, with a large increase in secondary cracking being observed, although this may be an artefact of the higher (~95%) conversion in the presence of CO. The C_4/C_{12} ratio before and after CO co-feeding is 1.8 and 4.8, respectively. Likewise, when CO is introduced, the total olefin selectivity rises from 0% to about 5% as shown in Table 5.10.

Table 5.10: Effect of CO on Olefin Selectivity (0.6 wt% Pd/H-MFI-90) (225°C, 20 bar, H_2/C_{16} = 10, WHSV = 1)[Reduced at 225°C]

Standard Olefin % Selectivity (49% Conversion)	Olefin % Selectivity with CO co-feed (95 % Conversion)
0	4.98

5.3.2.2 0.9 wt% Pd/H-MFI-90

The performance data of a 0.9 wt% Pd/H-MFI-90 catalyst in the presence of CO are presented in Tables 5.11 (conversion) and 5.12 (olefin selectivity), and in Figure 5.35 (product carbon number distribution).

Table 5.11: Conversion over 0.9 wt% Pd/H-MFI-90 (225°C, 20 bar, H_2/C_{16} = 10, WHSV = 0.75)

Feed	Conversion, mean (μ) (%)	Standard deviation (σ) (%)
C_{16}: 0.06 ml/min	35	0.4
C_{16}: 0.06 ml/min, H_2/CO = 2	87	0.5

Upon the introduction of CO to the 0.9 wt% Pd/H-MFI-90, conversion increases from 35% to 87% (Table 5.11).

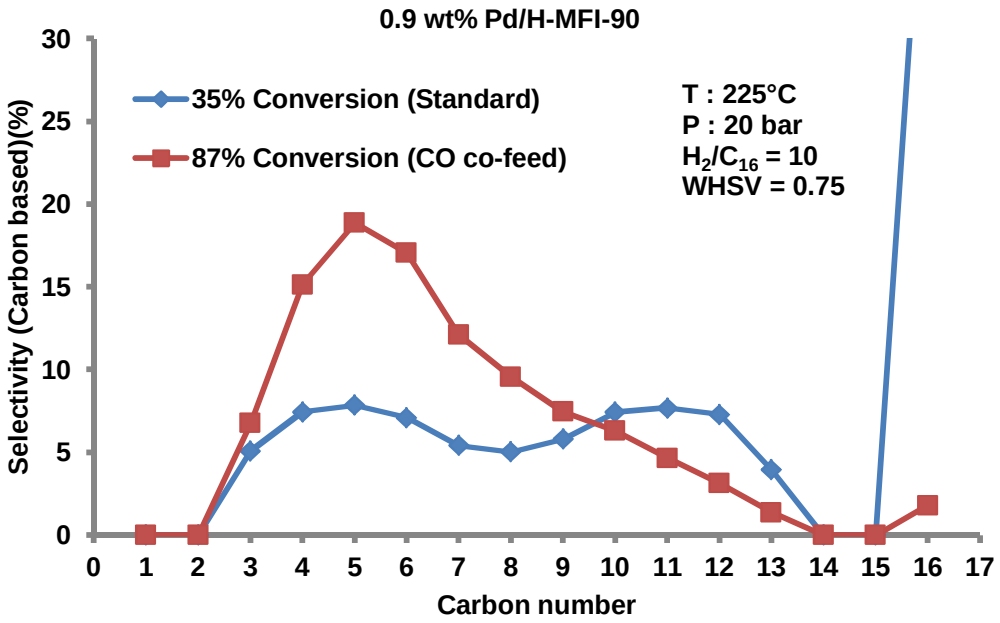

Figure 5.35: Effect of CO on 0.9 wt% Pd/H-MFI-90 total product distribution

Upon introducing CO, extensive secondary cracking sets in (Figure 5.35) over the 0.9 wt% Pd/H-MFI-90 catalyst, also olefins appear in the product spectrum when CO is introduced as shown in Table 5.12, suggesting that some of the metal hydrogenation function is deactivated. The C_4/C_{12} ratio, when CO is introduced increases from approximately 1 to 5.

Table 5.12: Effect of CO on Olefin Selectivity (0.9 wt% Pd/H-MFI-90) (225°C, 20 bar, H_2/C_{16} = 10, WHSV = 0.75)

Standard % Selectivity (35% Conversion)	% Selectivity with CO co-feed (87 % Conversion)
0	4.5

5.3.2.3 1.2 wt% Pd/H-MFI-90

The non-ideal 1.2 wt% catalyst was also tested in the presence of CO, the over view of the experiment is shown in Table 5.13.

Table 5.13: Conversion over 1.2 wt% Pd/H-MFI-90 (225°C, 20 bar, H_2/C_{16} = 10, WHSV = 0.75)

Feed at	Conversion, mean (μ) (%)	Standard deviation (σ) (%)
C_{16}: 0.06 ml/min	31	1.3
C_{16}: 0.06 ml/min, H_2/CO = 2	75	0.9

Upon the introduction of CO to the 1.2 wt% Pd/H-MFI-90, conversion increases from 31% to 75% Table 5.13.

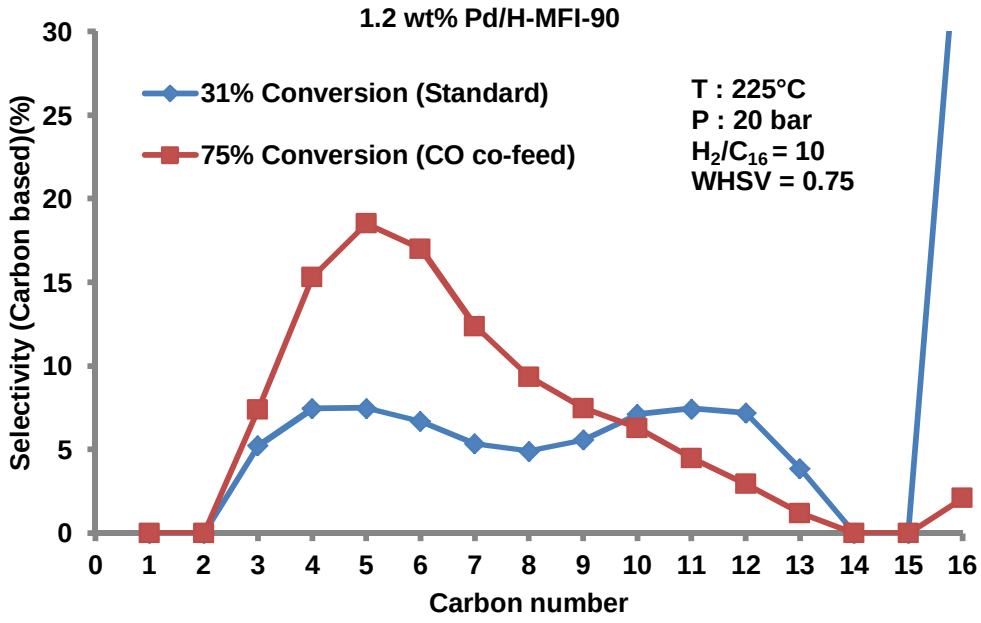

Figure 5.36: Effect of CO on 1.2 wt% Pd/H-MFI-90 total product distribution

Upon introducing CO, extensive secondary cracking sets in (Figure 5.36) over the 1.2 wt% Pd/H-MFI-90 catalyst, also olefins appear in the product spectrum when CO is introduced as shown in Table 5.14, suggesting that some of the metal hydrogenation function is deactivated. The C_4/C_{12} ratio, when CO is introduced increases from approximately 1 to 5.

Table 5.14: Effect of CO on Olefin Selectivity
(225°C, 20 bar, H_2/C_{16} = 10, WHSV = 0.3)

Standard % Selectivity (31% Conversion)	% Selectivity with CO co-feed (75 % Conversion)
0	4.6

5.3.2.4 Effect of Reduction Temperature on Pd/H-MFI-90 Catalyst Performance

The 0.9 wt% Pd/H-MFI-90 catalysts was pre-treated differently before testing to determine the effect reduction temperature has on the activity and selectivity of the impregnated hydrocracking catalyst. After drying, the catalyst was reduced in a hydrogen stream at reaction temperature (225°C) while all other conditions remained the same. The results of the catalysts reduced at reaction temperature and those reduced at 400°C are shown in Figures 5.37 and 5.38.

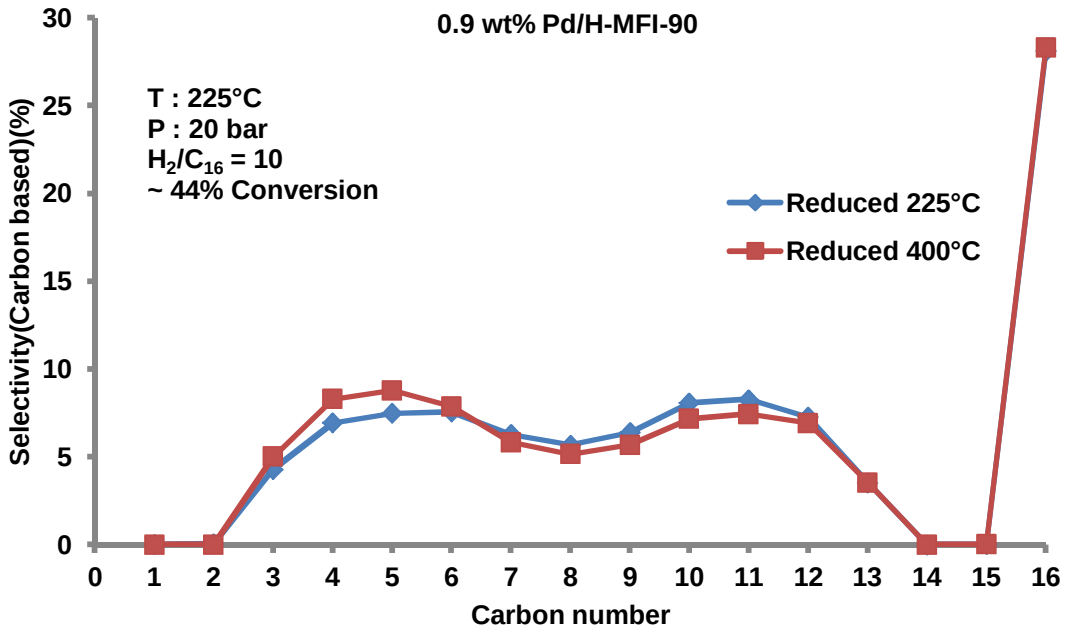

Figure 5.37: Comparison of product carbon number distribution at similar conversions for 0.9 wt% Pd/H-MFI-90 reduced at 225°C and 400°C.

The C_4/C_{12} ratio for the 0.9 wt% Pd/H-MFI-90 catalyst increases only marginally (from 1 to 1.3) upon an increase in reduction temperature from 225°C to 400°C. The total product carbon number distribution of the catalyst reduced at 400°C shows more secondary cracking than that of the catalyst reduced at reaction temperature (225°C), as can be seen from Figure 5.37. Figure 5.38 presents conversion against weight hourly space velocity. It can be seen that the activity of the 0.9 wt% catalyst is improved when reduction temperature is lower (225°C).

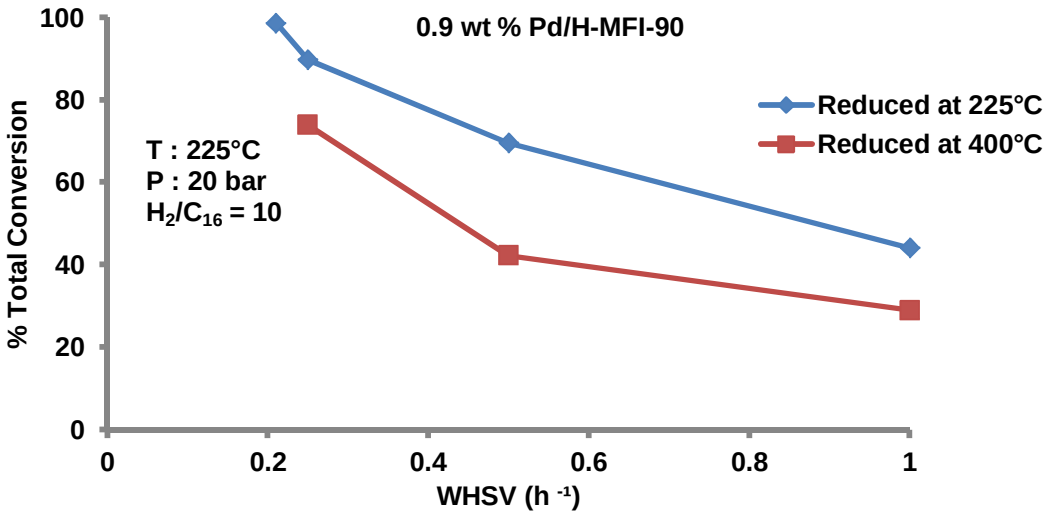

Figure 5.38: Conversion vs WHSV over 0.9 wt% Pd/H-MFI-90 reduced at different temperatures

6 Discussion

6.1 H-MFI-90 without Metal Function

The zeolite without any metal loaded was active and showed a typical cracking product distribution. This shows that even without the metal, at the LTFT reaction conditions employed, the zeolite is able to crack n-paraffins, presumably by acid cracking. However, the low olefin content observed seems to suggest that hydrocracking has a contribution to the observed product distribution. If a zeolite were to crack an n-parrafin without a metal function, the product would comprise of an olefin and paraffin. If the olefin product undergoes secondary cracking, the total cracked product spectrum will consist of paraffin and three olefins. This means that the observed product should be at least 75% olefins. The H-MFI-90 experiment showed 13% olefin content, despite prevalent secondary cracking. There are two possibilities to explain these results; the reactor wall (stainless steel) could be activating hydrogen/de-hydrogenating n-C_{16} or some olefins are dehydrogenated and deposited as coke on the zeolite, resulting in a more paraffinic product. A calculation of the possible amount of coke formed on the zeolite was undertaken. The calculated rate of formation was 0.00009 g/min at 18% conversion, 0.00013 g/min at 23% conversion and 0.00031 g/min at the highest conversion (about 52%) [See calculation in appendix]. If coke formation was occurring at 0.00031 g/min, a decline in catalyst activity should have been observed over the three days in which the experiment was run. No decline in activity was observed.

Blank experiments were carried out to evaluate the possibility of feed dehydrogenation on the reactor wall. The reactor was packed with SiC only (no catalyst) and run at standard hydrocracking conditions (20 bar, 225°C and H_2/n-C_{16} = 10). No olefins were detected in the reactor product. To rule out the activation of hydrogen by the reactor wall, the hydrocracking experiment would have to be carried out in a quartz reactor - an experiment which was not conducted.

When CO was introduced to the experiment with only the H-MFI-90 catalyst, the product distribution was essentially the same as that of the experiment without CO, although a slight increase in activity was observed in the presence of CO. Given that the total pressure of the system was kept constant for these experiments, the introduction of CO reduces the hydrogen partial pressure in the system, and since the hydrogen partial pressure is known to be inversely proportional to the hydrocracking reaction rate [Thybaut et al., 2005] the slight increase in activity on the H-MFI-90 upon the introduction of CO is ascribed to this phenomenon.

Thus, whereas it is unclear why the olefin content from the pure zeolite reaction is as low as it is and what mechanism prevails, the level of zeolite activity is low compared to the segregated catalysts or impregnated catalysts and thus the performance of these latter (metal-free) catalysts did not dominate the findings derived from the metal + zeolite and metal/zeolite catalysts.

6.2 Segregated Catalyst Performance

The activity of all segregated catalysts increased with increasing metal loading (i.e. increasing metal/acid site ratio). This means that the metal function was rate limiting and that the metal/ acid site 'balance' is dominated by the catalyst acidity. It was only for the Pd/SiO_2 + H-MFI-90 catalyst, at values of the metal/acid ratio higher than 0.1 that the activity (total conversion) of the catalyst did not increase further. In this region the metal was no longer limiting the hydrocracking reaction. The same observations were made by Wynne [2014], who used a Pt/SiO_2 + H-MFI-90 catalyst. The product carbon number distributions of all the catalysts tested shows that the product distribution did not change much with metal loading (i.e. with increasing metal/acid site ratio). The product carbon number distribution for all the segregated catalysts lacked symmetry and was peaking in the lower carbon numbers, a sign of secondary cracking. The segregated catalysts exhibited secondary cracking even at values of the metal/acid ratio above 0.1 (on the Pd/SiO_2 + H-MFI-90) which is the region where the activity should supposedly have been controlled by the acid function. Therefore, the occurrence of secondary cracking when the rate was not limited by the metal function indicates that the rate limiting step was not occurring on the acid site either and, for the catalysts of this study, ideal hydrocracking could not be achieved when the two functions were segregated, regardless of the metal co-catalyst used.

Mechanistically, the observations on the effect of metal loading on activity of the segregated catalysts can be explained as follows. According to Coonradt and Garwoods [1964], to prevent secondary cracking, the steady state concentration of olefins supplied by the metal sites is the key. When the concentration assumes its equilibrium value, it is considered high enough to cause rapid desorption of the alkylcarbenium ions from the acid sites through competitive adsorption. Segregating the metal function from the acid increases the diffusion distance for the olefins (according to the classical mechanism) or the activated hydrogen (according to the hydrogen spill over mechanism), generated on the metal sites to the acid sites. The occurrence of secondary cracking indicates that the rate limiting step is not occurring on the acid sites and nor, for metal/acid ratios greater than 0.1, is the metal function limiting. Thus, the only other rate that affects the overall hydrocracking reaction rate is the rate of diffusion of intermediates

between the two catalytic functions. The rate of diffusion becomes limiting when the distance between the metal and the acid sites is too great, resulting in secondary cracking

When CO is introduced, the general trend observed for all segregated catalysts tested was a decrease in activity. Secondary cracking was still prevalent in the presence of CO and all product distributions of all catalysts in the presence of CO were similar to those without CO. The catalysts showed an increase in olefin selectivity suggesting that the metal co-catalyst is partially deactivated.

Deactivation of the metal by CO has been reported in literature by Weiss et al. [1984], Al-Ammar et al. [1978] and Arnold et al. [1997]. They all reported that CO deactivated the metal function by competitive and strong adsorption on the metal sites. This deactivation disturbs the metal/acid ratio, i.e. the further aggravating of the secondary cracking conditions that were already in existence before CO was introduced, as observed in the study. Likewise, in keeping with a deactivation of the metal function by CO, when CO was co-fed, olefin selectivity increased.

6.3 Impregnated Catalyst Performance

For all the impregnated catalysts it was observed that increasing metal loading led to a decrease in activity (total conversion) of the catalyst. This is, at first glance, counter intuitive; one might expect an increase in metal loading to increase the activity of the hydrocracking catalyst, since the initial step in the hydrocracking reaction (paraffin dehydrogenation), occurs on the metal sites. More metal sites available for reaction therefore, should result in increased catalyst activity. The observed decrease in activity is thus postulated to be due to diffusion limitations resulting from metal cluster formation in the zeolite pores, since the H-MFI-90 zeolite does not possess super cages and the metal therefore sits in the channels of the zeolite restricting the diffusion of the feed molecules in the intrachannel spaces.

Generally, the impregnated catalysts showed a markedly higher selectivity toward iso-C_{16}, compared to that seen on any of the segregated catalysts. This is because the distance between the acid and metal functions is decreased on the impregnated catalyst, favouring high isomer yield and less secondary cracking - in keeping with the Weisz intimacy rule.

The cracking reactions in H-ZSM-5 zeolites occur through type C β-scission [Weitkamp et al., 1983]. According to Figure 2.8, the primary products of this type of β-scission are not branched. To account for the degree of branching in the product, Weitkamp et al. [1983] suggested secondary isomerization, i.e. skeletal rearrangement of the cracked product after primary cracking occurs. It is reasonable to assume that this secondary isomerization is influenced by

competitive adsorption at the acid sites [Coonradt and Garwood, 1964]. Due to the occurrence of competitive adsorption on the acid sites, the occurrence of secondary isomerization increases with increasing carbon number of the cracked product [Weitkamp et al., 1983]. Weitkamp et al. [1983] reported observing distinct minima in the product distributions on Pt/H-ZSM-5 and Pt/H-ZSM-11 catalysts for the conversion of n-decane. This minima, which shows the low probability of centre cleavage of hydrocarbon molecules, is a general feature of hydrocracking in Pt/H-ZSM-5 catalysts [Weitkamp et al., 1983]. The same minima was observed in this study. The distinct minima is very clear to see in the data from the 0.9 wt% Pd/H-MFI-90 catalyst. Weitkamp et al. [1983] suggested that for reasons unknown, cleavage near the edge of the carbon skeleton may very well be favoured in pentasil zeolites [Weitkamp et al., 1983].

When the metal loading was increased from 0.9 wt% to 1.2 wt%, secondary cracking increased (Figure 5.31). From observations made earlier, the distance between the metal and the acid sites is key to controlling secondary cracking. A possible explanation for the increased secondary cracking could stem from the temperature at which the catalyst was reduced (400°C) and the amount of metal loaded by ion exchange into the zeolite. When the metal is impregnated into the zeolite and reduced at high temperatures such as 400°C, the metal crystallites tend to sinter, resulting in a reduction of the surface area of the active metal [Scherzer and Gruia, 1996]. A reduction in surface area means the Pd clusters formed are large, resulting in an increase in the distance between the metal and acid sites which, in turn, results in increasing secondary cracking. A 0.9 wt% Pd loading is the maximum ion exchange limit of the H-MFI-90 zeolite. Above 0.9 wt% loading (e.g 1.2 wt%), the metal exceeds that limit resulting in Pd being in excess relative to the number of anions in the zeolite. It is proposed that this excess Pd in combination with the high reduction temperatures causes more sintering to occur in the 1.2 wt% catalyst than in the 0.9 wt% catalyst.

The impregnated catalysts also exhibit zero olefin selectivity. It follows that impregnating the metal function serves to reduce the diffusion distance of the species (activated hydrogen or olefins) between the two sites. When the number of metal sites is optimal, in the absence of diffusion limitations, an adequate supply of activated species to the acid sites will occur, which in turn assists rapid desorption of the primary products and the hydrogenation of olefins resulting in close to ideal behaviour as seen on the 0.9 wt% Pd/H-MFI-90 catalyst.

Co-feeding CO results in the activity of the impregnated catalysts approximately doubling (from 35% to about 87%, Figure 6.1). The activity of the 0.9 wt% Pd/H-MFI-90 catalyst, in the presence of CO, corresponds to the activity of a Pd/H-MFI-90 catalyst with a lower Pd loading (in the range 0.3 – 0.4 wt% Pd) as shown in Figure 6.1, suggesting CO in some way ‘deactivates’ some of the Pd active sites.

Decreasing the number of active Pd sites causes a deficiency in activated hydrogen or intermediate olefins, supplied to the acid sites, resulting in secondary cracking. The total product carbon number distribution of the 0.9 wt% Pd/H-MFI-90 in the presence of CO was similar to that of the catalysts with lower Pd loadings in the absence of CO. A comparison of the product carbon number distribution of the 0.9 wt% Pd/H-MFI-90 with CO co-feeding and that of 0.3 wt% Pd/H-MFI-90 catalyst without CO co-feeding is presented in Figure 6.2.

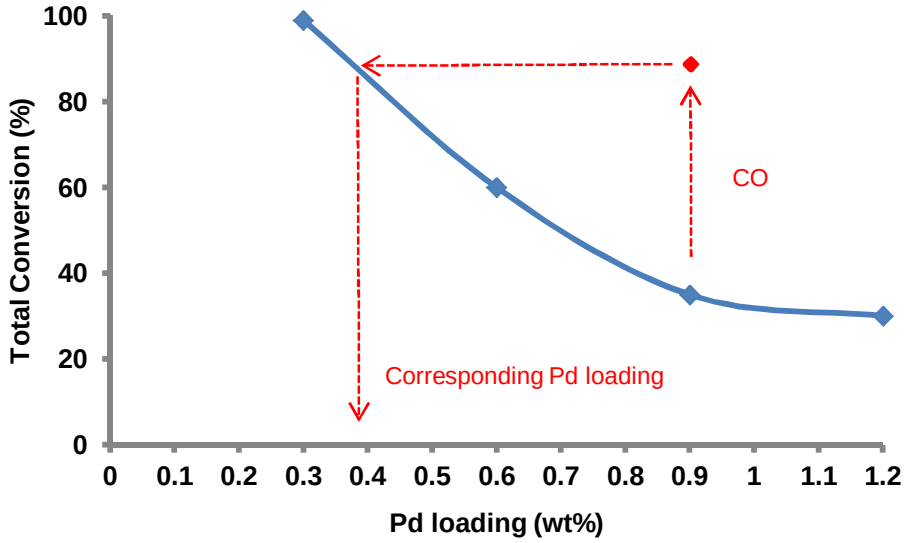

Figure 6.1: Effect of CO on the effective Pd loading on a 0.9 wt% Pd/H-MFI-90 hydrocracking catalyst. [225^{0}C, 20 bar, H_2/C_{16} = 10, WHSV = 0.75]

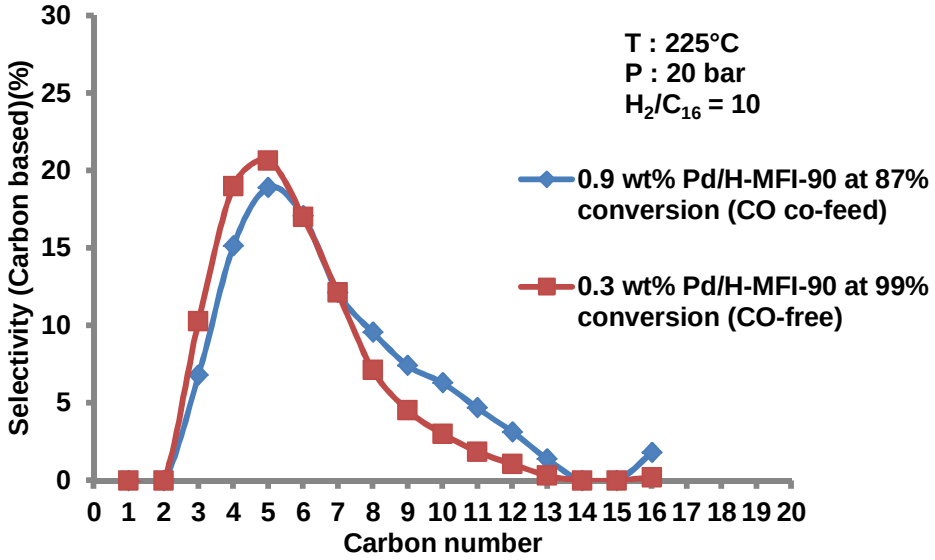

Figure 6.2: Effect of CO co-feeding on the product carbon number distribution of the 0.9 wt% Pd/HMFI-90 catalyst

The effect of metal loading on catalyst activity is clear, (Figure 6.1) - increasing metal loading decreases catalyst activity. If the suggested reason for this trend is true, it follows from Figure 6.1 that the introduction of CO reduces the effective amount of metal in the zeolite channels since the activity of the 0.9 wt% catalyst is similar to that of a catalyst with a lower metal loading. It may further be postulated that CO facilitates the migration of some of the Pd to the external surface of the zeolite therefore reducing the diffusional resistance introduced by such metal clusters in the zeolite channels, resulting in an increase in activity of the hydrocracking catalyst - although conclusive evidence for this postulation would require direct diffusion measurements.

The decrease in the number of metal sites also means the hydrogenation/dehydrogenation activity of the metal co-catalyst decreases, consistent with the increase in olefin selectivity over the impregnated hydrocracking catalysts when CO is co-fed (Table 5.12).

Results show that the activity of the 0.9 wt% Pd/H-MFI-90 catalyst, reduced at 225°C, was higher than that of the same catalyst reduced at 400°C. It is known that stable and well dispersed Pd clusters are formed in the zeolite channels when the catalyst is reduced at temperatures lower than 350°C, whereas above 350°C Pd_6 clusters migrate to the external surface of the zeolite [Okumura et al., 2004]. Improved dispersion implies that smaller stable metal clusters are formed, not only increasing the metal sites available for reaction, but also reducing diffusional limitations, both of which favour higher activity.

When reduction temperature is lowered from 400°C to 225°C, less secondary cracking (i.e decrease in C_4/C_{12} ratio) and an increase in activity are observed, from which it can be concluded that the Pd is better dispersed in the zeolite channels when reduced at 225°C than it is when reduced at 400°C. This conclusion is in agreement with the findings of Okumura et al. [2004] that showed the effect of reduction temperature on dispersion of Pd in ZSM-5 zeolites.

7 Conclusion

This work shows that on a segregated hydrocracking catalyst, at high metal/acid site ratios or metal loadings, the activity of the catalyst no longer increases, but secondary cracking still prevails. It can be concluded from these observations that the rate limiting step does not occur on the metal or the acid sites but that the performance is limited by the inter-site diffusion resistance. On an ideal hydrocracking catalyst, the rate limiting step occurs on the acid sites and there is no secondary cracking. On a non-ideal hydrocracking catalyst the rate limiting step does not occur on the acid sites and secondary cracking occurs. It follows that a segregated hydrocracking catalyst is not an ideal hydrocracking catalyst.

It was observed that co-feeding CO to the segregated hydrocracking catalyst not only aggravates the already prevalent secondary cracking, but also results in a loss of activity on the segregated hydrocracking catalyst. It has been shown in this work that co-feeding CO to the segregated catalyst poisons the metal function, which consequently reduces the number of active metal sites resulting in intensified secondary cracking and the loss of activity.

When the noble metal is impregnated, increasing metal loading decreases the activity of the hydrocracking catalyst. This is thought to be due to diffusional limitations the impregnated metal clusters introduce in the channels of the H-MFI zeolite.

When the noble metal co-catalyst is impregnated onto the zeolite, increasing metal loading on the zeolite from 0.3 wt% to 0.9 wt% Pd decreases secondary cracking. This is because the probability of intermediates seeing more acid sites before a metal site is very low for a higher metal loading than it is for a lower metal loading. Only at a Pd loading of 0.9 wt%, did secondary cracking not occur even at the highest conversion. Therefore almost ideal hydrocracking was achieved at this loading. To obtain such catalyst performance, sufficient metal must be loaded on the zeolite ensuring that the two types of active sites are as close as possible to each other.

Co-feeding CO to the impregnated hydrocracking catalyst results not only in a big increase in activity, but also introduces or exacerbates secondary cracking. Taking the almost ideal 0.9 wt% Pd/H-MFI-90 catalyst as an example, in the presence of CO its activity almost doubled and substantial secondary cracking was introduced. It is shown in earlier observations of this work that, in the absence of CO, the lower the metal loading, the higher the activity of the catalyst. When the conversion of the 0.9 wt% catalyst in the presence of CO is similar to that of a catalyst with a lower metal loading in the absence of CO, their product distributions are found to be very similar. From these observations, it is postulated that CO causes the impregnated metal to migrate and form clusters on the zeolite external surface, resulting in a reduction in diffusion

limitations and also a reduction in the ability of the noble metal to provide activated intermediate species. When diffusion limitations caused by the metal clusters are reduced, the activity of the catalyst increases, as does secondary cracking.

When the reduction temperature of the ideal catalyst is lowered from 400°C to 225°C without changing the metal loading, the activity of the catalyst increases and secondary cracking decreases. From these observations it is concluded that the Pd metal is better dispersed in the zeolite when reduced at 225°C than it is when reduced at 400°C.

References

Akhmedov, V.M. and Al-Knerahowaiter, S.H., 2002. Recent Advances and Future Aspects in the Low-Temperature Conversion of Saturated Hydrocarbons. Catalysis Reviews: Science and Engineering, volume 44, pp. 455-498

Al-Ammar, A. S., Webb, G., 1978. Hydrogenation of Acetylene over Supported Metal Catalysts. Part 1. Adsorption of [^{14}C]Acetylene and [^{14}C]Ethylene on Silica Supported Rhodium, Irridium and Palladium and Alumina Supported Palladium. Journal of Chemical Society, Faradaya Transcations, volume 75, pp. 2165-2186

Alvarez, F., Ribeiro, F. R., Perot, G., Thomazeau, C., Guisnet, M., 1996. Hydroisomerisation and Hydrocracking of Alkanes: 7. Influence of the Balance Between Acid and Hydrogenating Functions on the Transformation of n-Dodecane on Pt/H-Y Catalysts. Journal of Catalysis, volume 162, pp. 179–189

Arnold, H., Döbert, F., Gaube, J., 1997. Handbook of Heterogenous Catalysis. VCH Verlagsgesellschaft GmbH, Weinheim, volume 5, pp. 2165-2186

Benazzi, E., Leite, L., Marchal-George, N., Toulhoat, H., Rayband, P., 2003. New Insights into Parameters Controlling the Selectivity of Hydrocracking. Journal of Catalysis, volume 217, pp. 376 – 387

Bergerat, G., Gallezot, P., Imelik, B., 1981. X-Ray Study of the Activation, Reduction, and Reoxidation of Pd in Y-Type Zeolites. The Journal of Physical Chemistry, volume 85, pp. 411-416

Böhringer, W., Kotsiopoulos, A., de Boer, M., Knottenbelt, C., Fletcher, J.C.Q., 2007. Selective Fischer-Tropsch Wax Hydrocracking: Opportunity for Improvement of Overall Gas-to-Liquids Processing. Studies in Surface Science and Catalysis, volume 163, pp. 345–365

Böhringer, W., Wynne, P., Kukard, R., Fletcher, J.C.Q., 2009. Bifunctional Hydrocracking: The Sundown for a Hitherto Well Established Mechanism Model. National workshop on Catalysis, Tezpur University, Tezpur, Assam, India

REFERENCES

Bianchi, D., Lacroix, M., Pajonk, G. M., Teichner, S. J., 1981. Spilled-Over Hydrogen Transport from Platinum-on-Alumina Catalyst to Methoxylated Silica Aerogel. Journal of Catalysis, volume 68, pp. 411–418

Binneman, J., 2012. The Hydrocracking of Long Chain n-Paraffins under Fischer Tropsch Conditions. Center for Catalysis Research, University of Cape Town, MSc Thesis

Bouchy, C., Hastoy, G., Guillon, E., Martens, J. A., 2009. Fischer-Tropsch Waxes Upgrading via Hydrocracking and Selective Hydroisomerization. Oil and Gas Science and Technology-Review, volume 71, pp. 227-241

Calemma, V., Correra, S., Perego, C., Pollesel, P., Pellegrini, L., 2005. Hydroconversion of Fischer-Tropsch Waxes: Assessment of the Operating Conditions effect by Factorial Design Experiments. Catalysis Today, volume 106, pp. 282-287

Calemma, V., Gambaro, C., Parker, W. O., Carbone, R., Giardino, R., Scorletti, P., 2009. Middle Distillates from Hydrocracking of FT Waxes: Composition, Characteristics and Emissions. Catalysis Today, volume 149, pp. 40-46

Chevalier F., Guisnet, M., Maurel, R., 1977. Tracer Study of the Isomerization of Paraffins on Bifunctional Catalysts. Proceedings of the Sixth International Congress on Catalysis volume 1, pp. 478-487

Cimino, A., Boudart, M., Taylor, H. S., 1954. Ethane Hydrogenation-Cracking on Iron Catalysts with and without Alkali. The Journal of Physical Chemistry, volume 58, pp. 796–800

Claude, M. C., 1999. Isomérisation des Paraffins Longues par des Zéolites à pores Moyens selon les Mécanismes Ouverture de Pore et Clé Serrure, Université Paris VI, PhD Thesis

Collins, J. P., Font Freide, J. J. H. M., Nay, B., 2006. A History of Fischer-Tropsch Wax Upgrading at Bp-from Catalyst Screening Studies to Full Scale Demonstration in Alaska. Journal of Natural Gas Chemistry, volume 15, pp. 1-10

REFERENCES

Conner, W., Falconer, J., 1995. Spillover in Heterogeneous Catalysis. Chemical Reviews, volume 95, pp. 759–788

Coonradt, H. L., Garwood, W. E., 1964. Mechanism of Hydrocracking. Reactions of Paraffins and Olefins. Industrial Engineering Chemistry Process Design and Development, volume 3, pp. 38-45

Dittmeyer, R. and Emig, G., 2008. Simultaneous Heat and Mass Transfer and Chemical Reaction. Handbook of Heterogeneous Catalysis, volume 1, pp. 1727-1784

Csicsery, S. M., 1984. Shape Selective Catalysts in Zeolites. Zeolites, volume 4, pp. 202-213

Dauns, H., Ernst, S., Weitkamp, J., 1986. The Influence of Hydrogen Sulfide in Hydrocracking of n-Decane over Palladium/Faujasite Catalysts, in New Developments in Zeolite Science and Technology, Murakami, Y., Iijima, A., Ward, J.W., (eds), elsiever, Amsterdam, pp. 787-794

De Haan, R., Joorst, G., Mokoena, G. E., Nicolaides, C. P., 2007. Non-Sulphided Nickel Supported on Silicated Alumina as Catalysts for the Hydrocracking of n-Hexadecane and of Iron –Based Fischer-Tropsch Wax. Applied Catalysis. A, volume 327, pp. 247-254

Dry, M. E., 1981. Technology of the Fischer-Tropsch Process. Catalysis Review Science and Engineering, volume 23, pp. 265-278

Dry, M. E., 2001. High quality Diesel via the Fischer-Tropsch Process - a Review. Journal of Chemical Technology and Biotechnology, volume 77, pp. 43-50

Dry, M. E., 2002. The Fischer–Tropsch process: 1950–2000. Journal of Chemical Technology and Biotechnology, volume 71, pp. 227-241

Dry, M., 2003. Fischer-Tropsch Synthesis - Industrial. Encyclopaedia of Catalysis, volume 3, pp. 347-356

REFERENCES

Dufresne, P., Bigeard, P. H., Billion, A., 1987. New Developments in Hydrocracking: Low Pressure High-Conversion Hydrocracking. Catalysis Today, volume 1, pp. 367-384

Eilers, J., Posthuma, S. A., Sie, S. T., 1990. The Shell Middle Distillate Synthesis Process (SMDS). Catalysis Letters, volume 7, pp. 253–270

Fogler, H. S., 2006. External Diffusion Effects on Heterogeneous Reactions. Elements of Chemical Reaction Engineering, N.R. Amundson, pp. 757-801, Prentice-Hall Inc., New Jersey

Gallezot, P., 1979. The State and Catalytic Properties of Platinum and Palladium in Faujasite-Type Zeoolites. Catalysis Reviews: Science Engineering, volume 20, issue 1, pp. 121-154

Gates, B. C., Katzer, J. R., and Schuit, G. C. A., 1979. Chemistry of catalytic processes, Chemical Engineering Series, pp. 172-174. McGraw-Hill, New York.

Hamelinck, C. N., Faaij, A. P. C., den Uil, H., Boerrigter, H., 2004. Production of FT Transportation Fuels from Biomas: Technical Options, Process Analysis and Optimisation, and Development Potential. Energy, volume 29, pp. 1743-1771

Jacobs, A. P., Martens, J. A., Weitkamp, J., 1982. Hydroconversion of Long-Chain n-Alkanes on Pt/HZSM-5 Zeolite. Faraday Discussions, Chemical Society, volume 72, pp. 353 - 366

Kazansky, V. B., Senchenya, I. N., 1989. Quantum Chemical Study of the Electronic Structure and Geometry of Surface Alkoxy Groups as Probable Active Intermediates of Heterogeneous Acidic Catalysts: What are the Adsorbed Carbenium Ions?. Journal of Catalysis, volume 119, no. 1, pp. 108-120

Kemball, C. and Taylor, H. S., 1948. The Catalytic Decomposition of Ethane and Ethane Hydrogen Mixtures. Journal of American Chemical Society, volume 70, pp. 348–351

REFERENCES

Khodakov, A. Y., Chu, W., Fongarland, P., 2006. Advances in the Development of Novel Cobalt Fischer-Tropsch Catalysts for Synthesis of Long Chain Hydrocarbons and Clean Fuels. Chemical Review, volume 107, pp. 1692-1744

Kumar, H., Froment, G., 2007. A General Mechanistic Kinetic Model for the Hydroisomerization and Hydrocracking of Long-Chain Paraffins. Industrial and Engineering Chemistry Research, volume 46, pp. 4075-4090

Kukard, R., 2008. Effect of Zeolite Type on Hydrocracking of Long n-Parrafins. Center for Catalysis Research, University of Cape Town MSc Thesis

Kukard, K., Wynne, P., Böringer, W., Fletcher, J. C. Q., 2009. Hop Over or Spill Over-The End of a Hitherto Well Established Hydrocracking Mechanism. National Workshop on Catalysis, India

Lawson, K. H., Jothimurugesan, K., Espinoza, R. L., 2006. Catalyst For Hydroprocessing of Fischer-Tropsch Products. US Patent 20050274646 A1

Leckel, D., 2005. Hydrocracking of Iron-Catalysed Fischer-Tropsch Waxes, Energy and Fuels, volume 19, pp. 1795-1803

Leckel, D., Liwanga-Ehumbu, M., 2006. Diesel-Selective Hydrocracking of an Iron Based Fischer-Tropsch Wax Fraction (C_{15} – C_{45}) Using a MoO_3 – Modified Noble Metal Catalyst. Energy and Fuels, volume 20, pp. 2330-2336

Leckel, D., 2007. Noble Metal Wax Hydrocracking Catalysts Supported on High-Silica Alumina. Industrial and Engineering Chemistry Research, volume 46, pp. 3505-3512

Liu, Y., Hanaoka, T., Murata, K., Okabe, K., Inaba, M., Takahara, I., Sakanishi, K., 2007. Hydrocracking of Fischer-Tropsch Wax to Diesel-range Hydrocarbons over Bifunctional Catalysts Containing Pt and Polyoxocation-pillared Montmorillonite. Chemistry Letters, volume 36 pp. 1470-1471

REFERENCES

Martens, J. and Jacobs, P., 2001. Introduction to Acid Catalysis with Zeolites in Hydrocarbon Reactions. Studies in Surface Science and Catalysis, volume 137, pp. 633–671

Martens, J. and Jacobs, P., 1990. Conceptual Background for the Conversion of Hydrocarbons on Heterogeneous Acid Catalysts. Theoretical Aspects of Heterogeneous Catalysis, pp. 52–109

Marcilly, C., 2003, Réactivité et Modes de Transformation des Grandes familles d'Hydrocarbures, in Catalyse Acido-Basique, application au Raffinage et àla Pétrochemie, Technip, Paris

Maxwell, I.E., Stork, W. H. H., 1991. Chapter 17 Hydrocarbon Processing with Zeolites. Studies in Surface Science and Catalysis, volume 58, pp. 571-630

Maxwell, I. E., Minderhound, J. K., Stork, W. H. J., Van Veen, J. A. R., 1997. Hydrocracking and Catalytic Dewaxing, in Handbook of Heterogeneous Catalysis, volume 4, Ertl, G., Knözinger, H., weitkamp, J. Wiley-VCH, Weiinheim

Mena Subiranas, A. M. and Schaub, G., 2007. Combining Fischer-Tropsch (FT) and Hydrocarbon Reactions under FT Reaction Conditions – Catalyst and Reactor Studies with Co or Fe and Pt/ZSM-5. International Journal of Chemical Reactor Engineering, volume 5, no. A78

Mena Subiranas, A. M., Schaub, G., 2009. Combining Fischer-trpsch (FT) and Hydrocarbon Reactions under FT Reaction Conditions: Model Compound and Combined – Catalyst Studies. International Journal of Chemical Reactor Engineering, volume 7, no. A31

Mills, G., Heinemann, H., Milliken, T. Oblad, A., 1953. (Hydroforming Reactions) Catalytic Mechanism. The Journal of Industrial and Engineering Chemistry, volume 45, pp. 134–137

Munoz Arroyo, J. M., Martens, G. G., Froment, G. F., Marin, G. B., Jacobs, P. A., Martens, J. A., 2000. Hydrocracking and Isomerization of n-Paraffin Mixtures and a Hydrotreated Gasoil on Pt/ZSM-22: Confirmation of Pore Mouth and Key-Lock Catalysis in Liquid Phase. Applied Catalysis A General, volume 192, pp. 9-22

REFERENCES

Nat, P.J., 1988. NPRA Annual Meeting, San Antonio, TX, AM-88-75

Okumura, K., Yoshimoto, R., Uruga, T., Tanida, H., Kato, K., Yokota, S., Niwa, M., 2004. Energy-Dispersive XAFS Studies on the Spontaneous Dispersion of PdO and the Formation of Stable Pd Clusters in Zeolites. Journal of Physical Chemistry B. volume 108, pp. 6250-6255

Park, K. and Ihm, S., 2000. Comparison of Pt/zeolite Catalysts for n Hexadecane Hydroisomerization. Applied Catalysis A: General, volume 203, pp. 201–209

Park, S. H., Tzou, M. S., Sachtler, W. H., 1986. Temperature Programmed Reduction and Re-Oxidation of Pt in Y-Zeolites. Applied Catalysis, volume 24, pp 85-98

Pellegrini, L., Locatelli, S., Bonomi, S., Calemma, V., 2004. Modelling of Fischer-Tropsch Products Hydrocracking. Chemical Engineering Science, volume 59, pp. 4781-4787

Pellegrini, L., Gamba, S., Bonomi, S., Calemma, V., Molinari, D., 2007. The “All Components Hydrocracking Model”. Chemical Engineering Science, volume 62, pp. 5013-5020

Pinna, F., 1998. Supported Metal Catalyst Preparation. Catalysis Today, volume 41, pp. 129 – 137

Rastelli, H., Lok, B., Earls, D. J. and J. T., M., 1982. Characterization of Zeolitic Acidity: The Cracking of 2 mole% n-Butane over A Fixed Zeolite Bed. Canadian Journal of Chemical Engineering, volume 60, pp. 44-49

Riberio, F., Marcilly, C., Guisnet, M., 1982. Hydroisomerization of n-Hexane on Platinum Zeolites. Journal of Catalysis, volume 78, no. 2, pp. 267-280

Rigby, A. M., Kramer, G. J., and van Santen, R. A., 1997. Mechanisms of Hydrocarbon Conversion in Zeolites: A Quantum Mechanical Study. Journal of Catalysis, volume 170, pp. 1-10

REFERENCES

Roessner, F., Mroczek, U., Hagen, A., 1993. Hydrogen Spillover in the Conversion of Cyclohexane on ZSM-5 Zeolites. Studies on Surface Science Catalysis, volume 77, pp. 151-158

Roessner, F., Roland, U., 1996. Hydrogen Spillover in Bifunctional Catalysis. Journal of Molecular Catalysis A: volume 112, pp. 401–412

Roland, U., Braunschweig, T., Roessner, F., 1997. On the Nature of Spilt Over Hydrogen. Journal of Molecular Catalysis A, volume 127, pp. 61–84

Rollmann, L. and Walsh, D., 1979. Shape Selectivity and Carbon Formation in Zeolites. Journal of Catalysis, volume 56, pp. 139–140

Scherzer, J. and Gruia, A., 1996. Hydrocracking Science and Technology, Chapter 3. Marcel Dekker Inc., New York, 1st edition

Seki, H., Aoki, N., Ikeda, M., 2004. Development of Wax Hydrocracking Catalysts with Microcrystalline Zeolite, Abstracts Papers. American Chemical Scociety, volume 226, U252

Shah, P. P., Sturtevant, G. C., Gregor, J. H., Umbach, M. J. J., Padrta, F. G., Steigleder, K. Z., Fischer-Tropsch Wax Characterization and Upgrading: Final Report, UOP Inc., available on http://www.fischer-tropsch.org/, Accessed: 03/12/2010

Sie, S. T., Senden, M. M. G., Van Wechem, H. M. H., 1991. Conversion of Natural Gas to Transportation Fuels via The Shell Middle distillate Synthesis Process (SMDS). Catalysis Today, volume 8, pp. 371-394

Sinfelt, J. H., 1969. Catalytic Hydrogenolysis over Supported Metals. Catalysis Reviews, volume 3, pp. 175–205

Sinfelt, J. H., 1973. Specificity in Catalytic Hydrogenolysis by Metals. Advances in Catalysis, volume 23, pp. 91–119

REFERENCES

Steijns, M., Froment, G., Jacobs, P., Uytterhoeven, J., weitkamp, J., 1981. Hydrocracking and Hydroisomerisation of n-Decane and n-Dodecane. Industrial and Engineering Chemistry Research, volume 20, pp. 660 – 668

Steinberg, K., Mroczek, U., Roessner, F., 1990. Aromatization of Ethane on Platinum Containing ZSM-5 Zeolites. Applied Catalysis, volume 66, pp. 37–44

Thybaut, J. W., Laxmi Narasimhan, C. S., Denayer, J. F., Baron, G. V., Jacobs, P. A., Martens, J. A., Marin, G. B., 2005. Acid-Metal Balance of a Hydrocracking Catalyst: Ideal versus Nonideal Behaviour. Industrial and Engineering Chemistry Research, volume 44, pp. 5159-5169

Toulhoat, H., Raybaud, P., Benazzi, E., 2004. Effect of Confinement on the Selectivity of Hydrocracking. Journal of Catalysis, volume 221, pp. 500-509

Van Bekkum, H., Flanigen, E., Jacobs, P. Jansen, J. (eds.), 2001. Introduction to Zeolite Science and Practice. Elsevier, 2nd edition

Venuto, P. B., 1977. Aromatic Reactions over Molecular Sieve Catalysts: a Mechanistic Review in: 6th Catalysis Organization Synthesis, pp. 67-93, USA

Weisz, P. B., 1962. Polyfunctional Heterogenous Catalysis. Advances in Catalysis, volume 13, pp. 137-190

Weisz, P.B., Frilette, V. J., 1960. Intracrystalline and Molecular-Shape-Selective catalysis in Zeolite Salts. The Journal of Physical Chemistry, volume 64, pp. 382

Weisz, P. B., Swegler, E. W., 1957. Stepwise Reaction on Separate Catalytic Centers-Isomerization of Saturated Hydrocarbons. Science, volume 126, pp. 31-32

Weitkamp, J., 1975. Hydrocracking and Hydrotreating, American Chemical Society Symposium series, volume 20, pp. 1-27

REFERENCES

Weitkamp, J., Ernst, S., 1990. Factors Influencing the Selectivity of Hydrocarbons in Zeolites, in Guidelines for Mastering the Properties of Molecular Sieves, Barthomeuf, D., Deroune, E.G., holderich, W, (eds), Plenum Press, New York

Weitkamp, J., Jacobs, P., Martens, J., 1983. Isomerization and Hydrocracking of C_9 through C_{16} n-Alkanes on Pt/HZSM-5 Zeolite. Applied Catalysis, volume 8, pp. 123 –141

Weitkamp, J., Hedden, K., 1975. Reaktionsablauf beim Hydrocracken von n-Alkanen an Edelmetall/Zeolith-Katalysatoren. Chemie Ingenieur Technik, volume 47, pp. 537- 545

Weiss, A. H., LeViness, S., Nair, V., Guzci, L., Sarkany, A., Schay, Z., 1984. The Effect of Pd Dispersion in Acetylene Selective Hydrogenation. Proceedings of the 8th International Congress of Catalysis, volume 6, pp 143-196

Wynne, P., 2014. The Effect of Metal Type and Loading on Fischer-Tropsch Wax Hydrocracking Conversion and Selectivity. Center for Catalysis Research, University of Cape Town, MSc Thesis

Zhang, S., Zhang, Y., Tierney, W. J., Wender, I., 2001. Anion-Modified Zirconia:Effect of Metal Promotion and Hydrogen Reduction on Hydroisomerization of n-Hexadecane and Fischer-Tropsch waxes. Oil and Gas Science and Technology Review, Vol. 71, pp. 227-241

Zhou, Z., Zhang, Y., Tierney, J. W., Wender, I., 2003. Hybrid Zirconia Catalysts for Conversion of Fischer-Tropsch Waxy Products to Transportation Fuels. Fuel Process Technology, volume 83, pp. 67-80

Appendices

Segregated Catalyst Loading Calculation

For all segregated catalyst loadings a zeolite loading of 1g was used

Ruthenium

Metal Ruthenium

Avogadros Const	6.02E+23
Number of atoms/ nm2	12.5
Molar Mass (g)	101.07

	Ru-catalyst A	Ru-catalyst B	Ru-catalyst loading C	Ru-Catalyst loadng D
mass of metal on support	1.21E-02	7.15E-03	2.86E-04	2.86E-03
moles of metal on support	0.000113552	6.71904E-05	2.68762E-06	2.68762E-05
atoms loaded on support	6.84E+19	4.05E+19	1.62E+18	1.62E+19
metal atoms exposed	2.05E+18	1.21E+18	4.86E+16	4.86E+17
actual Metal/acid	0.009	0.006	0.00022	0.002

Rhodium

Metal Rhodium

Avogadros Const	6.02E+23
Number of atoms/ nm2	13.3
Molar Mass (g)	102.91

	Rh-catalyst A	Rh-catalyst B	Rh-catalyst C	Rh-catalyst D
mass of metal on support	0.011449644	0.006774937	0.000270997	0.002709975
Number of moles of metal in support	0.000111259	6.58336E-05	2.63334E-06	2.63334E-05
Number of metal atoms on support	6.70E+19	3.97E+19	1.59E+18	1.59E+19
Number of atoms available for reaction (those exposed)	6.61E+19	3.91E+19	1.57E+18	1.57E+19
Actual Metal/Acid	0.30	0.18	0.01	0.07

Metal Pd

Avogadros Const	6.02E+23
Number of atoms/ nm2	13.3
Molar Mass (g)	106.42

	Pd - catalyst A	Pd - catalyst B	Pd - catalyst C	Pd - catalyst D	Pd - catalyst E	Pd - catalyst F	Pd - catalyst G
Metal : Acid site ratio	0.0004	0.0013	0.004	0.020	0.040	0.100	0.169
number of metal sites on support	5.81E+17	1.89E+18	5.81E+18	2.91E+19	5.81E+19	1.45E+20	2.46E+20
Number of moles of metal on support	9.65E-07	3.14E-06	9.65E-06	4.83E-05	9.65E-05	2.41E-04	4.08E-04
Mass of metal on support	1.0272E-04	3.3383E-04	1.0272E-03	5.1358E-03	1.0272E-02	2.5679E-02	4.3397E-02
Mass of metal plus support	0.0022	0.0070	0.0216	0.1079	0.2157	0.5393	0.9113

Impregnated Catalyst

Total weight of all impregnated catalyst tested was 2g.

Weight of impregnated catalyst weight tested

Pd Loading (Wt%)	Mass of Pd Loaded (g)	Mass of H-MFI-90 (g)
0.3	0.0060	1.9940
0.6	0.0120	1.9880
0.7	0.0140	1.9860
0.8	0.0160	1.9840
0.9	0.0180	1.9820
1.2	0.0240	1.9760

Calculation of Coke Deposited on Zeolite

This calculation is for the impregnated catalyst. A hydrogen and carbon balance was done on the system as follows:

The carbon to hydrogen ratio of the feed ($[H/C]_{feed}$) and product ($[H/C]_{product}$) were determined to be 2.13 and 2.30 respectively at 58% conversion

Density n-$C_{16}H_{34}$	0.887	g/ml
Molar Mass n-$C_{16}H_{34}$	226	g/mole
No. carbons	16	
No. hydrogens	34	

Flow rate (ml) n-hexadecane	0.01	ml/min
Moles C16 in	3.92E-05	moles/min
Moles Carbon flowing in	6.28E-04	moles/min
moles of hydrogen flowing In	1.33E-03	moles/min

The molar carbon balance for the system that relates carbon in the feed (C_{feed}), carbon in the product ($C_{product}$), carbon in unconverted feed ($C_{unconverted\ feed}$) and carbon as coke (C_{coke}) is shown below

$$C_{feed} = C_{product} + C_{unconverted\ feed} + C_{coke} \ldots\ldots\ldots (1)$$

The hydrogen balance for the system relating the hydrogen in the feed molecule (H_{feed}), the hydrogen in the product molecules ($H_{product}$) and the hydrogen in the unconverted feed molecules ($H_{unconverted}$) is shown below:

$$H_{feed} = H_{product} + H_{unconverted} \quad \text{..... (2)}$$

Since the hydrogen to carbon ratio of the feed is known ($[H/C]_{feed}$) and the hydrogen to carbon ratio in the products is known ($[H/C]_{product}$), the molar carbon deposited as coke is then calculated in terms of hydrogen as follows.

$$C_{coke} = H_{feed}/[H/C]_{feed} - H_{product}/[H/C]_{product} - H_{unconverted}/[H/C]_{feed} \quad \text{.....(3)}$$

$$C_{coke} = 0.00030551\text{g/min}$$

$$C_{coke} = 0.0001268\text{g/min (at 23\% conversion)}$$

$$C_{coke} = 0.00009205\text{g/min (at 18\% conversion)}$$